NCHRP
REPORT 468

NATIONAL COOPERATIVE HIGHWAY RESEARCH PROGRAM

Contributions of Pavement Structural Layers to Rutting of Hot Mix Asphalt Pavements

TRANSPORTATION RESEARCH BOARD

NATIONAL RESEARCH COUNCIL

NATIONAL COOPERATIVE HIGHWAY RESEARCH PROGRAM

NCHRP REPORT 468

Contributions of Pavement Structural Layers to Rutting of Hot Mix Asphalt Pavements

THOMAS D. WHITE
Mississippi State University
Starkville, MS

AND

JOHN E. HADDOCK
ADAM J. T. HAND
HONGBING FANG
Purdue University
West Lafayette, IN

SUBJECT AREAS
Pavement Design, Management, and Performance • Materials and Construction

Research Sponsored by the American Association of State Highway and Transportation Officials
in Cooperation with the Federal Highway Administration

TRANSPORTATION RESEARCH BOARD — NATIONAL RESEARCH COUNCIL

NATIONAL ACADEMY PRESS
WASHINGTON, D.C. — 2002

NATIONAL COOPERATIVE HIGHWAY RESEARCH PROGRAM

Systematic, well-designed research provides the most effective approach to the solution of many problems facing highway administrators and engineers. Often, highway problems are of local interest and can best be studied by highway departments individually or in cooperation with their state universities and others. However, the accelerating growth of highway transportation develops increasingly complex problems of wide interest to highway authorities. These problems are best studied through a coordinated program of cooperative research.

In recognition of these needs, the highway administrators of the American Association of State Highway and Transportation Officials initiated in 1962 an objective national highway research program employing modern scientific techniques. This program is supported on a continuing basis by funds from participating member states of the Association and it receives the full cooperation and support of the Federal Highway Administration, United States Department of Transportation.

The Transportation Research Board of the National Research Council was requested by the Association to administer the research program because of the Board's recognized objectivity and understanding of modern research practices. The Board is uniquely suited for this purpose as it maintains an extensive committee structure from which authorities on any highway transportation subject may be drawn; it possesses avenues of communications and cooperation with federal, state and local governmental agencies, universities, and industry; its relationship to the National Research Council is an insurance of objectivity; it maintains a full-time research correlation staff of specialists in highway transportation matters to bring the findings of research directly to those who are in a position to use them.

The program is developed on the basis of research needs identified by chief administrators of the highway and transportation departments and by committees of AASHTO. Each year, specific areas of research needs to be included in the program are proposed to the National Research Council and the Board by the American Association of State Highway and Transportation Officials. Research projects to fulfill these needs are defined by the Board, and qualified research agencies are selected from those that have submitted proposals. Administration and surveillance of research contracts are the responsibilities of the National Research Council and the Transportation Research Board.

The needs for highway research are many, and the National Cooperative Highway Research Program can make significant contributions to the solution of highway transportation problems of mutual concern to many responsible groups. The program, however, is intended to complement rather than to substitute for or duplicate other highway research programs.

Note: The Transportation Research Board, the National Research Council, the Federal Highway Administration, the American Association of State Highway and Transportation Officials, and the individual states participating in the National Cooperative Highway Research Program do not endorse products or manufacturers. Trade or manufacturers' names appear herein solely because they are considered essential to the object of this report.

NCHRP REPORT 468

Project C1-34A FY'99

ISSN 0077-5614

ISBN 0-309-06721-9

Library of Congress Control Number 2001099801

Price $24.00

NOTICE

The project that is the subject of this report was a part of the National Cooperative Highway Research Program conducted by the Transportation Research Board with the approval of the Governing Board of the National Research Council. Such approval reflects the Governing Board's judgment that the program concerned is of national importance and appropriate with respect to both the purposes and resources of the National Research Council.

The members of the technical committee selected to monitor this project and to review this report were chosen for recognized scholarly competence and with due consideration for the balance of disciplines appropriate to the project. The opinions and conclusions expressed or implied are those of the research agency that performed the research, and, while they have been accepted as appropriate by the technical committee, they are not necessarily those of the Transportation Research Board, the National Research Council, the American Association of State Highway and Transportation Officials, or the Federal Highway Administration, U.S. Department of Transportation.

Each report is reviewed and accepted for publication by the technical committee according to procedures established and monitored by the Transportation Research Board Executive Committee and the Governing Board of the National Research Council.

Published reports of the

NATIONAL COOPERATIVE HIGHWAY RESEARCH PROGRAM

are available from:

Transportation Research Board
National Research Council
2101 Constitution Avenue, N.W.
Washington, D.C. 20418

and can be ordered through the Internet at:

http://www.trb.org/trb/bookstore

Printed in the United States of America

FOREWORD

By Staff
Transportation Research Board

This report presents the findings of a research project to investigate whether the relative contributions of the structural layers to rutting in a hot mix asphalt (HMA) pavement can be determined from an analysis of its transverse surface profile. The report presents a recommended method for estimating the relative contributions of pavement layers to total rutting. The report will be of particular interest to engineers in the public and private sectors with responsibility for the design, construction, maintenance, and rehabilitation of HMA pavements.

Rutting is the load-induced permanent deformation of a flexible pavement. Depending on the magnitude of the load and the relative strength of the pavement layers, permanent deformation can occur in the subgrade, the base, or the upper hot mix asphalt (HMA) layers. Vulnerability of pavement layers to rutting varies at different times of the year. For example, rutting of HMA layers is more common during hot summer months than it is during the winter, and permanent deformation is more likely in an aggregate base during wet spring months. A second important factor is the stress level in an individual pavement layer, which is a function of total pavement thickness and magnitude of the load. For example, application of a heavy load on a thin pavement over unstabilized subgrade may induce excessive rutting in the subgrade as well as in the HMA layers.

Appropriate remedial action for existing rutting requires a knowledge of the relative contributions of the layers (i.e., subgrade, base, and HMA) to the total permanent deformation in the pavement. Early analysis of the long-term pavement performance (LTPP) database suggested that the layers primarily responsible for the rutting of a flexible pavement could be identified from an analysis of the shape of the pavement's transverse surface profile. Measuring a transverse surface profile is easier, less hazardous, and far less costly than cutting a transverse trench to examine underlying layers.

Under NCHRP Project 1-34A, "Contributions of Pavement Structural Layers to Rutting of Flexible Pavements," Purdue University was asked to investigate whether the relative contributions of the layers to rutting in a flexible pavement can be determined from an analysis of the pavement's transverse surface profile and then prepare a practical method for estimating the relative contributions of pavement layers to total rutting.

The research team first conducted extensive computer analyses using finite element analysis to simulate rutting failures in HMA surface mixtures, base courses, and subgrades. Transverse surface profile characteristics indicative of failure within specific structural layers were then determined in the form of simple distortion parameters, and specific criteria were developed for these distortion parameters. The criteria were applied to an analysis of full-scale accelerated pavement test (APT) data, confirming that the relative contributions of the layers to rutting in an HMA pavement could be determined from an analysis of its transverse surface profile.

In the second phase of the project, the initial criteria were further refined through additional finite element analysis and then validated using trench data collected from in-service pavements in seven states. Good agreement was found between the predicted and field-observed location of failure in the pavement structure. A method to estimate the contributions of individual pavement layers to the total rutting was then developed in the form of a recommended test method in AASHTO standard format.

The final report includes a critical literature review, a detailed description of the analytical and experimental programs, a discussion of the research results, and five supporting appendixes:

- Appendix A: Recommended Method for Determining the Failed Layer of a Flexible Pavement;
- Appendix B: Relationship Between Rut Width and Affected Depth in Pavements;
- Appendix C: General Approach to Performing a Finite Element Analysis;
- Appendix D: Surface Profile Data from Field Projects; and
- Appendix E: Distortion Parameters Determined for the Different Transverse Measurement Increments for Each Failure Mode.

This published report includes the main text and Appendix A. Appendixes B through E are available on request from NCHRP.

CONTENTS

AUTHOR ACKNOWLEDGMENTS

The research reported herein was performed under the National Cooperative Highway Research Program, Project 1-34A, by the School of Civil Engineering, Purdue University, and the Department of Civil Engineering, Mississippi State University. Purdue University was the contractor for the study. The work undertaken at Mississippi State University was under a subcontract with Purdue University.

Thomas D. White, former Professor and Materials Area Head in the School of Civil Engineering at Purdue University, now Professor and Head of Civil Engineering at Mississippi State University, was the principal investigator. The other authors of this report are co-principal investigator John E. Haddock, Assistant Professor in the School of Civil Engineering at Purdue University; co-principal investigator Adam J. Hand, Assistant Professor in the School of Civil Engineering at Purdue University; and Hongbing Fang, Graduate Research Assistant in the School of Civil Engineering at Purdue University.

The work was conducted under the general supervision of Professor White. The work performed at Purdue University was conducted under the supervision of Professors Hand and Haddock with the assistance of Mr. Fang, Graduate Research Assistant. Professor White performed the work conducted at Mississippi State University.

The authors acknowledge the cooperation of several agencies that provided valuable accelerated pavement test data to the project. The agencies and specific individuals include Federal Highway Administration (Accelerated Load Facility test data—Dr. Walaa Mogawer); Cold Regions Research Engineering Laboratory (Heavy Vehicle Simulator data—Dr. Vincent Janoo); Federal Highway Administration/ National Cooperative Highway Research Program (WesTrack test data—Dr. Terry Mitchell and Dr. Edward Harrigan); Indiana Department of Transportation (INDOT/Purdue APT test data—Dr. Barry Partridge); and Minnesota Department of Transportation (MnROAD test data—Mr. Duane Young).

The authors also acknowledge the cooperation of several state highway agencies that provided resources to identify and trench in-service pavements in support of this research project. The states include Alabama, Indiana, Minnesota, Mississippi, Nevada, North Carolina, Ohio, Texas, and West Virginia.

CHAPTER **1**

INTRODUCTION AND RESEARCH APPROACH

1.1 PROBLEM STATEMENT, RUTTING AND ITS RELATIONSHIP TO CLASSIC PAVEMENT DESIGN PRACTICES, AND RESEARCH OBJECTIVES

1.1.1 Problem Statement

In recent years, many states have experienced an increase in the severity and extent of permanent deformation (rutting) in hot mix asphalt (HMA) pavements. The increased rutting has been attributed to increases in truck tire pressures, axle loads, and traffic volumes. Tire pressure and axle load increases mean that HMA near the pavement surface is exposed to higher stresses than the levels assumed when structural designs are performed in accordance with the 1993 AASHTO Guide for Design of Pavement Structures. These design criteria are based on 80-kN (18,000-lb) axle loads and tire contact pressures of 517–552 kPa (75–80 psi) [1].

In 1987, concern about high truck-tire pressures and rutting led to a national symposium on the subject [2]. Symposium participants concluded that increased truck weights and tire pressures had led to an increase in rutting. They also believed that giving more attention to material selection, mix design, and construction practices could minimize rutting. Field studies have been conducted in the last 15 years in an effort to identify material properties, design parameters that relate to rutting, or both [3, 4].

More recently, a study was conducted by the National Center for Asphalt Technology (NCAT) entitled, "A National Study of Rutting in Hot Mix Asphalt Pavements." This study included 42 pavements in 14 states dispersed throughout all regions of the United States. The projects represented various climatic zones and aggregates of differing origins and angularity. The projects also involved different specifying agencies and construction practices [5]. Concurrently, the Strategic Highway Research Program (SHRP) included a large component targeted at understanding the permanent deformation phenomenon in HMA [6]. The SHRP program resulted in the development of materials selection, mix design and analysis procedures, and performance prediction tools, formally termed the Superpave mix design and analysis system [7, 8]. The FHWA has assisted with implementation of Superpave binder and volumetric mixture design procedures. However, implementation of more sophisticated components of the Superpave system, specifically the mix analysis and performance modeling, has been slowed because of the need for additional research and refinements. These efforts are currently underway with the support of NCHRP and FHWA [9].

The research associated with Superpave and its implementation, along with the plethora of other pavement-related research recently conducted or currently underway in the United States and abroad, has and will continue to provide a better understanding of the permanent deformation phenomenon, which is a load-related distress [10]. A classic description of rutting and its relationship to pavement design is provided in the following section. Trenching studies at the AASHO Road Test, as well as at other full-scale test tracks, have indicated that shear deformation, rather than densification, is the primary rutting mechanism in HMA surface mixtures when reasonably stiff supporting layers are present [11, 12]. In asphalt-bound surface layers, permanent deformation is limited to the upper 100 mm (4 in.) of the HMA and the rut depth is proportional to the number of load applications [11].

1.1.2 Rutting and Its Relationship to Classic Pavement Design Practices

Rutting develops with an increasing number of load applications [9]. Rutting is caused by a combination of densification and shear-related deformation and may occur in any layer of a pavement structure [11]. A typical structural section is illustrated in Figure 1-1 (figures appear at the end of each chapter). The layer(s) in which rutting occurs is determined by loading magnitude and the relative strength of the pavement layers. Stresses within each layer of a pavement structure are determined by applied load, individual and combined layer thickness, and layer material properties. Structural designs, mixture designs, and construction are performed with a goal of minimizing permanent deformation.

Classic pavement design procedures are based on limiting the vertical stress on top of the subgrade and the tensile stress at the bottom of the lowest HMA layer. The stress and strain are illustrated in Figure 1-1. Stresses and strains are limited by increasing layer thickness and stiffness. As a result, pavement structures are composed of layers possessing successively higher moduli (i.e., stiffness) approaching the surface. These layers attenuate load-induced stresses and limit subgrade stress and deflection. For a given subgrade, a stiffer layer possesses

better load distribution capabilities. A stiff surface course may reduce the risk of subgrade deflection, but it thus increases tensile stress at the bottom of the layer and increases horizontal shear stresses. Therefore, a designer must ensure that the flexural and shear resistance of the stiff layer are great enough to sustain these high-stress states.

Pavement structural design has historically focused on protecting the subgrade, and shear resistance of the HMA layers has been left to mixture designers. Adequacy of HMA mixture shear resistance is commonly assessed with empirical methods, such as Marshall and Hveem Stability. More recently, assessments have been made using an array of mechanical test methods, such as laboratory wheel-track tests, creep and triaxial tests, and Superpave shear tests. There is a conscious effort to move toward the use of fundamental performance-related test methods.

Figure 1-2 shows classic rutting over time. Typically, with the application of traffic, a small amount of permanent deformation (3–5 mm) due to densification of both unbound and bound layers within the structure will occur. The accumulation of deformation then slows as the HMA strain hardens (i.e., stiffens). Stiffening due to aging of the HMA also contributes to shear resistance with time. A power function can be used to represent the strain rate.

Pavement fatigue cracking is also associated with traffic accumulation. Cracking reduces the stiffness of the HMA surface, and water can infiltrate and lower the strengths of the unbound granular layers and subgrade, which will then lead to accelerated rutting. Wear due to studded tires also contributes to rutting.

Figure 1-3 shows the potential effects of seasonal temperature and moisture variation on rutting. Rutting is not common during fall and winter months, when HMA is typically very stiff because of cold temperatures; unbound aggregate layers and subgrade materials may even be frozen. In the spring, unbound aggregate layers and subgrade material strengths are low because of high moisture contents. As a result, rutting potential increases. In late spring and early summer, rutting potential decreases as moisture contents in unbound aggregate layers and subgrade decrease. During the summer months, when temperatures are relatively high, HMA stiffness decreases and the propensity for rutting increases.

1.1.3 Research Objectives

For years, researchers and practitioners alike in the pavements and materials industry have been performing forensic investigations to determine the origin of HMA permanent deformation failures. Usually, the investigations involve traffic control, coring, excavation, and significant materials testing. These investigations are costly and can be very inconvenient for road users. A method of estimating the contribution of individual pavement layers to rutting from analysis of transverse surface profiles would provide the industry with an extremely valuable analytical tool. Additionally, such a method could save taxpayers much of the costs associated with typical forensic investigations. It would also provide highway engineers with information necessary for selecting appropriate maintenance, rehabilitation, or reconstruction alternatives.

The objectives of this research project were to (1) investigate whether the relative contributions of the layers to rutting in a flexible pavement could be determined from an analysis of its transverse surface profile and (2) prepare a method for estimating the relative contributions of pavement layers to total rutting.

1.2 SCOPE OF STUDY

The scope of this study included a review and analysis of available literature on the subject of nondestructive evaluation of transverse surface profiles to assess the source of rutting in HMA pavements. The scope incorporated a theoretical analysis that examined surface profiles generated when substandard material properties were assumed for specific pavement layers. Simulations, using the finite element modeling technique, were employed for this purpose. Information in the literature was coupled with the theoretical analysis to develop relationships between transverse surface profile characteristics and contributions of the individual pavement layers to rutting in HMA pavements. Limited full-scale accelerated pavement test (APT) data were used to evaluate the reasonableness of the relationships. The relationships were found to be very reasonable; thus, a field study was initiated to collect data for validating the relationships, refining the relationships, or both. Finally, using the refined relationships, a method to estimate the contributions of pavement layers to total rutting was developed and documented in the form of a draft AASHTO recommended practice.

1.3 RESEARCH APPROACH

The research approach undertaken follows the general outline provided in the research prospectus, NCHRP Project 1-34A, “Contributions of Pavement Structural Layers to Rutting of Flexible Pavements.” The research was separated into two phases, each of which consisted of three individual tasks. The Phase 1 tasks consisted of (1) review literature and analyze existing data in the literature, (2) prepare a work plan for Tasks 4 and 5, and (3) prepare an interim report. The Phase 2 tasks were (1) conduct the work plan, (2) validate developed relationships, and (3) prepare the final project report.

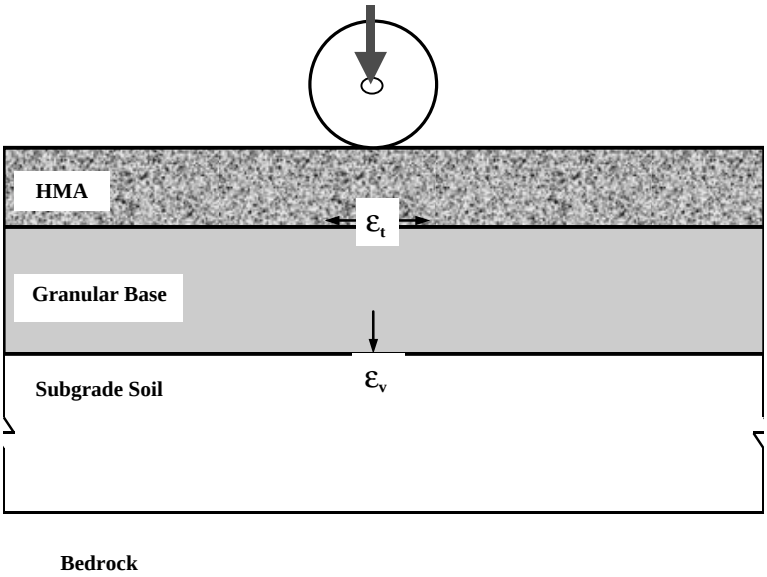

Figure 1-1. Illustration of stress and strain within pavement layers.

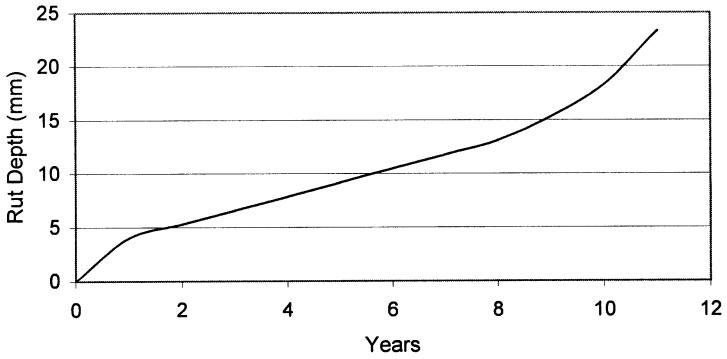

Figure 1-2. Classic rutting behavior over time.

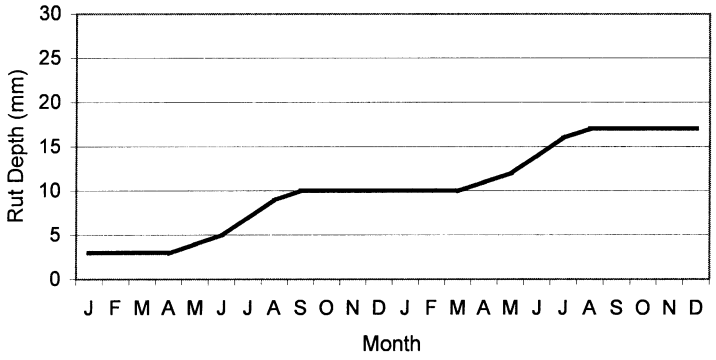

Figure 1-3. Potential seasonal effects on rutting.

CHAPTER **2**

LITERATURE REVIEW

2.1 INTRODUCTION

A literature review was conducted on the subject of nondestructive evaluation of transverse surface profiles to assess the source of rutting in HMA pavements. The task objective was to identify, collect, review, and analyze data from field studies of observed rutting in flexible pavements. The following databases were searched for information regarding the subject research topic:

- Transportation Research Information Services (TRIS),
- National Technical Information Service (NTIS),
- TRB Publications Index,
- *ASCE Journal of Transportation Engineering* database,
- ASTM Publications database,
- *Asphalt Paving Technology* (Journal of the Association of Asphalt Paving Technologists [AAPT]) database, and
- Other conference proceeding databases.

A conscious effort was made to encompass the multiple research efforts currently underway in the United States to further advance Superpave technology. This effort ultimately led to literature on projects employing prototype accelerated-loading facilities such as the FHWA Accelerated Loading Facilities (ALF), South African Heavy Vehicle Simulator (HVS), Texas Mobile Load Simulator (TxMLS), Indiana DOT/Purdue University Accelerated Pavement Testing (INDOT/Purdue APT) Facility, and full-scale test tracks such as the Minnesota Road Research Project (MnROAD), the Pennsylvania Transportation Institute (PTI) test track, and WesTrack. Accelerated testing was considered attractive because performance data are generated in a short period compared with in-service pavements. Also, pavement sections in such facilities are small enough that the evaluated materials and pavements can be thoroughly investigated. Other positive attributes include close control of construction and inclusion of pavement instrumentation in test sections. A particularly important aspect of this project was that extensive performance monitoring (including transverse profile measurements) was conducted on a regular basis on most projects that incorporated accelerated loading. At the time this project was initiated, several accelerated pavement performance studies were in progress, and extensive performance data had already become available. Such studies included the National Pooled Fund Study 176 (PFS 176), FHWA ALF, MnROAD, and WesTrack.

The remainder of this section provides details about the literature search and review. At the time the research proposal was written, a TRIS search was performed and three interesting publications that specifically referenced correlating transverse surface profiles and the contributions of specific pavement layers to rutting were summarized. It was anticipated that other publications would be identified when the search was expanded to include other databases. Significant literature was available relative to predicting permanent deformation. In particular, significant literature presented comparisons of predicted and measured rut depths. However, limited literature provided surface transverse profiles, subsurface transverse profiles, or both, rather than rut depth data. A summary of each relevant publication reviewed follows.

Gramling et al. analyzed rut depth measurement techniques and the benefits of surface transverse profiles as opposed to simple rut depth measurements [13]. The primary objective of this research was to compare methods of measuring rut depths for the SHRP long-term pavement performance (LTPP) study sites. Both static and dynamic methods of measuring transverse profile and rut depth were evaluated. Static procedures that were considered included rod and level, string line, long straightedge, short straightedge, and Face Dipstick® device. Dynamic methods included sensor systems (both ultrasonic and laser) and 35-mm photography systems. The 35-mm photography systems project a line onto and across the pavement surface. This line, which assumes the pavement's transverse profile, is then photographed. Using the film record of the transverse profile, selected coordinates along the line are analyzed by a computer that simulates stretching a wire across the high points of the transverse profile. Rutting is determined by measuring the difference in elevation (perpendicular to the wire) between the wire and pavement surface. Figure 2-1 illustrates the procedure. This method is commonly termed the "wire method" of analysis. A commercially available system for rutting analysis was used by SHRP on LTPP study sites. On the basis of their research, Gramling et al. suggested that transverse profiles, rather than simple rut depths, be measured and that the wire method be used as a standard for reporting rut depths using analysis of the transverse profiles. They also identified several benefits associated with transverse surface profile measurements. They stated the following:

> Transverse profiles can provide the shape, depth, and lateral location of longitudinal pavement deformations. From the

transverse profile, an estimate of the actual rutting mechanism that is useful in selecting corrective actions can be made. The type of rutting observed on the transverse profile can provide information helpful in selecting rehabilitation methods. If rutting appears to be mostly consolidation and shear, then added structural strength might be needed and a heavier overlay used. If rutting appears to be primarily from lateral distortion, then rehabilitation by milling or leveling, with a new wearing course, or by recycling the surface might be appropriate. This information can be used in determining the causes of the deformations and in determining quantities of leveling, milling, or grinding required to correct deformations [13].

Unfortunately, Gramling et al. provided no data to illustrate these statements. However, their publication does provide definitions of rut depths that will be used later in this report.

In the mid-1970s, a limited investigation was conducted in Oklahoma with the primary objectives of investigating rutting on high-quality flexible pavements and detecting, if possible, evidence of the contribution of bituminous-bound pavement materials to permanent deformation failures [14]. A "transverse profile gauge" was developed and used to plot transverse surface profiles of pavement sections considered in the research. Heaving, or upward displacement adjacent to ruts, was considered an indication of outward or lateral creep of the material from beneath the wheel paths. Stereographic photogrammetry was used to obtain quantitative estimates of differential rutting in wheel paths. Visual pavement surface condition ratings were also obtained.

Sixteen field sites selected along Interstates 35 and 40 were considered in this 1970s research. Four base course material types were present within the 16 selected sites. They included hot mix sand asphalt (HMSA), soil-cement base (SCB), stabilized aggregate base course (SABC), and black base (BB). Each of the 4 base course types was present in the structure of 4 of the 16 selected sites. The effort did not directly address the influence or contributions of subgrade and unbound base materials to rutting.

After rutting measurements were obtained, cores were extracted from each of the sites and subdivided into surface course; leveling course; and upper, middle, and bottom thirds of the bound base course. Densities of the respective subdivisions were determined. Significant differences in densities between materials in the wheel paths and outside the wheel paths were considered evidence of differential densification. Table 2-1 summarizes the performance measures and density data and estimates the contribution of rutting due to densification, surface wear, lateral creep, and base or subgrade deformation. It is important to note that rutting measurements were made only once, after 36–169 months of service. Conclusions drawn by the authors of this early study included the following:

- HMA densification contributed significantly to total surface rut depths;
- Lateral creep (i.e., upheaval due to shear failure in the HMA), identified from transverse surface profiles, was predominate in the absence of base and subgrade deformation; and
- Surface subsidence, indicated by the transverse profiles (with the absence of lateral creep), was observed at sites where base and subgrade deformations influenced the magnitude of rutting.

This early work showed the potential for transverse surface profiles to indicate the layers primarily responsible for flexible pavement rutting.

Significant rutting occurred in a major coal haul road in eastern Kentucky. As a result, a forensic analysis of the pavement was conducted [15]. The pavement consisted of a 25-mm (1-in.) HMA wearing surface and a 300-mm (12-in.) large-stone HMA base course. The base course was placed on a 100-mm (4-in.) open-graded drainage layer, which was placed on a 100-mm (4-in.) dense-graded aggregate base that rested on the natural subgrade soil. The pavement carried approximately

TABLE 2-1 Modal contributions to rutting

Site	Base Course Type	Age (Months)	Maximum Rut Depth (mm)	Estimated Contribution to Rut Depth (%)			
				Densification	Surface Wear	Lateral Creep	Base or Subgrade Deformation
10	HMSA	36	25.15	28	2	70	-
60	HMSA	169	10.90	40	5	55	-
70	HMSA	169	14.58	40	5	55	-
120	HMSA	105	9.65	42	8	50	-
20	BB	82	14.50	58	12	30	-
30	BB	56	15.42	25	2	-	73
40	BB	56	16.33	22	2	-	76
50	BB	86	19.96	8	2	-	90
80	SABC	165	14.50	9	5	-	86
90	SABC	165	15.88	9	13	-	78
100	SABC	156	15.42	18	5	-	77
110	SABC	156	12.24	20	6	-	74
130	SCB	148	5.56	43	8	49	-
140	SCB	148	7.34	30	5	65	-
170	SCB	169	12.70	14	8	78	-
180	SCB	169	12.14	25	6	69	-

4 million equivalent single axle loads (ESALs) annually. After 2 years in service, rut depths of 30–46 mm (1.2–1.8 in.) were observed on steep uphill grades where loaded trucks traveled at low speeds. Among other things, the forensic study incorporated a transverse surface profile at one location; coring at the pavement centerline, in each wheel path, and between the wheel paths; and a trench. Figure 2-2 shows the thickness of the HMA materials based on the cores, and Figure 2-3 shows the transverse surface profile measured at the same location. It is clear from Figure 2-2 that the top 100 mm (4 in.) of the large-stone HMA consolidated significantly in the wheel paths. However, the transverse surface profile does not show significant upheaval along the edge of the wheel paths. Further investigation revealed inadequate stone-to-stone contact in the large-stone HMA and a significant reduction in air voids in the top 100 mm (4 in.) of the mix. The rutting was primarily due to consolidation rather than shear failure. The transverse profile reflects a base failure rather than a near surface failure in the HMA.

Several literature sources [5, 16, 17] reported findings of the NCAT study. This study included 42 pavements from all regions (i.e., 14 states) of the United States. The pavements represented various climatic zones and aggregates of differing origins and angularity. The pavements also involved different specifying agencies and construction practices. The objectives of the NCAT study were to identify material properties and mix design parameters that affected rutting, to provide information necessary to produce HMA mixtures that would perform satisfactorily, and to provide information to identify mixes with a tendency to rut under heavy traffic and loads. Oteng-Seifah and Manke [14] state the following:

> One of the criteria for selection of asphalt pavements to be evaluated in this study was that rutting was the result of an asphalt mix problem and not a result of subgrade or base problems. Hence, pavements were selected for investigation in which it appeared that rutting had occurred in the various layers of asphalt.

This statement implies that sites could be selected from a visual inspection of the pavement surface.

Extensive field, laboratory, and analysis plans were associated with the study. The field-testing operations included extraction of 12 cores across the traffic lane, rut depth measurements, and trenching. Rut depth measurements were made using a 3.6-m (12-ft) level, elevated straightedge. The distance from the straightedge to the pavement surface was measured at 0.3-m (1-ft) transverse intervals over the proposed coring locations. These data constituted a rough transverse surface profile. The profile and the lift thickness determined from cores were used to estimate the amount of rutting that occurred in each pavement layer or, in other words, quantify where in the structure the rutting had occurred. Figures 2-4 and 2-5 are example plots of such data. The plots clearly show upheaval along the sides of the wheel paths even though the transverse distance between measurements is quite large. Visual inspection in trenches indicated that the majority of rutting was occurring in the top 75–100 mm (3–4 in.) of the pavements and that the amount of rutting in base courses was insignificant.

In 1987, the City of Lethbridge, Alberta, Canada, initiated a study of premature rutting in asphalt concrete pavements within its arterial street system. The study addressed causes of the rutting and means of mitigating future rutting [18]. The authors state that three types of ruts can develop in asphalt concrete pavements. Figure 2-6 depicts the three types, which consist of the following: (1) wear rutting, which is due to progressive loss of coated aggregate particles from the pavement surface and which is caused by combined environmental and traffic influences (the rate at which wear rutting develops may be accelerated when winter ice control abrasives [i.e., sand] accumulate); (2) structural rutting, which is due to the permanent vertical deformation of the pavement structure under repeated traffic loads and which is essentially a reflection of permanent deformation within the subgrade; and (3) instability rutting, which is due to lateral displacement of material within the pavement layer and which occurs within the wheel paths (instability rutting occurs when the structural properties of the compacted pavement are inadequate to resist the stresses imposed upon the pavement, particularly by frequent repetitions of high axle loads). The following observations were made from distress surveys: (1) modest to severe rutting typically existed over several blocks in length, and a preponderance of severe rutting existed on the deceleration side of signal-controlled intersections; (2) at bus bays, severe rutting existed, but with little wear rutting; and (3) a substantial portion of the rutting resulted from mixture instability, but some of the rutting could have been due to mixture instability, structural inadequacy, or both. In order to differentiate positively between structural and mixture instability rutting, trenches were excavated at 11 sites. The trenches revealed that essentially all of the rutting at each site was confined to the HMA surface layer (i.e., instability rutting). Trenching locations at bus bays, where extreme distortions were observed, provided an interesting observation: the alignment of the aggregate particles on the vertically sawed faces of the pavement demonstrated that shear failure had occurred within the pavement layer. The authors have made similar observations at Wes-Track and other field sites.

The City of Lethbridge, Alberta, Canada, concluded that materials other than HMA might be necessary for pavements used to construct bus bays and proposed refinements to its material and mix design specifications. Using the proposed refinements, the city built full-scale test sections to evaluate the recommendations. At the time of publication, only early performance data were available, but these results indicated that much of the rutting problem would be alleviated with the proposed specification changes.

In the late 1980s, Lenngren at the Royal Institute of Technology in Sweden [19] analyzed multiple longitudinal and transverse surface profiles. The objective of the analysis was to determine whether the cause of rutting could be ascertained from statistics associated with the profiles. Knowing the cause,

appropriate maintenance actions could be recommended. It was known that studded tire wear contributed significantly to rutting in Sweden at the time. Lenngren suggested that variation of rut depth in the longitudinal direction, extracted from multiple transverse profile measurements along a roadway, could be used because studded tire wear should be lengthwise more uniform than deformations due to inadequate structural capacity. The basis for Lenngren's hypothesis relied on his statement that "ruts caused by studded tire wear are directly related to the number of studded tires passing on the section." Figure 2-7 was presented in his work to illustrate this point.

Lenngren plotted frequency distributions from rut depths measured every meter over 100-m-long sections. Figures 2-8 and 2-9 are example frequency distributions for low-volume (i.e., thin-HMA-surface) and high-volume (i.e., thick-HMA-surface) facilities, respectively. The following interpretations were provided relative to the figures. For Figure 2-8, Lenngren suggested that if rutting resulted from deformations occurring deep in the pavement structure, a relatively thin HMA might sustain a certain degree of deformation, after which degree cracking would be exhibited, giving way to even greater deformation. A frequency distribution of rut depth would then show two maximums: one for the uncracked portion and one for the areas with thoroughly propagated cracks.

If the process had been allowed to continue, severe fatigue cracking would have occurred and the HMA would no longer have been able to provide load distribution over the underlying layers. If this situation had been the case, a third group of ruts might have been agglomerated around a still deeper rut depth value, as illustrated in Figure 2-8. Lenngren did recognize that a thorough understanding of the consistency of the structure would be required in order to form such an interpretation. He also acknowledged the temperature dependency of HMA and suggested that variation could occur because of shadows over portions of a roadway, in addition to differences in materials within the structure. Figure 2-9 is an example from a high-volume facility with a thick HMA layer (300 mm [11.8 in.]), which did not exhibit any cracking. The average rut depth is large, approximately 25 mm (1 in.), but does not vary greatly. The rutting was primarily due to studded tire wear.

The variance (i.e., square of deviations from the mean), skewness (i.e., asymmetry of the distribution), and kurtosis (i.e., peakedness of the distribution) of such distributions were examined, and the data showed that a low-volume facility with a thin HMA pavement yielded high variance and skewness, but low kurtosis. High-volume facilities with thick HMA pavements yielded more symmetrical distributions, or less skewness. On the basis of the analyses, Lenngren suggested that the statistics could be useful in determining criteria for overlay and maintenance activities, especially for thin pavements. It must be noted that there is potential for fallacy in the interpretations provided.

For example, a distribution such as that presented in Figure 2-8 could be obtained for thick pavement under heavy loading (i.e., traffic) conditions, as well as a thin pavement under light loading conditions. Furthermore, distributions such as the one presented in Figure 2-9 could also be observed for structural failure as long as the structural section was consistent throughout the length of the pavement. Figure 2-6 Cases A and B are examples of such rutting.

Lenngren also analyzed transverse surface profiles directly attempting to distinguish studded tire wear from load-related deformations. He considered the width and distance between ruts. He felt that deformations were typically caused by heavily loaded commercial vehicles with tire configurations that differed from passenger cars with studs (namely dual versus single tire and width). Because commercial vehicles are wider than passenger cars, the outer distance from tire wall to tire wall is greater. The inner distance from tire wall to tire wall is about the same as for passenger cars. To determine if vehicle type could be associated with the ruts, Lenngren measured the mean distance between tires and compared these distances with the distance between the ruts. He assumed that a rut would be deepest in the center if it were due to the same type of vehicle. However, when typical traffic distributions and vehicle wander were considered, he recognized that this approach could lead to erroneous conclusions.

At that point, Lenngren closely examined the worn or depressed area of individual wheel paths, looking for a better indication of the cause. He determined the distance, transverse to the direction of traffic, between points where each rut profile area was divided into two equal halves. Figure 2-10 illustrates this distance (note that Areas A1 and A2 are equal, as are Areas A3 and A4). In other words, the vertical line separating a pair of areas does not necessarily coincide with the total width of the wheel path divided by two. The location of the line is determined by locating it such that equal areas are observed on each side of it. Lenngren then defined the horizontal distance between the two vertical lines separating the pairs of areas as the "gauge" and said that this distance was equal to the distance between ruts. He assumed that the gauge would indicate the vehicle type predominately causing the rutting. Again, when typical traffic distributions and vehicle wander were considered, he recognized that this approach could also lead to erroneous conclusions.

Lenngren then compared transverse profiles from lanes dominated by passenger cars and slow-moving heavy traffic (e.g., commercial trucks). Figures 2-11 and 2-12 show example profiles. Lenngren noted that the commercial vehicles resulted in wider ruts than ruts due to studded tire wear for the same total rut profile area. Figure 2-13 illustrates this rut width. Lenngren further noted that ruts due to deep-lying deformations were even wider for the same total rut profile area.

On the basis of these analyses, Lenngren suggested that quantifying transverse profile measurements presented a potential method of determining the cause of rutting in the absence of traffic, structural, and environmental data. However, he did acknowledge that typical traffic and vehicle wander distributions could lead to erroneous conclusions.

TABLE 2-2 Rutting origin sorting criteria

Hypothesized Rutting Mode or Type	Total Distortion (mm^2)	Ratio of Distortion (Positive/Negative)	Number of Sections
Subgrade	< -4500	< 0.4	61
Base	-4500 <x< 700	0.4 <x< 1.25	24
Surface	700 <x< 5000	1.25 <x< 3.0	15
Heave	>5000	>3.0	28

In 1995, Simpson et al. [20] hypothesized that the area under the transverse surface profile could be used to predict the source of rutting from within the pavement structure. Simpson et al. wanted to distribute a large data set into subsets using a profile characteristic that isolated the cause of rutting (i.e., rutting mode) in an effort to develop and refine rutting prediction models.

Simpson et al. placed transverse surface profiles of rutted pavements in four general categories: subgrade rutting, base rutting, surface course rutting, and heave. Figure 2-14 presents the shape of the transverse surface profile associated with each category. Simpson et al. sited elastic theory, both Boussinesq and Burmister, as the basis for the profile shapes. This work suggests that one should be able to establish weaknesses in a pavement structure on the basis of the shape and dimensions of deformations at the pavement surface. Unfortunately, Simpson et al. provide no details as to the generation of the profiles (e.g., assumed structures, loading conditions, material properties, and vehicle wander) presented in Figure 2-14. It is simply assumed that plastic deformation follows a trend similar to that of elastic deformation.

In the study by Simpson et al., 134 transverse surface profiles were obtained from LTPP General Pavement Studies (GPS) Experiments 1 and 2. The algebraic area between the transverse profile and the straight line connecting its end points was calculated to identify into which of the four categories the various transverse profiles fit. Area above the straight line connecting the profile end points was considered to be positive, and area below the line was considered to be negative. It is clear from Figure 2-14 that sections within the subgrade category would be entirely negative and sections within the heave category would be entirely positive. Distinguishing between base and surface rutting, which involved both positive and negative area, was handled using the general perception that marginally positive areas would be considered surface rutting and marginally negative areas would be considered base rutting.

Two criteria were ultimately used to hypothesize the origin of the rutting. They were total area, which was termed "distortion," and the ratio of positive to negative area, which was termed "ratio of distortion." Ranges of the two criteria were established, and each of the LTPP GPS profiles was classified on that basis. Table 2-2 summarizes the criteria, criteria ranges, hypothesized rutting mode, and number of LTPP GPS sections that fit within each category. Six of the sections did not fit within the dual criteria and were excluded from the database used for performance-modeling efforts.

Neural-network modeling techniques were employed to develop performance relationships. Five models were developed. One was developed for the entire data set (without distribution into the categories). Then a model was developed for each category using the data after distribution into the categories. The models were then compared with a model developed under SHRP Contract P-020 using the same data set (i.e., entire data set) and regression techniques. Table 2-3 presents the results of the comparison.

The models developed by Simpson et al. were all excellent. Table 2-4 provides a summary of independent variables that were significant in each model developed using the neural networks technique. The independent variable sets for each of the models are oriented toward the rutting mode noted. This orientation suggests that the models appear to be appropriate not only from a statistical standpoint, but also from an engineering standpoint.

Simpson studied the characterization of pavement transverse surface profiles [11]. In this study, Simpson examined 10 potential characterizations (i.e., indexes). They were

- Area of rutting below and area of pavement above a straight line connecting the profile end points;
- Area between the pavement surface and a series of straight lines connecting the peak points on the pavement surface;

TABLE 2-3 Performance model comparison

Data Set	R^2	RMSE	Model Type
P-020 (Entire Data Set)	45%	0.18	Regression
Entire Data Set	82%	0.07	Neural Networks
Subgrade Rutting Data Set	94%	0.05	Neural Networks
Base Rutting Data Set	90%	0.04	Neural Networks
Surface Rutting Data Set	98%	0.02	Neural Networks
Heave Rutting Data Set	96%	0.02	Neural Networks

TABLE 2-4 Significant independent variable sets associated with each model

Model	Independent Variables
Entire Data Set	HMA thickness, air voids, viscosity @ 60ºC, annual precipitation, avg. no. of days>32.ºC, avg. freeze thaw cycles, PI, subgrade moisture, subgrade p0.075mm, base thickness, log (Cumm KESALs)
Subgrade Rutting Data Set	Annual precipitation, avg. no. of days>32.ºC, avg. freeze thaw cycles, PI, subgrade moisture, subgrade p0.075mm, base thickness, log (Cumm KESALs)
Base Rutting Data Set	Annual precipitation, avg. no. of days>32.ºC, base thickness, base compaction, log (Cumm KESALs)
Surface Rutting Data Set	HMA thickness, asphalt content, air voids, viscosity @ 60ºC, HMA aggregate <4.75mm, annual precipitation, avg. no. of days>32.ºC, log (Cumm KESALs)
Heave Rutting Data Set	Annual precipitation, avg. freeze thaw cycles, PI, subgrade moisture, subgrade p0.075mm, log (Cumm KESALs)

- Maximum vertical distance for each wheel path between a 1.2-m (4-ft) straightedge and the pavement surface below the straightedge in each wheel path;
- Maximum vertical distance for each wheel path between a 1.8-m (6-ft) straightedge and the pavement surface below the straightedge in each wheel path;
- Maximum depth of the outside wheel path between a horizontal line from the edge of the pavement and the pavement surface (i.e., the depth of water that may accumulate before drainage onto the shoulder);
- Maximum depth of the inside wheel path between a horizontal line from the maximum elevation between the wheel paths and the pavement surface (i.e., the maximum depth of water that may accumulate before drainage into the outside wheel path, assuming elevations in an adjacent lane greater than the maximum depth between wheel paths);
- Maximum vertical distance between a 3.7-m (12-ft) string line stretched across the lane and the pavement surface;
- Width of rut using a 3.7-m (12-ft) string line;
- Radius of curvature of deformation; and
- Parallel Symbolic Computation (PASCO) typecasting.

After individually examining each of these options, Indexes 3, 6, 9, and 10 were removed from the list of recommendations included in the National Information Management System (NIMS). Index 3, which uses a 1.2-m (4-ft) straightedge, is generally considered an unreliable measurement. Index 6, which uses the maximum water depth in each wheel path, directly relates to the safety issue of hydroplaning and is easily understood. This index would not have been removed from the list had the longitudinal variability not greatly affected the level of water held on the pavement surface.

After removal of the four indexes, Simpson performed a correlation analysis on those indexes remaining. The result shows that rut depth (Indexes 4 and 7), negative area (Index 1), and fill area (Index 2) have relatively high correlations, which means that they measure the same properties. However, indexes for rut depth have a poor correlation with Index 8, which is the rut width given by a 3.7-m (12-ft) string line.

Brown and Gibb [21] conducted experiments at the Nottingham Pavement Test Facility (PTF) to assess the results of repeated load uniaxial compression and small-scale wheel tracking tests on cores and slabs taken from small-scale test pavements. The objective was to determine whether the laboratory tests could correctly rank the rutting performance observed in the small-scale test pavements. The rutting tests performed at the Nottingham PTF were part of the SHRP A003A contract. In these tests, four combinations of two aggregates and two binders were tested. Mixtures included gravel and crushed granite aggregate blended with a neat 100-penetration binder and with a styrene-butadiene rubber (SBR) modified binder. The pavement structure tested consisted of 100 mm (4 in.) of HMA placed over 200 mm (8 in.) of crushed aggregate base that rested on a silty clay subgrade. The PTF is a not a full-scale APT facility, as Figure 2-15 shows. For the testing described, a single wheel load of 10 kN (2,250 lb) was employed, with a tire inflation pressure of 620 kPa (90 psi). The test sections were trafficked in only one direction at a speed of 4 km/h (2.5 mph), at a test temperature of 30°C (86°F), and no transverse wheel wander was used. Transverse surface profile measurements were made several times during a test. Figure 2-16 presents profiles measured at the completion of the tests. Although the quality of the published figure makes it difficult to read, mixtures containing the modified binder (i.e., Sections B and D) clearly show superior performance. More importantly, the profiles are consistent with those presented by others in the literature where significant upheaval is observed along the sides of the wheel paths when shear failure has occurred in the HMA surface layer. It is important to note that the vertical scales are not consistent for all the plots in Figure 2-16. Strain measurements in the base course indicated that only 2 mm (0.08 in.) of the total rut depths were due to permanent deformation in the base course layer.

An FHWA-sponsored study is currently underway at the U.S. Army Corps of Engineers Cold Regions Research and Engineering Laboratory (CRREL) with a primary objective of developing pavement subgrade failure criteria as a function of soil type and moisture content [22]. Full-scale pavement test sections are being constructed and subjected to loading with a Mark IV Heavy Vehicle Simulator (HVS). Researchers will test several soil types over a range of moisture content and density levels, in addition to a range of load levels. Two soils have already been tested at two moisture contents and several load

levels. The test results on one soil are available. These test sections, referred to as "Windows" by the author, were constructed with the same materials and layer thickness. Figure 2-17 shows a plan view of the test sections, or "Windows." Each test section consists of 76 mm (3 in.) of HMA placed on 229 mm (9 in.) of crushed gravel base that rests on 3 m (10 ft) of silty gravel subgrade (AASHTO A-2-4). Figure 2-18 depicts the structural section. Each test section is instrumented at seven levels. Figures 2-19 and 2-18 show the instrumentation plan and levels, respectively. Load levels applied to the four different test sections with the HVS were 78 kN, 85 kN, 89 kN, and 102 kN (17,500 lb; 19,100 lb; 20,000 lb; and 22,900 lb). Loading was bidirectional, with a standard dual-wheel configuration and tire pressure of 690 kPa (100 psi). Transverse wheel wander was applied over a width of 0.9 m (3 ft). Tests were continued until rut depths of 12.5 mm (0.5 in.) developed. In addition to collecting data from the instrumentation throughout the loading, transverse surface profiles were measured with a laser profilometer. When tests were terminated, test pits were excavated and visual inspections were made. Unfortunately, transverse profiles were not reported. Most of the accumulated permanent strain occurred in the base and at the top of the subgrade (i.e., 70 percent occurred in the subgrade and more than 20 percent occurred in the base). The remainder (less than 10 percent) occurred in the HMA. Because transverse profiles were not published, one of the authors was contacted, and he indicated that there was an absence of upheaval along the sides of the wheel path. This observation is consistent with the previously discussed literature.

Two South African HVS devices are being used by the California Department of Transportation in its Accelerated Pavement Testing (CAL/APT) program [23–25]. The CAL/APT program is a 5-year, multimillion-dollar, research-and-development program jointly being conducted by the California Department of Transportation (Caltrans), the University of California at Berkeley, the Division of Roads and Transport Technology of the Council of Scientific and Industrial Research (CSIR) (in South Africa), and Dynatest Consulting Incorporated. The research program includes not only accelerated pavement testing, but also laboratory material testing, pavement design and analysis, and implementation components. Significant testing of HMA pavements has been conducted in the last 5 years as part of this program. The focus has been on HMA pavement fatigue performance, but significant data on rutting performance have also been collected.

Rutting-related studies have included the effects of channelized traffic that would occur with automated vehicle control systems (AVCS), a comparison of dense-graded HMA and gap-graded asphalt rubber mixes, and a comparison of asphalt-treated permeable base (ATPB) mixes and conventional aggregate base. Transverse surface profile measurements were used to evaluate rutting performance. The findings of the CAL/APT program are similar to other APT-related research relative to transverse surface profile and the contribution of pavement layers to rutting. Specifically, the transverse surface profiles reveal significant upheaval along the wheel paths when rutting occurs in the HMA surface mixture; such rutting is typically confined to the top 75 mm (3 in.) of the HMA. Figure 2-20 is an example of transverse profiles measured on a CAL/APT HVS test of HMA where transverse wander was employed.

The Texas Department of Transportation (TxDOT) has implemented an APT program with the following objectives: (1) select rehabilitation strategies, (2) improve design equations, (3) evaluate new materials and construction techniques, and (4) study the effects of truck configurations on pavement [26, 27]. TxDOT is using TxMLS, which is a mobile testing device. The TxMLS incorporates six bogie carriages with tandem axles and suspension systems, loaded to the legal limit in Texas of 151 kN (34,000 lb). Transverse wheel wander of 1.04 m (41 in.) is used during loading [28]. Figure 2-21 schematically depicts the TxMLS.

Data collected from a flexible pavement test pad located in TxDOT's Yoakum District were tested and analyzed. The structural section consisted of 75 mm (3 in.) of HMA placed on 300 mm (12 in.) of lime-treated gravel base (LTGB) placed on 150 mm (6 in.) of lime-stabilized subgrade. Figure 2-22 depicts the loaded area of the test pad. After 630,000 axle repetitions were applied, the test was terminated. Transverse surface profile measurements were made at several intervals during the test. Trenches were excavated at the completion of the test. Figure 2-23 presents transverse profiles measured at 4.5 m and 6.3 m (14.8 ft and 20.7 ft) from the end of the test section. The significant difference in rut depths between the left and right wheel paths shown in the figure was investigated. It was determined that dry density was highest and moisture content was lowest in the right wheel path. Deflection testing prior to the initiation of TxMLS loading also indicated greater stiffness in the right wheel path. Figure 2-24 presents profiles of all layer interfaces that were measured at the face of the trench walls. Chen et al. [26] refer to Figure 2-24 and state that profile data show information about the layer thickness after trafficking and can be used to study layer contributions to rutting. Table 2-5 presents layer thickness and summary statistics. The data in Table 2-5 show that as depth increases, variability in thickness increases, as indicated by increasing standard deviation and coefficient of variation values. From Figure 2-24 and the data in Table 2-5, it was determined that there was no permanent deformation in the HMA. It was also determined that more than 50 percent of the rutting occurred in the 300-mm (12-in.)-thick lime-treated base (LTB). The accuracy of the transverse surface profile measurements was verified using a straightedge, and it was determined that there was up to 2 mm (0.08 in.) of error in the data that was due to inaccuracy of the measuring systems. The transverse surface profiles do not show any upheaval at the edge of the wheel paths, which is consistent with previously reviewed literature.

A study on rut-depth measurement was conducted by TxDOT [29] on Farm to Market (FM) 600, FM 922, FM 970, US 281, I 20, I 10, US 77, and State Highway (SH) 34. The rut

TABLE 2-5 Average pavement layer thickness

	Trench Wall Location					
	4.5 m			6.3 m		
	HMA (mm)	LTB (mm)	LTS (mm)	HMA (mm)	LTB (mm)	LTS (mm)
Average	75.33	284.09	112.33	71.90	275.51	74.08
Standard	5.77	22.97	31.95	3.98	25.04	17.08
Coefficient of Variation	7.66	8.09	28.44	5.54	9.09	23.06

depths were measured transversely using the following seven measurement spacings: 25 mm (1 in.), 50 mm (2 in.), 100 mm (4 in.), 150 mm (6 in.), 200 mm (8 in.), 305 mm (12 in.), and 610 mm (24 in.). The string line method was used to determine the rut depth for all spacings. For purpose of analysis, the 25-mm (1-in.) measurement spacing was considered to give 100-percent accuracy; the accuracy for all other spacings was then determined by comparison to the rut depth at 25-mm (1-in.) measurement spacing. The average accuracies were taken over the six profiles and had values of 97 percent, 95 percent, 89 percent, 90 percent, 80 percent, and 68 percent for spacings of 50 mm (2 in.), 100 mm (4 in.), 150 mm (6 in.), 200 mm (8 in.), 305 mm (12 in.), and 610 mm (24 in.), respectively. On the basis of the results, 100-mm (4-in.) measurement spacing was suggested for use in measuring field data.

The FHWA has conducted pavement performance tests over the last 13 years using its Accelerated Loading Facility (ALF) pavement test machines [30, 31]. An ALF device consists of a moving half-axle wheel assembly housed in a 29-m (95-ft)-long steel frame. Loads ranging from 45 kN to 100 kN (10,000–22,500 lb) can be applied while the wheel assembly travels at 18.5 km/h (11.5 mph). Unidirectional trafficking with or without transverse wander may be applied with the device. The devices are mobile and have been used to perform tests of in-service pavements. However, more extensive testing has been conducted at the permanent pavement-testing laboratory, the Pavement Testing Facility (PTF), located at the FHWA Turner Fairbanks Highway Research Center (TFHRC). Figure 2-25 shows a plan view of 48 individual test sites currently at the PTF. Several pavement research projects have been conducted since the FHWA accelerated pavement test program was established. The effectiveness of accelerated pavement testing has been clearly demonstrated through these pavement-performance and pavement-response studies.

A study conducted at the PTF focused on initial validation of some of the SHRP asphalt research program findings. The research emphasized the effect of binder properties on rutting and fatigue cracking in flexible pavements and had the following objectives [31]:

> (1) Confirm that the binder properties identified by the SHRP research as determinants of pavement performance do significantly affect pavement performance; (2) verify the performance prediction capability of the proposed Superpave accelerated laboratory mixture tests; and (3) provide controlled loading performance data that can be used in the validation of the pavement performance models in Superpave.

The research comprises full-scale APT tests, laboratory binder and mixture testing, and comparisons of predicted and observed performance. Twelve test lanes with four test sites per lane (48 individual test sites) were constructed at the PTF using binders expected to be associated with a range of rutting and fatigue performance based on Superpave binder test results. Table 2-6 presents the combinations of binder grades, mixture types, and structural layer thickness of the test sites. The SM-3 mixture is a 19.0-mm (0.75-in.) nominal maximum aggregate size mixture with an asphalt content of 4.8 percent. The BM-3 mixture is a 37.5-mm (1.5-in.) nominal

TABLE 2-6 FHWA ALF Superpave validation study pavements [25]

Lane Number	Binder Grade	Mixture Type	HMA Thickness (mm)	Base Thickness (mm)	Subgrade Thickness (mm)
1	PG58-34	SM-3B	102	559	610
2	PG64-22	SM-3B	102	559	610
3	PG58-34	SM-3B	204	457	610
4	PG64-22	SM-3B	204	457	610
5	PG58-28	SM-3B	204	457	610
6	PG64-22	SM-3B	204	457	610
7	PG82-22*	SM-3B	204	457	610
8	PG76-22*	SM-3B	204	457	610
9	PG58-34	SM-3B	204	457	610
10	PG64-22	SM-3B	204	457	610
11	PG58-34	BM-3	204	457	610
12	PG64-22	BM-3	204	457	610

* Modified binders.

maximum aggregate size mixture with an asphalt content of 4.0 percent.

In addition to other efforts, the validity of Superpave binder specification parameters is being directly assessed on the basis of the ALF and Superpave binder tests conducted over a range of temperatures. For the rutting portion of the study, Test Lanes 5–8 identified in Figure 2-25 and Table 2-6 were tested. The rest of the lanes were used for the fatigue portion of the study. In the rutting study, the ALF loading consisted of a 44.5-kN (10,000-lb) load on a wide-based single tire inflated to 689 kPa (100 psi). Transverse wheel wander loading was not employed. In the fatigue study, a load of 53 kN (11,900 lb) was used with the same tire, but transverse wheel wander of 1.1 m (45 in.) was incorporated.

Transverse surface profiles have been collected during ALF tests since 1986. These profiles are measured with a semiautomatic surface profiler developed by researchers at the PTF. A multilayer deflectometer was also used to measure vertical compressive strains and rutting in each pavement layer for the Superpave validation study. Figure 2-26 is an example of selected transverse surface profiles generated as part of the rutting study at a test temperature of 58°C. Bonaquist et al. [30] noted that even though a relatively thick HMA layer was used to minimize rutting in the supporting layers, significant rutting did occur at the top of the base course. The result was associated with the high test temperature. Bonaquist et al. also noted that at the temperatures used in the rutting tests, the lanes with unmodified binders showed significant upheaval along the wheel paths, but lanes with the modified binders showed very little upheaval. Figure 2-26 illustrates lack of upheaval, where a modified binder was used. This finding is inconsistent with other reviewed literature. The research team also noted that cracks formed parallel to the wheel path in this mixture after the total pavement rut depth reached approximately 25 mm (1 in.). The cracking was associated with tensile strains at the pavement surface in the region of high curvature just outside the loaded area. The research team further suggested that the cracking was the result of deep rutting caused by the high pavement temperatures and the lack of lateral wander in the ALF loading. Such cracks would not be expected on typical in-service pavements.

The FHWA provided transverse surface profile and multidepth deflectometer data from the fatigue portion of this study for use in the NCHRP 1-34A study. The fatigue data were obtained on the basis of the NCHRP 1-34A panel recommendation that only APT data generated with wheel wander be used for analyses.

On the basis of instrumentation data and observations in trenches at WesTrack, Epps et al. [12, 32] reported that shear deformation, rather than densification, is the primary rutting mechanism in HMA surface mixtures when reasonably stiff supporting layers are present. Rutting at WesTrack was confined entirely to the top 50–75 mm (2–3 in.) of the 150-mm (6-in.) HMA surface. WesTrack is the FHWA/NCHRP full-scale accelerated pavement test facility project located approximately 100 km (62.2 mi.) southeast of Reno, Nevada. The primary objectives of the project were to (1) continue the development of performance-related specifications (PRS) for HMA pavements by evaluating the impact on performance of deviations in materials and construction properties from design target values and (2) provide early field verification of the Superpave mix design method.

As originally constructed, the track consisted of 26 HMA test sections. The original test sections included both fine- and coarse-graded Superpave mixtures that incorporated a crushed-gravel source and a neat PG64-22 binder. Binder content, in-place air voids, and gradation (minus 0.075 mm [#200] only) were systematically varied among the test sections to simulate construction variability.

Approximately 4.7 million 80-kN (18,000-lb) ESALs were applied on the facility test section pavements as of June 1, 1998. Four autonomous (i.e., driverless) tractor/triple-trailer vehicles were used to apply the traffic. The vehicles consisted of a typical three-axle tractor/single-axle semi-trailer and two trailers, each with two single axles. The tractor steering axle carried 54 kN (12,000 lb), and all other axles carried 89 kN (20,000 lb), resulting in the application of 10.5 ESALs per vehicle pass. The 295/75R22.5 truck tires were inflated to 700 kPa (100 psi). Truck speed was constant at 64 km/h (40 mph). With the application of 2.8 million ESALs, excessive rutting and/or fatigue cracking forced the replacement of ten of the original test sections; eight of these sections were coarse-graded Superpave mixes [12]. It was initially hypothesized that the poor rutting performance was due to the partially crushed gravel used in the mixtures [33]. However, an extensive interlaboratory study revealed that the poor performance did not relate to the angularity of the coarse aggregate [34]. Eight of the replacement section mixtures were coarse-graded Superpave mixtures using a local crushed aggregate and a neat PG64-22 binder. As with the original test sections, researchers systematically varied binder content, in-place air voids, and gradation (minus 0.075 mm [#200] only) among the replacement test sections to simulate construction variability. The replacement mixtures performed worse than the original coarse-graded mixtures, with several of the replacement mixtures failing (rut depth ≥25 mm [1 in.]) after the application of only 0.58 million ESALs.

WesTrack pavement performance was monitored on a regular basis, and climatic data were collected with an LTPP weather station located on site. Longitudinal and transverse surface profiles, as well as Falling Weight Deflectometer (FWD) tests, were included in the performance-monitoring efforts. Additionally, two LTPP seasonal monitoring devices were used to measure pavement temperatures with depth and moisture contents in the base, engineered fill, and subgrade. Figure 2-27 is an example of a transverse profile measured at WesTrack using the laser profilometer. WesTrack transverse profile data were obtained with permission of the FHWA and NCHRP for use on NCHRP Project 1-34A. Transverse surface profiles measured at WesTrack are consistent with those

expected for shear failure in the HMA in that depressions existed in the wheel paths and considerable upheaval occurred along both sides of the wheel paths.

The WesTrack findings are also consistent with background discussed by Monismith et al. [6]. Monismith et al. discussed trenching studies at the AASHO Road Test, as well as other full-scale test tracks that indicated that shear deformation was the primary failure mechanism in HMA surface mixtures when stiff supporting layers were present. In such cases, the HMA surface layer permanent deformation was limited to the upper 100 mm (4 in.).

The shape of the transverse surface profiles measured at WesTrack is similar to shapes predicted by Weissman during and after SHRP while attempting to assess the effects of tire pressure, pavement thickness, and underlying support on relationships between maximum permanent shear strain and rut depth using finite element modeling (FEM) techniques [6, 35–37]. Unfortunately, only transverse profiles associated with two-layer systems containing very thick HMA layers and stiff underlying support were presented. Figure 2-28 is the two-dimensional finite element mesh representation of the pavement cross section modeled by Weissman. Note that the HMA thickness is 380 mm (15 in.) and the underlying support layer is considered to be a linear elastic material. Figure 2-29 represents the deformed mesh after a given loading duration. Figure 2-30 shows predicted surface profiles for different loading times and a contact stress of 3,450 kPa (500 psi). The surface profiles are simply the surface of the finite element mesh. Results shown in Figure 2-31 are based on a contact stress of 1,380 kPa (200 psi). These tire inflation pressures are not realistic for truck tires.

On the basis of his analysis of profiles generated using different material behavior assumptions, Weissman stated that there is a need to model nonlinear behavior of HMA if realistic profiles are to be predicted [35, 37]. In the SHRP-funded research, Weissman and others proposed the use of, and actually employed, a nonlinear visco-elastic constitutive relationship. Weissman found that when coefficients of the elastic parameters were set to zero in his constitutive model, he generated profiles that did not show upheaval at the edges of the tires. This finding was inconsistent with field-observed profiles and, thus, the basis for his reasoning. It is well established that HMA behavior, at the temperatures at which rutting occurs, is nonlinear visco-elastic. There is a plethora of physical and theoretical evidence of this established phenomenon in the literature [38–47].

In an initial effort to determine minimum crushed aggregate requirements necessary to provide satisfactory rutting performance of HMA surface mixtures in Indiana, Purdue University designed, built, and continues to operate a full-scale APT facility for INDOT [48, 49]. The facility has been fully operational since 1992, and it has a history of successful research focusing on HMA rutting phenomenon. The APT is capable of applying up to an 89-kN (20,000-lb) load on a dual or super-single wheel assembly at 8.3 km/h (5 mph). Traffic can be applied with or without wheel wander. When wander is required, the wheel path is randomly selected to achieve a normal distribution over a total width of 260 mm (10.2 in.) [50, 51]. Traffic can be applied in one or two directions, but one-directional traffic is typically employed.

Approximately 85 percent of the roadways owned by INDOT are composite (Portland cement concrete overlaid with HMA) pavements [52]. As a result, tests in previous studies in the APT facility were initiated with asphalt overlays constructed on a concrete slab. A pavement temperature conditioning system was developed that uses water pumped through hoses embedded in the concrete. Air heating/conditioning is also used to minimize air/pavement temperature differential. Tests can be conducted at pavement temperatures ranging from 20°C to 60°C (68–140°F). The test pit is 1.8 m (6 ft) deep, so it easily accommodates most typical pavement structural sections. Figure 2-32 is a schematic that illustrates the APT and pavement structure. Figure 2-33 is a picture of the APT device. Test sections are constructed using conventional production, placement, and compaction methods. Rutting is assessed after various load repetitions using a device developed to record transverse profiles. A profile measurement is made by lowering a small wheel onto the pavement surface and rolling it transversely across the test lane. Vertical and horizontal wheel position is measured with cable-based transducers and recorded on a PC-based data acquisition system. Software was written to automatically reduce and store the data in a spreadsheet.

In the minimum crushed aggregate study that initially used the APT facility, 27 sections were tested. Laboratory tests provided comprehensive information on mixture and constituent material properties. The effects of the percentage of crushed coarse aggregate and the ratio of natural to manufactured fines on the rutting performance of the mixtures was clearly established. A commercially available finite element program, ABAQUS, was used in this study to model the pavement structure and permanent deformation. An approximate approach was used to simulate the APT loading conditions. A creep model was used to represent the actual pavement rutting. On the basis of mixture performance in the APT, material constants in the creep model were back-calculated. Regression analyses were conducted to correlate these material constants with mixture physical properties. Excellent correlation was developed between measured and predicted rutting. Unfortunately, wheel wander was not employed in this study, so the data could not be used for NCHRP Project 1-34A.

As part of PSF 176 (“Validation of SHRP Asphalt Mixture Specifications Using Accelerated Testing,” recently completed at Purdue University), the effect of wheel wander on permanent deformation in HMA surface mixtures was assessed [47]. The finite element method was applied to model the rutting. The study focused on validation of various aggregate specifications and volumetric relationships established by Superpave. The work used the APT, laboratory wheel tracking, triaxial testing,

and Superpave shear tests. Mixtures having gradations above, through, and below the Superpave restricted zone were tested. Mixtures were tested with different coarse and fine aggregates. Data collected relative to the APT testing include asphalt layer temperature, transverse surface profile, and core properties in and out of the wheel path. Figure 2-34 shows the effect of wander on rutting in APT tests. It is clear from the figure that observed rutting is quite different for the three levels of wander (0, ±130 mm [±5.1 in.], and ±260 mm [±10.2 in.]). If loading is applied with dual wheels, single wheel path traffic produces significant uplift between and outside of the tires. The effect of wander is to substantially compress the uplift between the wheels. Figure 2-35 compares a measured surface profile with a surface profile predicted using the FEM simulation. Consistent with Weissman's recommendation and other work by White, a nonlinear material model was used in the FEM simulation. Because wander was incorporated in the loading of several test sections, the PFS 176 data were used for analysis in NCHRP Project 1-34A.

2.2 ANALYSIS OF LITERATURE

The literature review reinforces the fact that a relationship exists between transverse profile and location of rutting in the pavement layers. Prior and current research clearly document that the shapes of transverse surface profiles differ between failures in the HMA surface mixture and failures in the underlying support layers. When failure occurs in the HMA surface layer, depressions in the wheel paths are accompanied by upheaval along the sides of the wheel paths. When failure occurs in the supporting layers, there are depressions in the wheel paths, but upheaval along the sides of the wheel paths is minimal to none. These conditions were identified in the literature for both in-service and accelerated (i.e., APT) loading conditions. The literature does not provide a clear distinction as to the source of rutting among supporting layers (i.e., base versus subgrade). The work presented by Simpson et al. strongly suggests that the distinction can be made using an evaluation of more than 125 in-service pavements, 85 of which are represented as base and subgrade failures [20]. The data presented by Oteng-Seifah and Manke [14] were consistent with Simpson's evidence. There was an absence of data in the literature relative to heave.

2.3 THEORETICAL ANALYSIS

In accordance with the project work plan, limited theoretical analysis was conducted to define initial distortion parameters and criteria similar to those defined by Simpson. The purpose of this effort was to develop criteria that could be evaluated using available data from the literature and APT tests. If the criteria appeared to be reasonable on the basis of this evaluation, then extensive theoretical modeling and field data collection (i.e., trenching) efforts would be initiated. Five rutting failure modes were simulated. They included rutting due to failures in the HMA surface, base, subbase, and subgrade layers. The case of heave in the subgrade was also analyzed. The heave failure represents the conditions of frost heave, as well as heave due to expansive subgrade soils. Modeling techniques similar to those used in PFS 176 [53] were applied to assess the effects of wheel loads on typical structural sections. The predicted surface profiles are associated with material failure in specific layers of the structure.

The analysis incorporated typical low- and high-volume pavement structures. Finite element modeling techniques using the ABAQUS software and a nonlinear material model were employed. The analyses were two-dimensional simulations (four-node quadrilateral plane strain elements). Single-axle loads of 80 kN (18,000 lb) were assumed with uniform tire contact pressure of 620 kPa (90 psi) and normally distributed wheel wander. Pavement cross slope was not considered. The low-volume pavement structure consisted of 75 mm (3 in.) of HMA placed on 300 mm (12 in.) of unbound aggregate base over a silty-clay subgrade soil. The high-volume structure consisted of 150 mm (6 in.) of HMA, 300 mm (12 in.) of unbound aggregate base, and 300 mm (12 in.) of unbound aggregate subbase over the same silty-clay subgrade soil. Each of five potential failure modes was modeled to generate a range of rut depths approximately 5–25 mm (0.2–1.0 in.). There were two levels of rut depth for each rutting mode and pavement structure to obtain enough pooled data to initially define distortion criteria that would represent typical low- and high-volume pavement. These analyses required approximately 35 FEM computational runs. The reason that more than 20 computational runs (2 structures × 5 failure modes × 2 rut depth levels) were required is that rut depths are controlled not only by the structure and material models, but by the loading time as well. Loading time to achieve the desired rut depths had to be established by trial and error; thus, there were additional runs. Mesh optimization also required several runs. Complete details of this modeling effort are presented in Chapter 3.

Figures 2-36 through 2-40 represent predicted surface layer deformations (HMA layer mesh only) for each of the failure modes for the high-volume structure with equal loading times. An examination of the predicted deformations indicates they represent typical deformations observed in actual in-service pavements. Figure 2-41 shows a comparison of the predicted surface profiles associated with Figures 2-36 through 2-40. Recall that the upper boundary of the deformed surface mesh is equivalent to a transverse surface profile. The predicted deformations have been magnified for presentation in Figures 2-36 through 2-40. The predicted surface profiles are consistent with profiles observed for actual rutted pavements due to failures in the specific layers identified.

In order to obtain distortion parameters, the area between the original (i.e., unloaded) mesh surfaces and the deformed mesh surfaces was determined. It was calculated by integrating the areas, defined by the x- and y-coordinates of nodes of the deformed FEM mesh. Area above the original mesh sur-

face was considered to be positive, while area below the mesh surface was considered negative, as illustrated in Figure 2-42. The distortion parameters obtained from each FEM simulation are summarized in Table 2-7.

Data in Table 2-7 are pooled for both rutting levels and structures and shown in Table 2-8. Simpson's criteria are also presented in Table 2-8. The data indicate whether the parameters generated through the FEM simulations agreed with Simpson's criteria. In reviewing Simpson's criteria, one must remember that field investigations were not conducted to verify actual failure modes. Rather, Simpson's criteria were based simply on elastic theory and the assumption that plastic deformations follow trends similar to those of elastic deformations [20]. It is also important to recognize that only two structural sections were considered in the FEM simulations. The discussion that follows reviews the data in Table 2-8.

For both heave and subgrade failure modes, the FEM-generated data agree with Simpson's criteria. However, Simpson's criteria appear to be conservative for both cases when compared with the theoretical analysis. Simpson did not present criteria for the subbase failure mode. The FEM-generated data fall within Simpson's subgrade criteria, with the exception of the total area for the high-volume, low-rutting level. The total area for this case was –4,368, which is greater than Simpson's criterion of <–4,500 for subgrade. It appears as though the subgrade and subbase failure modes could be combined if this total-area criterion were somewhat larger. For the base failure mode, the FEM data agree with Simpson's criteria for the ratio of areas and all of the data except the high-volume, high-rutting level case. The exception is very close to meeting the criteria: the minimum total-area criterion recommended by Simpson is –4,500, and the FEM data range from –872 to –4,612. This exception suggests that the total-area criterion is too restrictive on the low side. The base course modeled was only 300 mm (12 in.) thick. It is likely that smaller (i.e., more negative) total areas could occur if thicker, lower modulus base courses were modeled.

For the surface failure mode, there is clearly lack of agreement between Simpson's recommendations and the FEM-generated data. A comparison of Figures 2-20 and 2-38 clearly shows the discrepancy. The difference is because Simpson used linear elastic theory to estimate the shape of the surface profiles while the research team used a nonlinear creep material model to predict pavement deformation. Surface profiles Simpson predicted for the surface failure mode show upheaval extending the entire distance between the wheel paths. This upheaval is inconsistent with multiple profiles observed by the research team members when shear failures have occurred in HMA surface layers. The upheaval typically does not extend the entire distance between the wheel paths; rather, there is a reverse in curvature of the surface profile at the peak of the upheaval. This reverse in curvature is clearly shown in Figures 2-36 and 2-42. Simpson's total-area criterion for the surface failure mode is entirely positive because the profile upheaval extends the entire distance between the wheel paths. This extension is also the reason for Simpson's high ratio criterion. The FEM simulation–generated data are reasonable, and initial criteria of 0 to –7,500 for total area and 0.3 to 0.8 for the ratio appear to be more appropriate.

On the basis of the previous discussion, initial criteria were proposed for further study and are summarized in Table 2-9. It should be noted that significant changes were proposed that extended even beyond the bounds observed using the FEM simulations. In addition to the total-area and ratio criteria, criteria were placed on the surface and base failure modes. The additional criteria were that there must be a reversal of curvature in the transverse surface profile between the wheel paths for the surface failure mode, and there must not be a reversal of curvature in the transverse surface profile between the wheel paths for the base failure mode. These criteria are illustrated in Figure 2-43. All of the FEM-generated profiles showed a reversal of curvature for the surface failure mode, while none of them showed a reversal of curvature for the base failure mode. These criteria address the overlap of total-area and ratio criteria for the surface and base failure modes. The initial criteria proposed for further study were assessed using limited data from APT tests. The analysis is presented in the following section.

TABLE 2-7 Distortion parameters based on FEM analyses

Failure Mode	Rutting Level	Distortion Parameters (mm^2)							
		Low-Volume Structure				High-Volume Structure			
		Total	Positive	Negative	Ratio	Total	Positive	Negative	Ratio
Surface	Small	-1433	1080	-2513	0.43	-856	2408	-3264	0.74
	Large	-2119	5928	-8047	0.74	-2430	8828	-11258	0.78
Base	Small	-872	3619	-4491	0.81	-1693	2939	-4632	0.63
	Large	-2207	10666	-12873	0.83	-4612	9584	-14196	0.68
Subbase	Small	n/a	n/a	n/a	n/a	-4368	702	-5070	0.14
	Large	n/a	n/a	n/a	n/a	-21307	952	-22259	0.04
Subgrade	Small	-9189	250	-9439	0.03	-8822	294	-9116	0.03
	Large	-24745	1440	-26385	0.05	-28365	1628	-29993	0.05
Heave	Small	18081	18081	0	∞	19378	19378	0	∞
	Large	71695	71695	0	∞	70765	70765	0	∞

TABLE 2-8 Range of distortion parameters pooled for rutting levels and structures

Failure Mode	Distortion Parameters (mm^2)						Agreement with Simpson's Criteria	
	Combined Ranges Based on FEM				Simpson's Criteria			
	Total	Positive	Negative	Ratio	Total	Ratio	Total	Ratio
Surface	-2430 to -856	1080 to 8828	-11258 to -2513	0.43 to 0.78	700 to 5000	1.25 to 3.0	No	No
Base	-4612 to -872	2939 to 10666	-14196 to -4491	0.63 to 0.83	-4500 to 700	0.4 to 1.25	No	Yes
Subbase	-21307 to -4368	702 to 952	-22259 to -5070	0.04 to 0.14	n/a	n/a	n/a	n/a
Subgrade	-28365 to -8822	250 to 1628	-29993 to -9116	0.03 to 0.05	< -4500	<0.4	Yes	Yes
Heave	18081 to 71695	18081 to 71695	0	∞	>5000	>3.0	Yes	Yes

2.4 EVALUATION OF PROPOSED INITIAL CRITERIA

Transverse surface profile data were requested from several sources that have used APT techniques to evaluate pavement performance. Data were obtained from tests performed at the following facilities:

- U.S. Army Corps of Engineers Cold Regions Research and Engineering Laboratory (CRREL),
- FHWA ALF,
- INDOT/Purdue University APT,
- WesTrack, and
- MnROAD.

In addition, limited data were obtained from the literature associated with TxMLS and CAL/APT.

Extensive discussion was provided on all of these facilities and on studies in the literature review (see Section 2.1), with the exception of MnROAD. The Minnesota Department of Transportation (MnDOT) Road Research Project [54], MnROAD, is located on I-94 northwest of Minneapolis, Minnesota. Two parallel lanes of the existing interstate highway serve as the location for what is termed the "mainline" experiment. A low-volume facility is located adjacent to the mainline site. Actual traffic from the existing interstate highway can be diverted onto the mainline test lanes. The low-volume facility is trafficked with controlled loading. The facilities are heavily instrumented. MnDOT was very cooperative in providing data for use in conduct of the current research. For NCHRP Project 1-34A, data were obtained from two mainline and one low-volume test section. The mainline, or high-volume, sections were numbers 15 and 21, and the low-volume section was number 28. Section 15 is a full-depth asphalt pavement comprised of 275 mm (10.75 in.) of HMA placed directly on the subgrade (AASHTO A-6). Section 21 has 200 mm (7.75 in.) of HMA placed on 585 mm (23 in.) of base course, which rests on the subgrade. Section 28 has 75 mm (3 in.) of HMA placed over 330 mm (13 in.) of base that rests on the subgrade. The expected traffic on the mainline sections is 3.4 million ESALs for a 10-year design life, and the low-volume section is expected to experience 115,000 ESALs for a 5-year design life.

TABLE 2-9 Potential initial distortion parameters based on literature and FEM

Failure Mode	Distortion Criteria (mm^2)		Other Conditions
	Total	Ratio	
Surface	-7500 to 0	0.30 to 0.8	Reversal in Curvature Between the Wheel Paths
Base	-7500 to 5000	0.4 to 3.0	No Reversal in Curvature Between the Wheel Paths
Subbase or Subgrade	< -2000	<0.5	n/a
Heave	>5000	0	n/a

Several criteria were used to select data for this analysis. They included the following:

- Transverse profiles must have been measured with a high degree of accuracy,
- Traffic must have incorporated transverse wheel wander,
- Measured rut depths had to be at least 5 mm (0.2 in.), and
- The data had to be readily available.

In order to use data for the purpose of assessing distortion criteria, the data had to be closely spaced. In other words, the transverse distance between sequential elevation measurements had to be taken at small intervals (i.e., less than 50 mm [2 in.]). When elevation data are collected at greater intervals, near-surface distortions can be bridged. One exception was made to include the TxMLS data, which were collected at 150-mm (6-in.) intervals. The data used were obtained at the completion of 160,000 passes at the initial load level. At the subsequent load level, cracking was observed. Use of data from tests with wheel wander was essential in that transverse profiles generated with and without wander are very different, as is illustrated in Figure 2-34. The minimum rut depth requirement was placed on the data to ensure that the rut depths were large enough that the precision of the profilometers used to measure the profiles did not mask the true profiles. Typical precision of most laser and bogie-wheel-type profilometers is on the order of ±1 mm (±0.04 in.). The criterion that the data had to be readily available was relaxed to a degree in that some of the data obtained were in raw form and had to be digitized so that profiles could be plotted.

During the initial literature study, data were readily available from all of the sources listed previously, with the exception of CRREL. Raw profile data had been collected at CRREL, but were not in a releasable form as of September 15, 1999. There was no reluctance on the part of CRREL to provide the data; rather, the data simply were not yet available. An offer to visit, collect, and analyze data was extended to the research team by CRREL, but such work would have been beyond the scope of the planned work, at least for the first phase of the project.

Upon obtaining data from various sources, distortion parameters were first calculated. Data in the literature that were not in electronic format were analyzed by overlaying the figures with small-scale semitransparent graph paper. The profiles were traced, and squares on the graph paper were counted to determine distortion parameters. In some cases, the test sections for which profiles were measured incorporated cross slope. If the data were in electronic format, the cross slope was removed mathematically prior to calculating distortion parameters. Plots were also rescaled to improve the precision of area measurements and to ensure consistent units of elevation and transverse distance. These plots are illustrated in Figures 2-27 and 2-44 for one of the WesTrack test sections. Figure 2-27 was obtained in electronic format from the WesTrack research team. Figure 2-44 shows the same data after mathematically removing the pavement cross slope and converting the data to consistent units. The profile is measured from the pavement edge or shoulder stripe toward the pavement centerline. Thus, the right wheel path of the truck is the one closest to the y-axis. Figure 2-44 illustrates the fact that the cross slope at WesTrack is toward the inside of the track. This cross slope is opposite to that on most highways, particularly undivided highways. Figure 2-44 also illustrates a very important point. The measured profile for this section extends 3.55 m (11.5 ft) rather than the full 3.65-m (12-ft) lane width and, thus, does not capture all of the distortion in the section. This point is very clear from the right side of the figure, which does not capture all of the upheaval at the edge of the wheel path. This point was also true for some of the other profiles analyzed. The example in Figure 2-44 was an extreme case used to illustrate the point. Also illustrated by the figure is that the distortion is not the same for both wheel paths when cross slope is present. This point is illustrated more clearly in Figure 2-27.

The calculated distortion parameters for all of the data obtained from APT tests and the literature are presented in

TABLE 2-10 Summary of APT distortion criteria

Data Source	Test Section ID	Calculated Distortion Parameters			Failure Mode Based on Table 2-9	Observed Failure Mode	Comments
		Total	Ratio	Curvature Reversal			
FHWA ALF	L2S4	-14324	∞	No	Subbase or Subgrade	Base	
PFS 176	44B low	-4120	0.34	Yes	Surface	Surface	Agreement
	44B high	-6593	0.29	Yes	Surface	Surface	Agreement
WesTrack	1	-4339	0.45	Yes	Surface	Surface	Agreement
	5	-16063	0.34	Yes	Surface	Surface	Total < -7500
	35	-12981	0.13	Yes	Surface	Surface	Total < -7500 and Ratio < 0.30
MnROAD	15	4598	3.83	No	Base	Base	Ratio > 3.0
	21	5968	3.85	No	Base	Base	Total > 5000 And Ratio > 3.0
	28	-20362	0.22	Yes	HMA	Base	Underdesign
TxMLS	Field	-5422	0.04	No	Subbase or Subgrade	Subbase or Subgrade	Agreement
CAL/APT	Phase II	-12766	0.07	N/A	Subbase or Subgrade	Deep HMA	

Table 2-10. The examples used to calculate the parameters were the following:

- CAL/APT (see Figure 2-20),
- TxMLS (see Figure 2-23),
- INDOT/Purdue APT (see Figure 2-35),
- WesTrack (see Figures 2-44 and 2-45),
- MnROAD (see Figures 2-46 through 2-48), and
- FHWA ALF (see Figure 2-49).

The proposed criteria based on the literature and modeling need additional refinement. In general, the criteria point to the appropriate failure mode. The between-wheel curvature criteria are important in this respect. There are limitations on the theoretical results and available data. A standard 80-kN (1,800-lb) axle load was applied in the FEM simulations. In contrast, several of the test sections analyzed were placed under extremely heavy loading. For example, the CAL/APT test section was exposed to 150,000 load repetitions at a load of 40 kN (9,000 lb), 50,000 load repetitions at a load of 80 kN (18,000 lb) and 100,000 load repetitions at a load of 100 kN (40,000 lb) on a half axle-wheel assembly. This loading is extremely heavy. The FHWA ALF loading was also extreme: 53.5 kN (12,000 lb) on a single wide-base tire. Axle loads at WesTrack were 89 kN (20,000 lb). In general, the negative portion of the total distortion areas was quite large for many of these cases. Thus, the proposed total negative-area criteria were exceeded in several cases. For data where standard load levels were applied, as was the case with INDOT/Purdue APT and TxMLS sections, the criteria appeared to be appropriate. The MnROAD data slightly exceeded the total-area and/or ratio criteria in some cases. The reverse curvature criteria were violated for Section 28. A forensic study and further analysis suggest that the HMA thickness was significantly underdesigned for the applied loading. This suggestion is reasonable in that the structures were actually quite different than those modeled. Additionally, wander employed in some of the APT tests was less than the wander that would be observed on in-service pavements.

2.5 SUMMARY

Analysis of existing data suggests the need to refine the initial criteria. Combining the APT data and modeling efforts served as an excellent means of assessing the initial distortion criteria. However, the analysis suggests that in-service performance, rather than APT performance, should be used to develop refined criteria. The analysis, as well as the literature, has provided strong evidence that a relationship exists between transverse surface profile and location of rutting in the pavement layers.

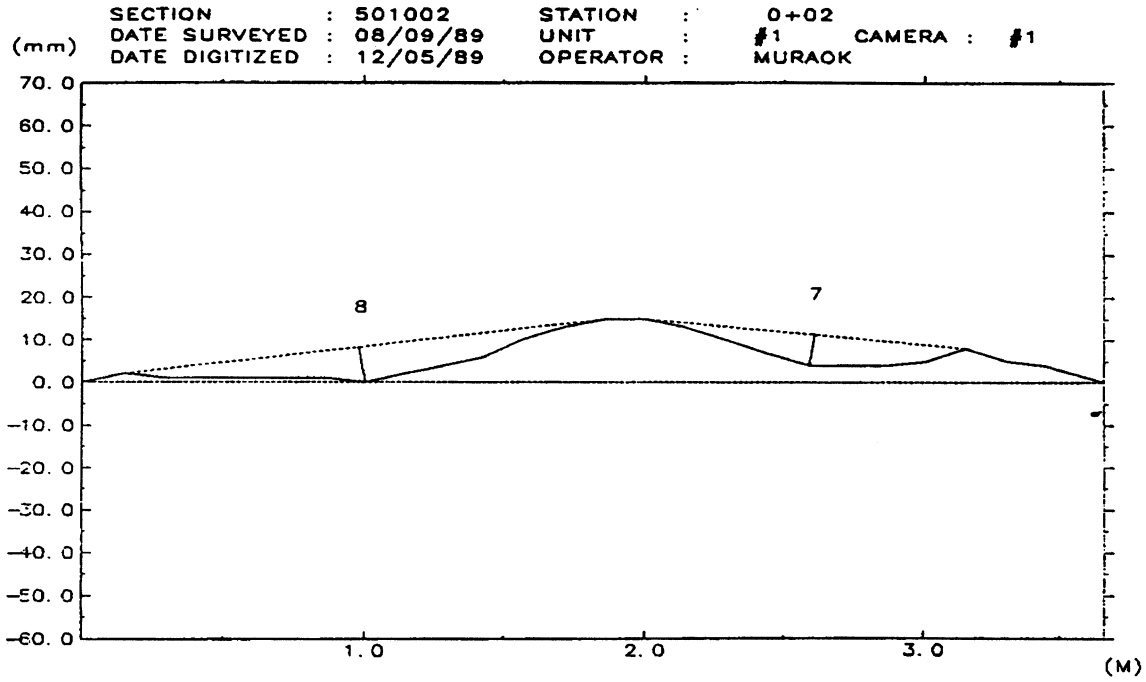

Figure 2-1. Typical plot of transverse profile and "wire method" of rut depth determination [13].

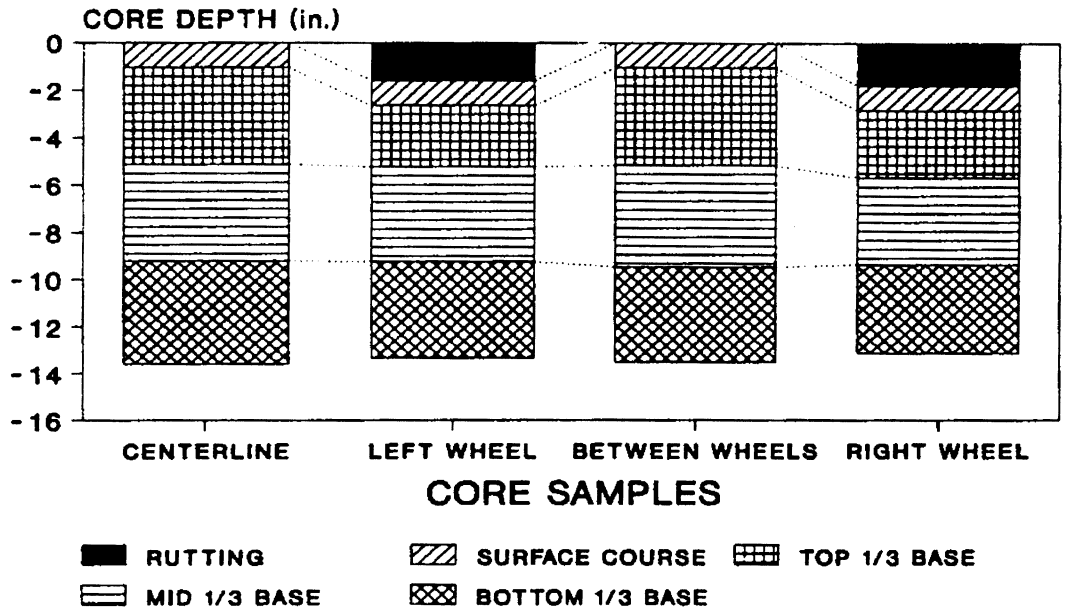

Figure 2-2. HMA pavement section based on core data for Kentucky haul road [15].

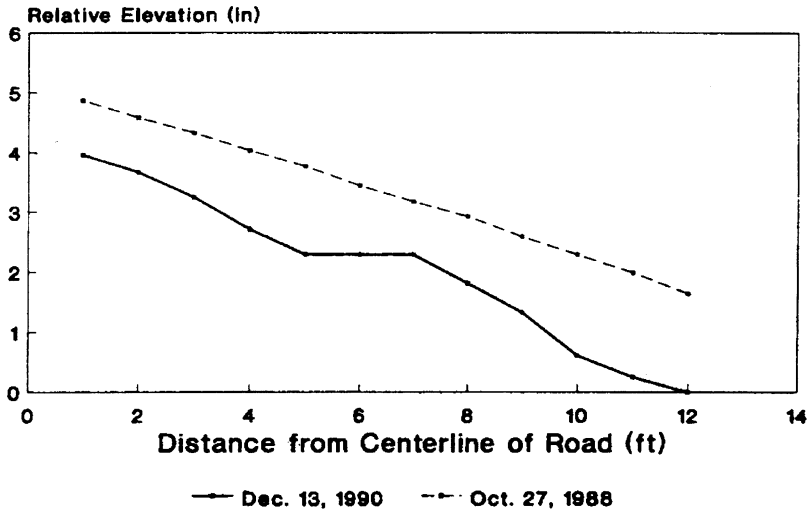

Figure 2-3. Transverse profile data for Kentucky haul road as constructed and after 2 years in service [15].

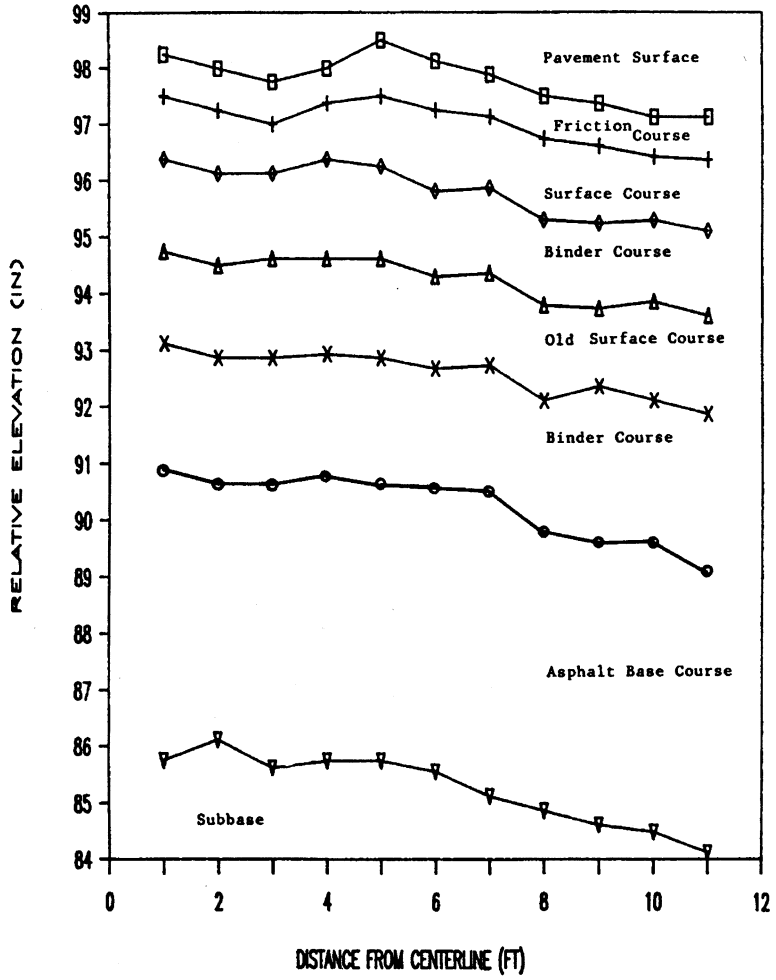

Figure 2-4. Relative layer elevation for NCAT Site 5 [16].

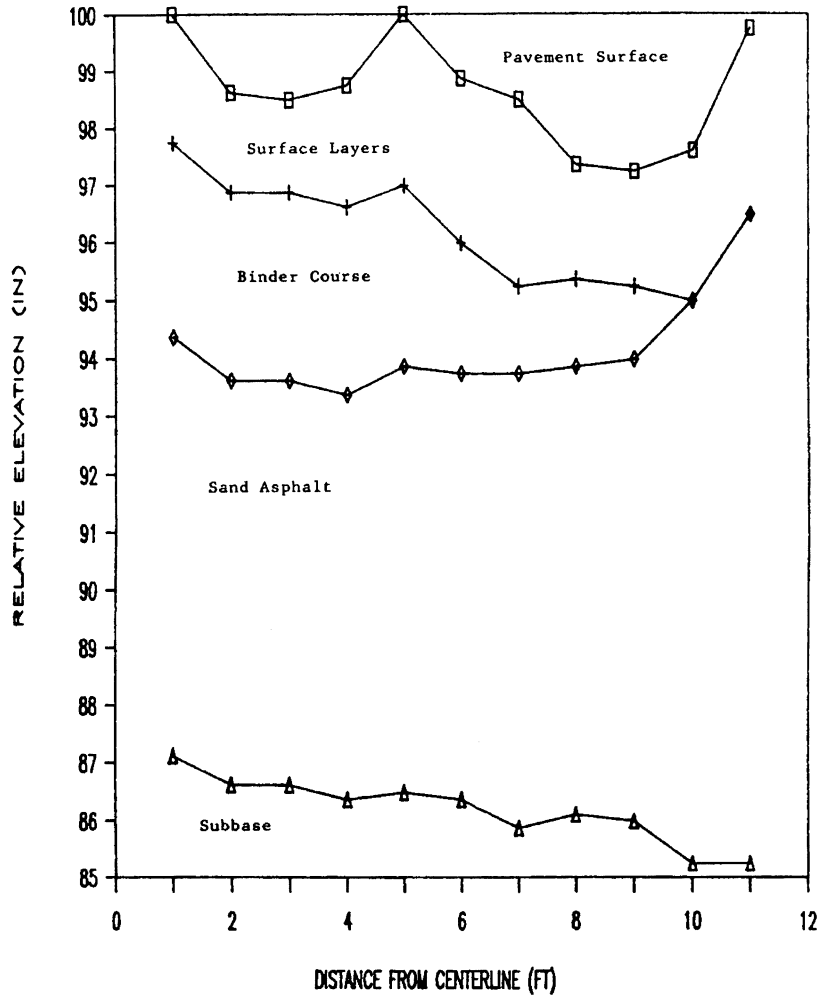

Figure 2-5. Relative layer elevation for NCAT Site 1 [16].

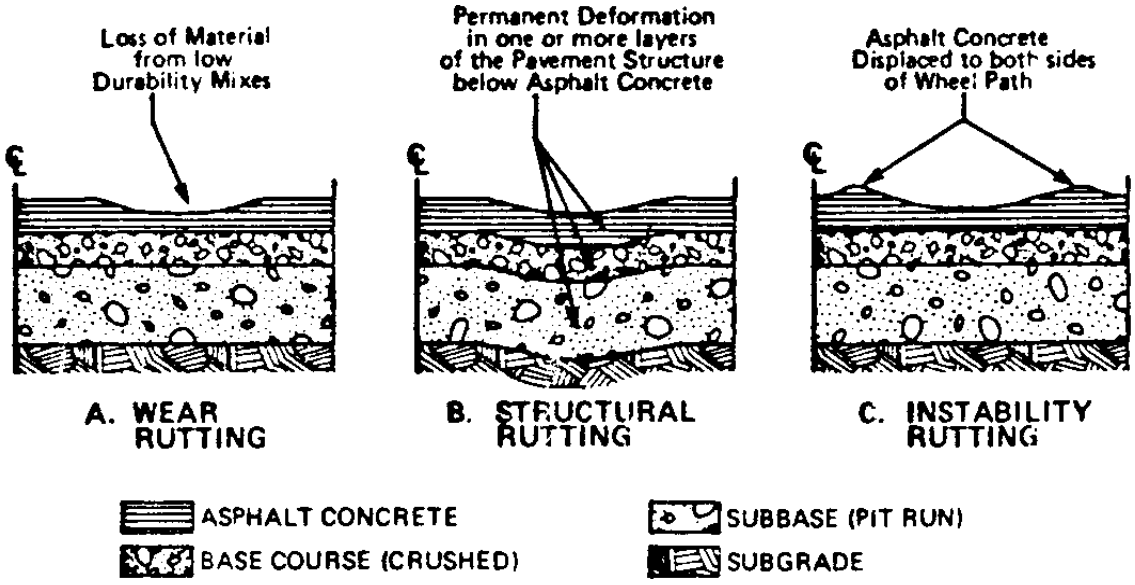

Figure 2-6. Description of rutting types [18].

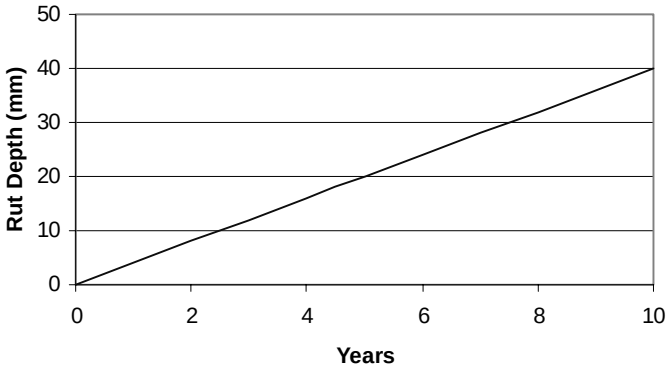

Figure 2-7. Studded tire wear growth [19].

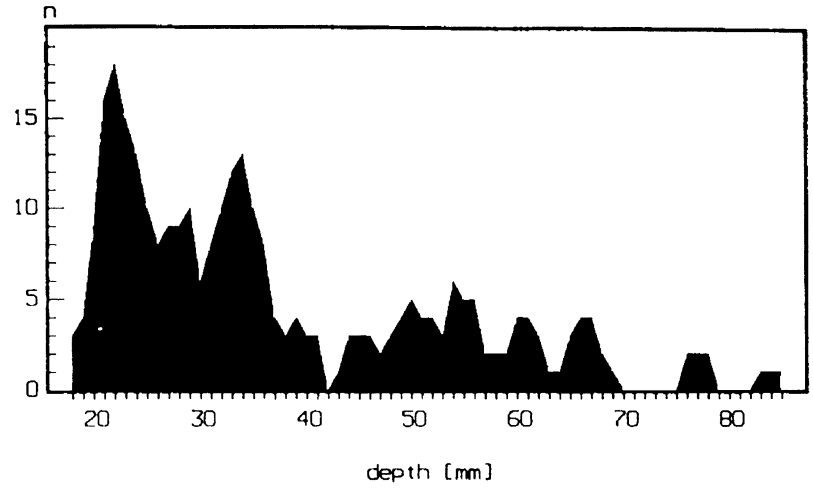

Figure 2-8. Frequency diagram of rut depth: low-volume roads [19].

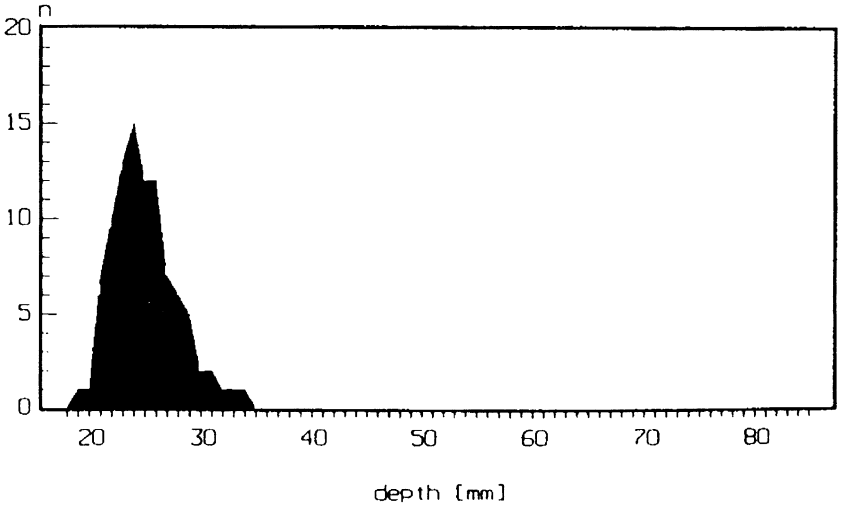

Figure 2-9. Frequency diagram of rut depth: high-volume roads [19].

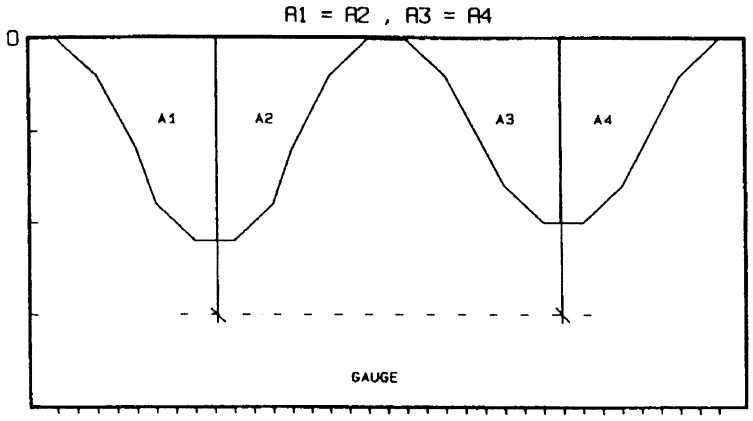

Figure 2-10. Definition of rut gauge [19].

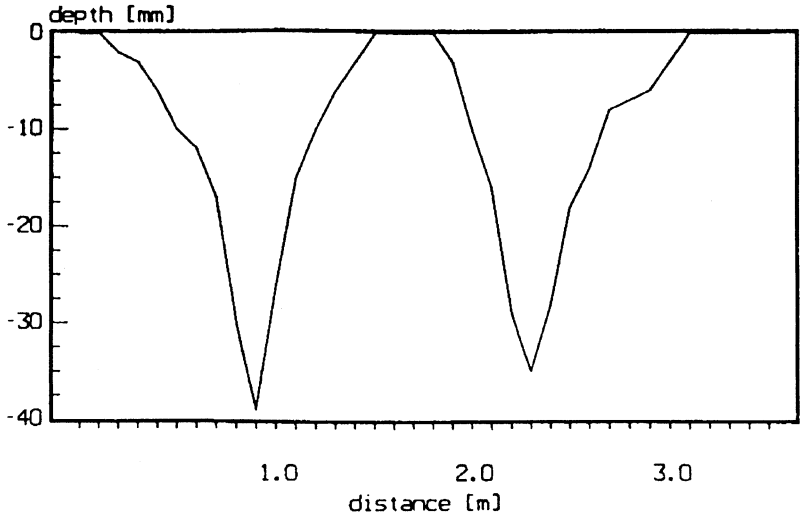

Figure 2-11. Profile of studded tire wear [19].

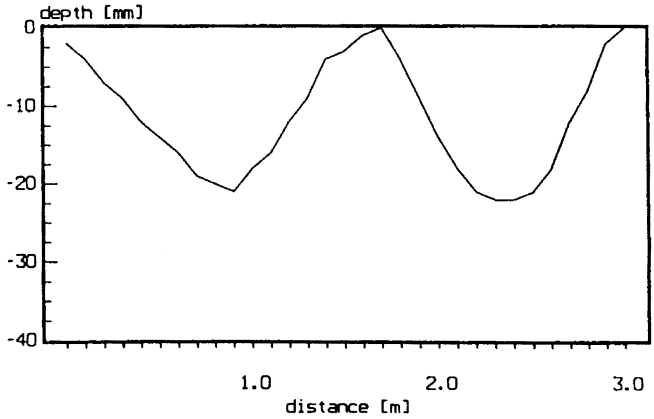

Figure 2-12. Profile of deformation [19].

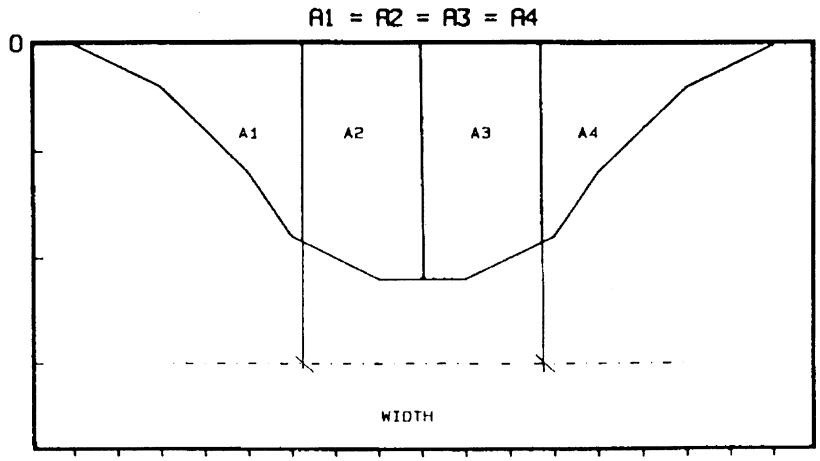

Figure 2-13. Definition of rut width [19].

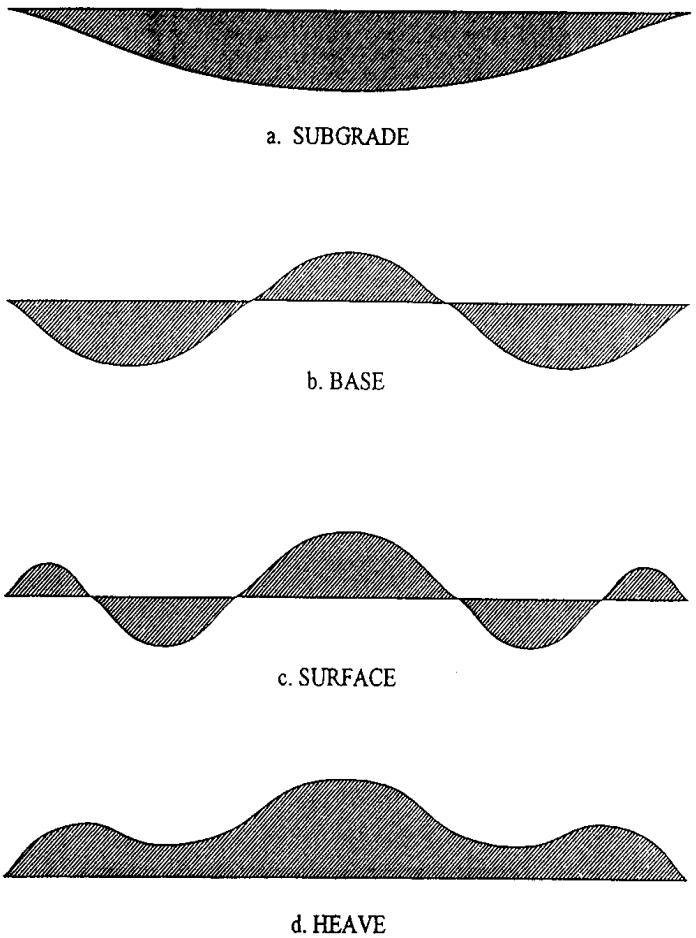

Figure 2-14. Transverse surface profiles by rutting failure mode [20].

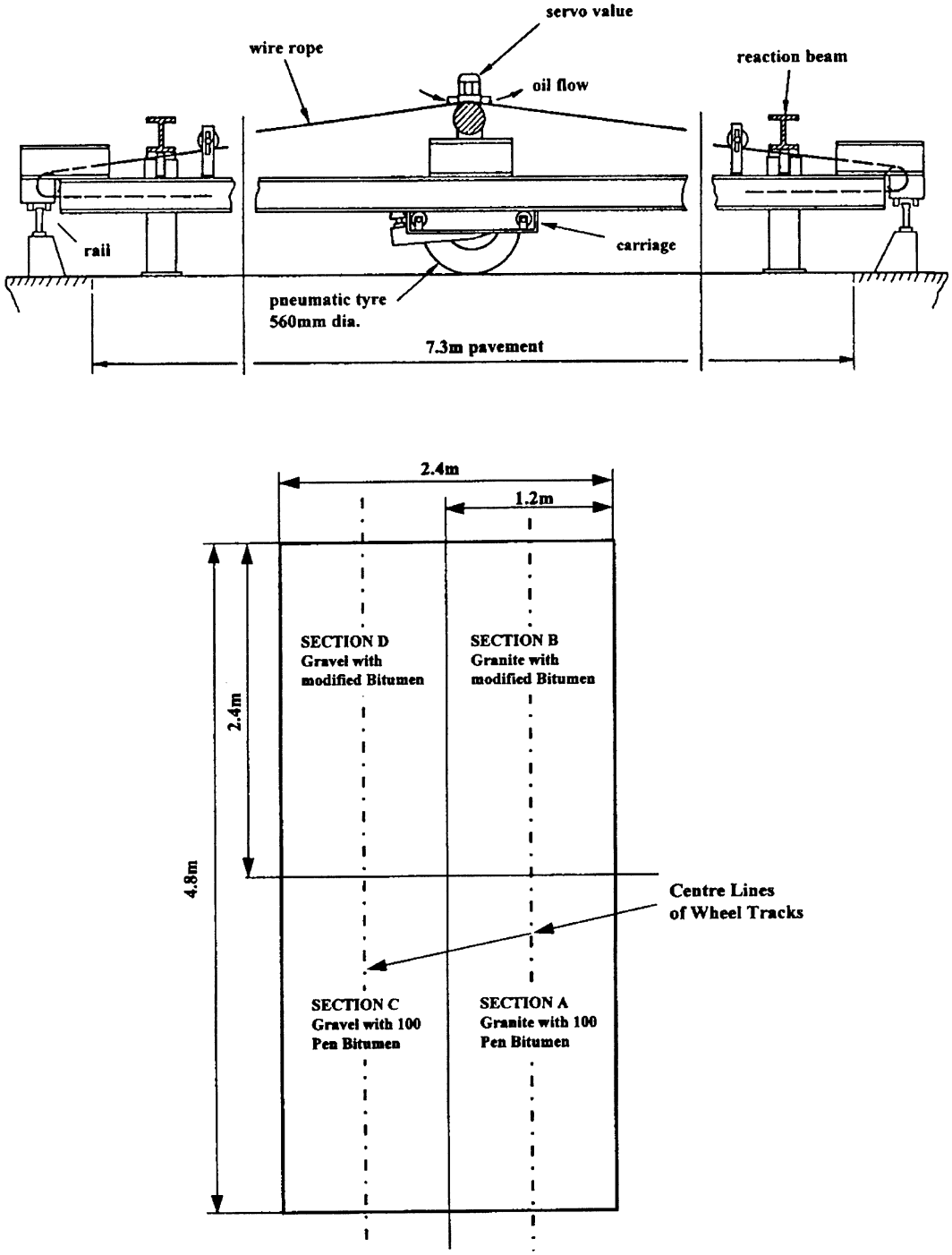

Figure 2-15. Nottingham PTF and plan view of test sections [21].

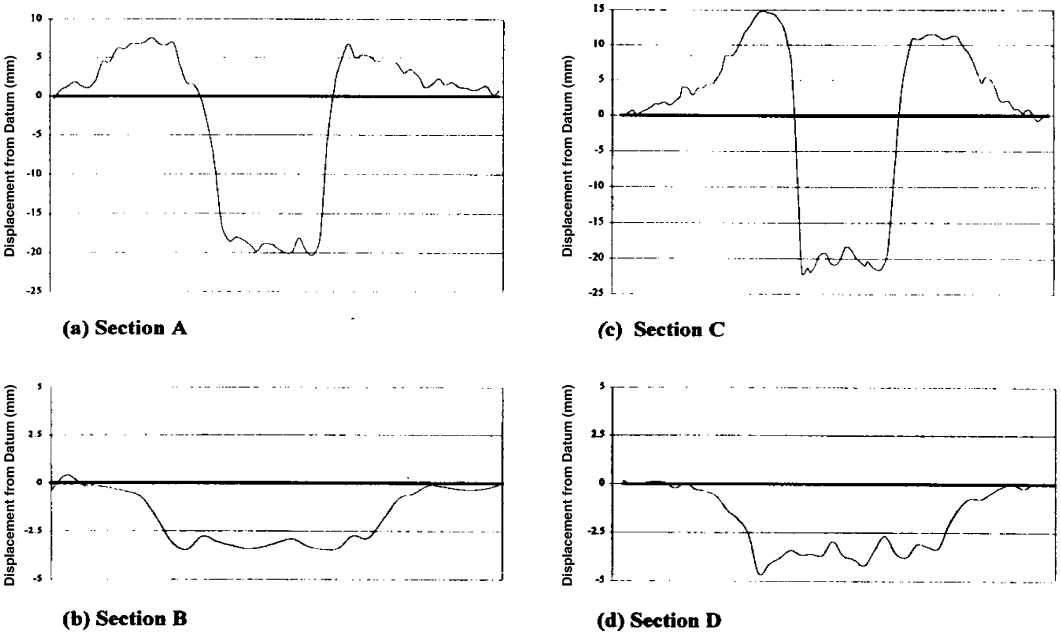

Figure 2-16. Final PTF rut profiles [21].

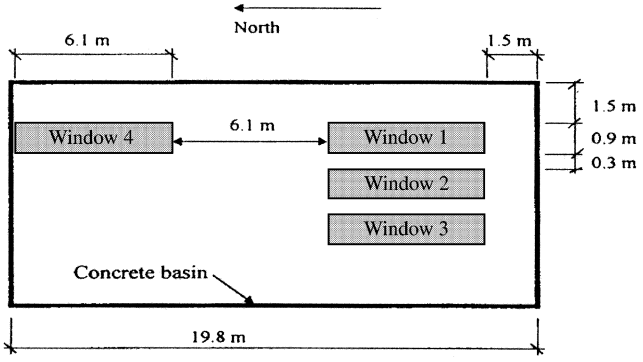

Figure 2-17. Plan view of test sections, or "Windows" [22].

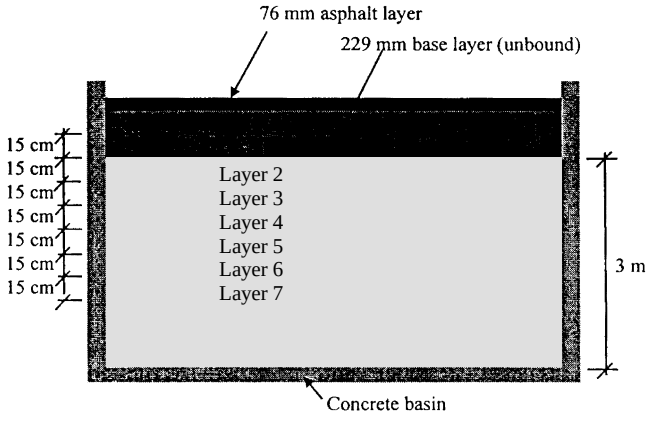

Figure 2-18. Structural section showing instrumentation plan and levels of test sections, or "Windows" [22].

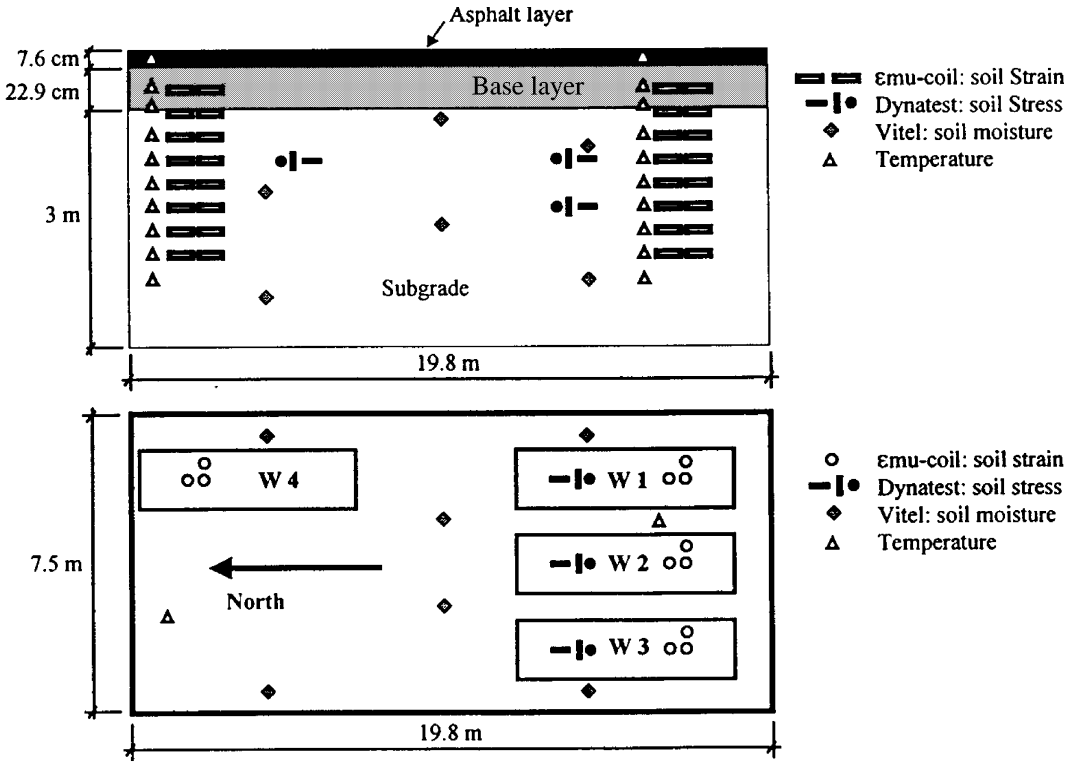

Figure 2-19. Instrumentation of test sections at CRREL [22].

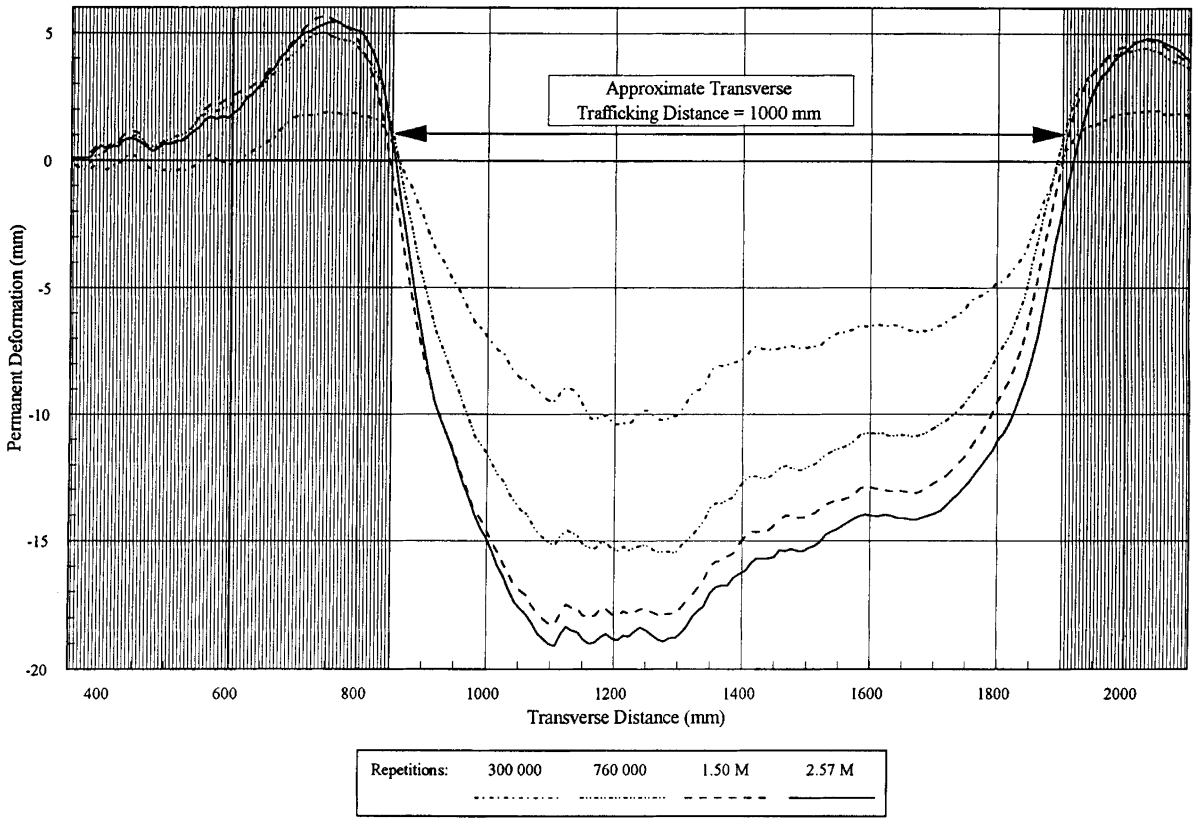

Figure 2-20. Multiple profiles of a CAL/APT HVS HMA test [23].

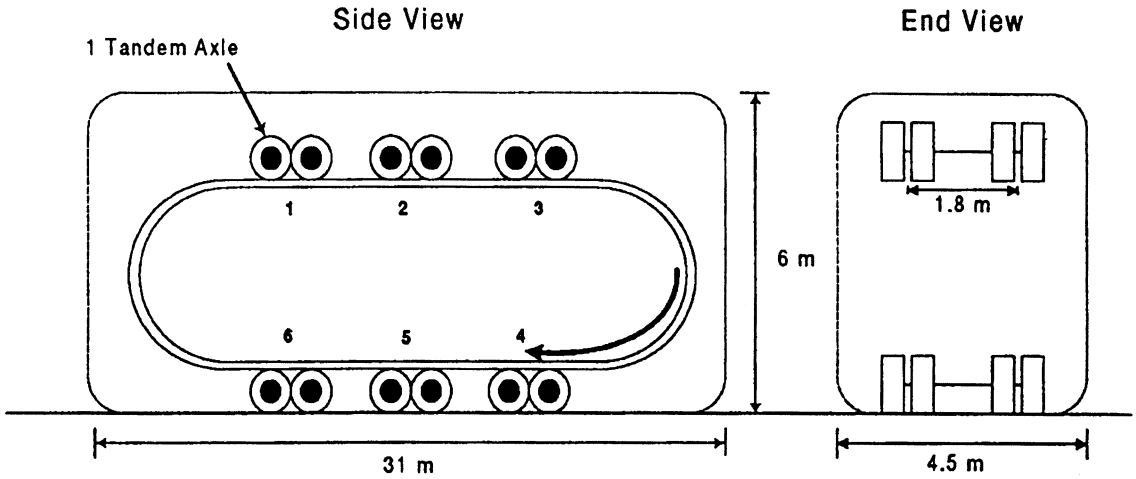

Figure 2-21. Schematic of TxMLS [27].

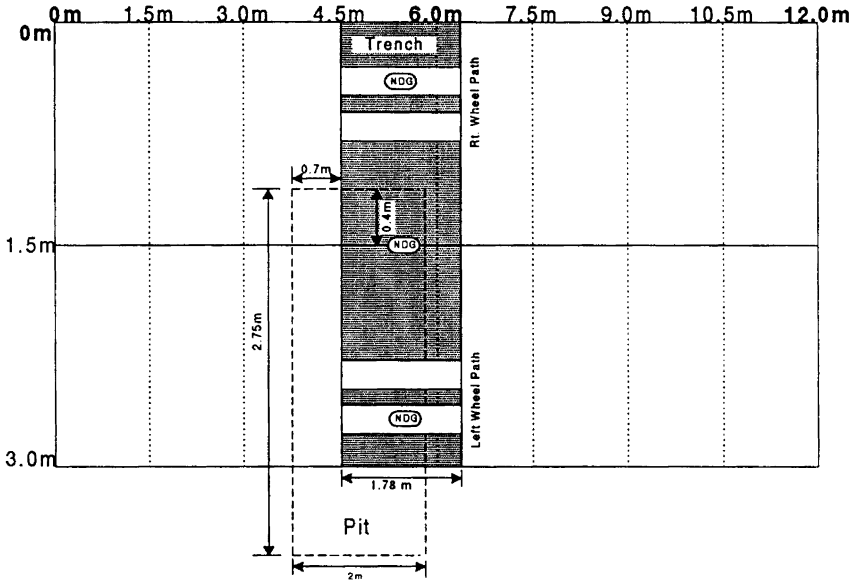

Figure 2-22. Test section with locations of interest and test pit identified [26].

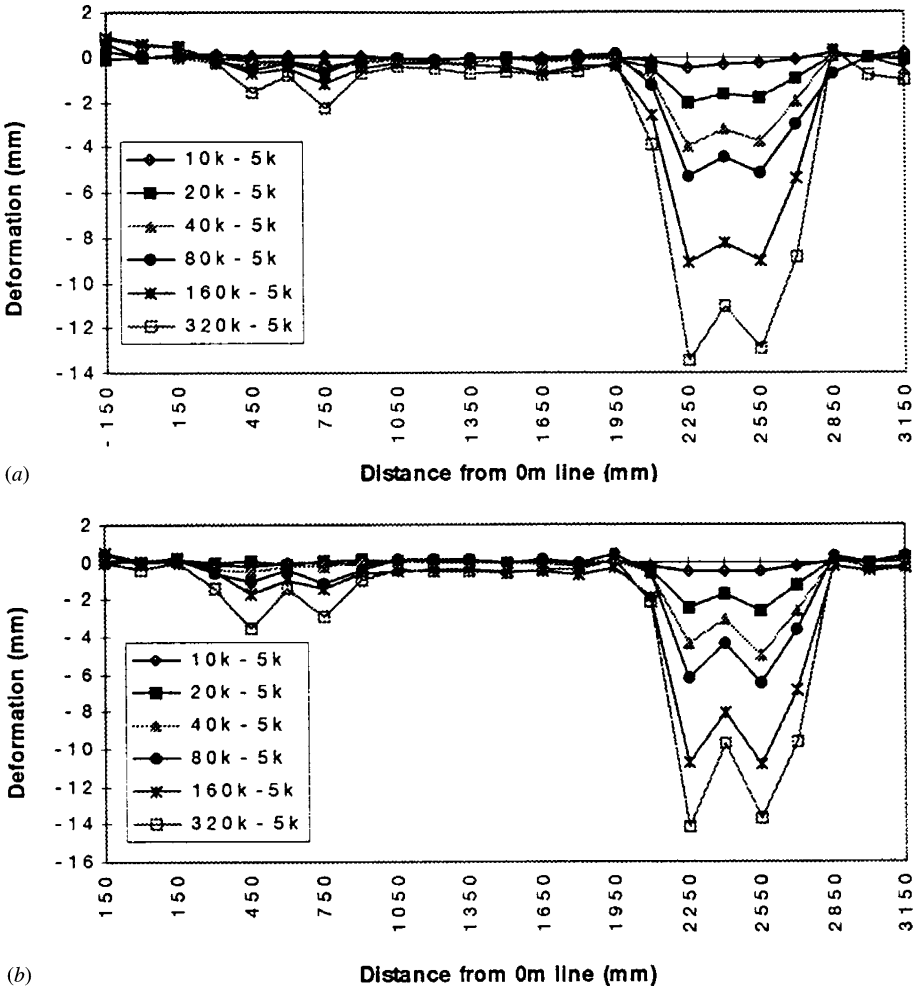

Figure 2-23. Transverse surface profiles as a function of load repetitions (a) at 4.5-m lines and (b) at 6.3-m lines [26].

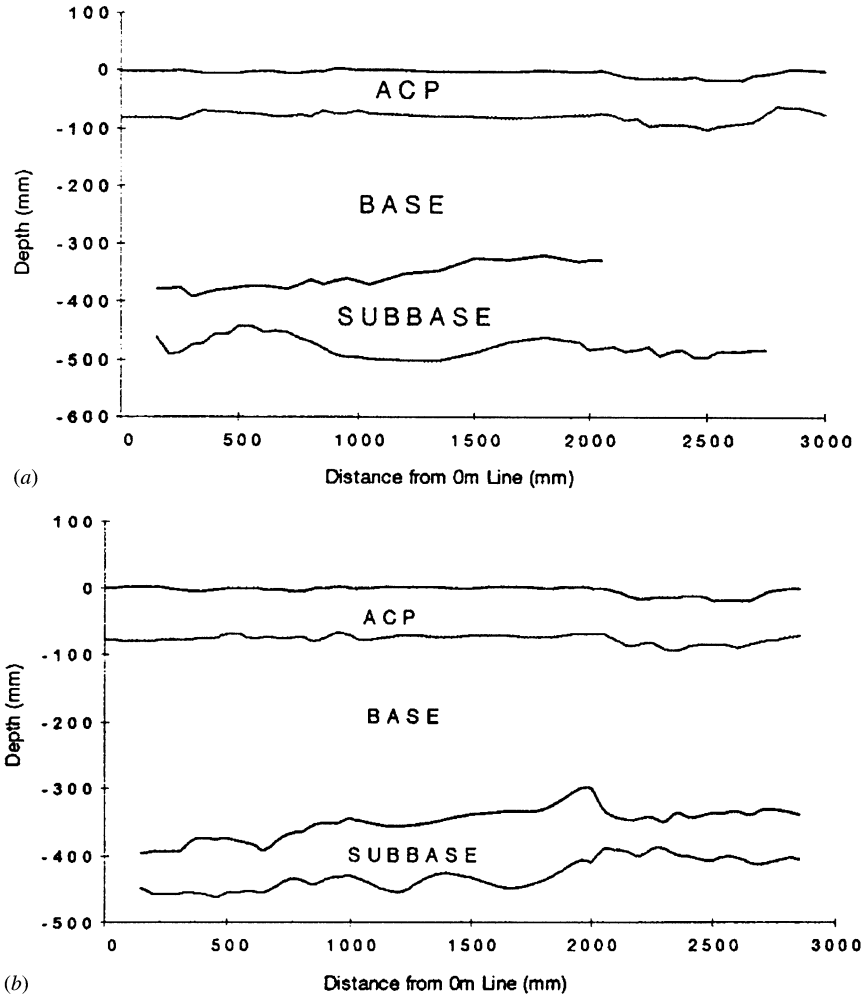

Figure 2-24. Trench wall layer profiles (a) along 4.5-m lines and (b) along 6.3-m lines [26].

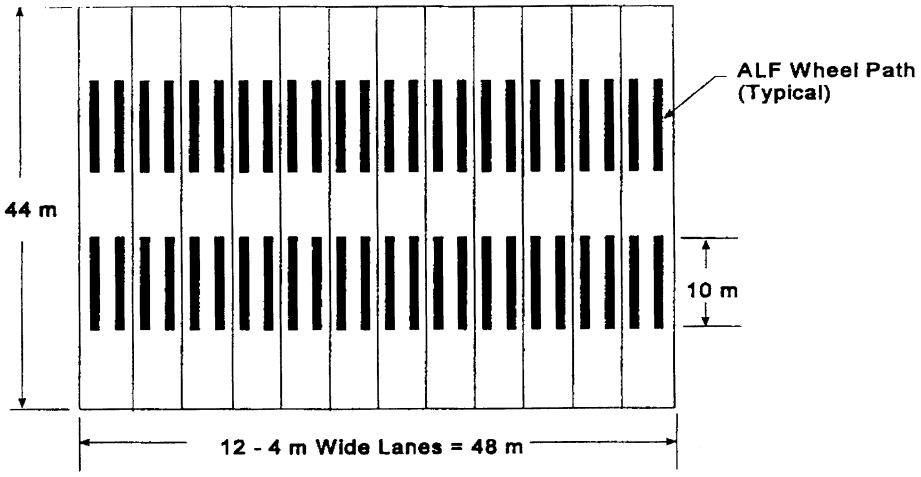

Figure 2-25. Plan view of PTF test lanes [31].

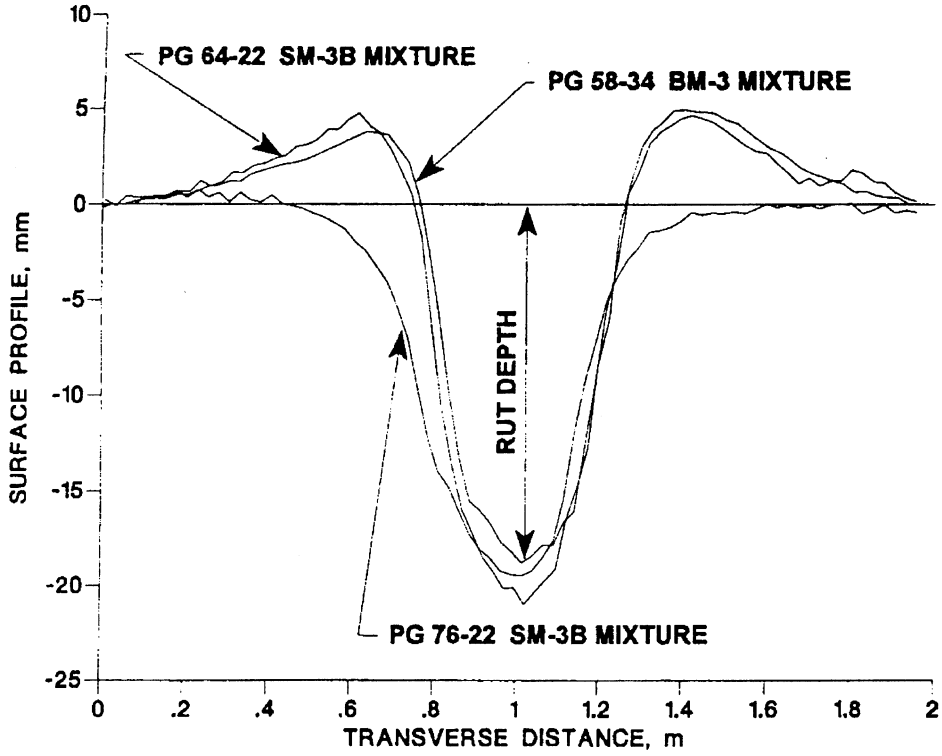

Figure 2-26. Surface profiles from selected ALF rutting tests [30].

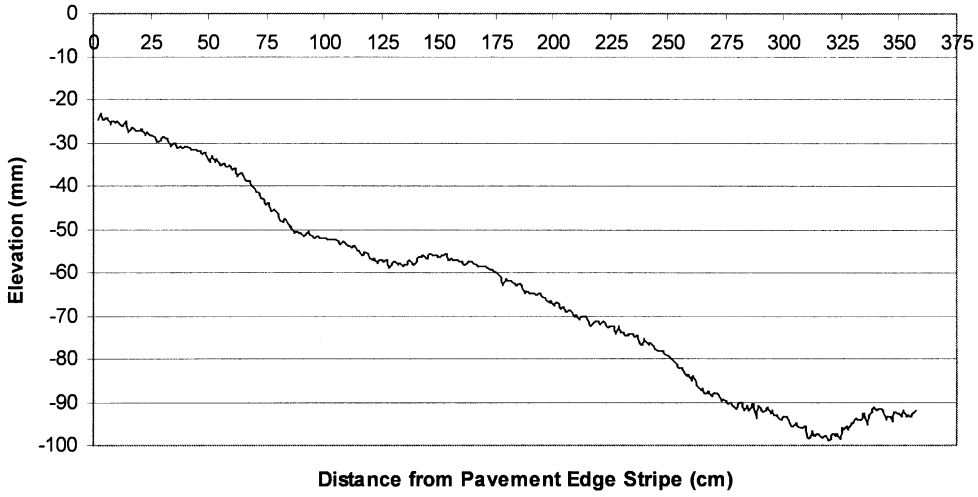

Figure 2-27. Typical transverse surface profile observed at WesTrack.

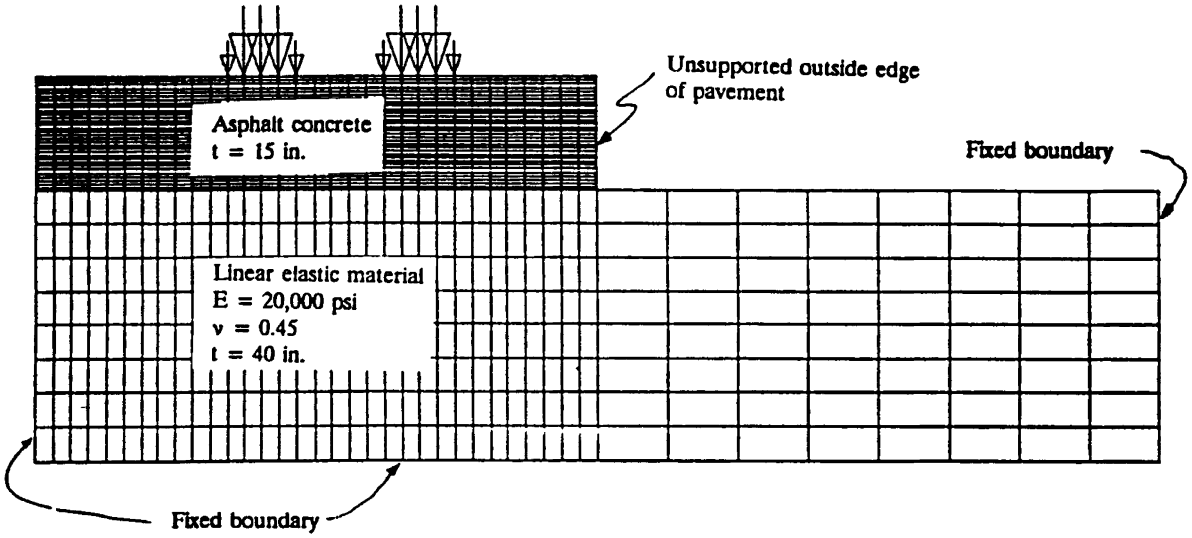

Figure 2-28. Pavement cross section represented by two-dimensional finite element mesh [11].

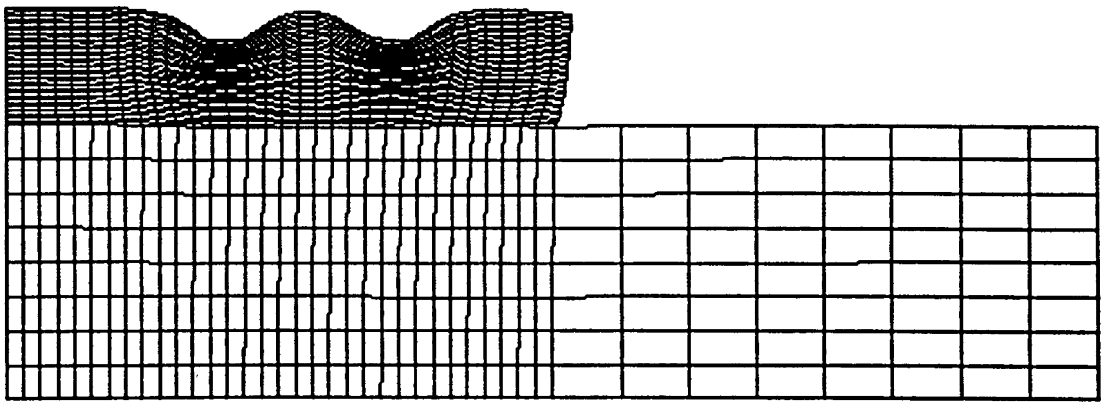

Figure 2-29. Deformed finite element mesh [11].

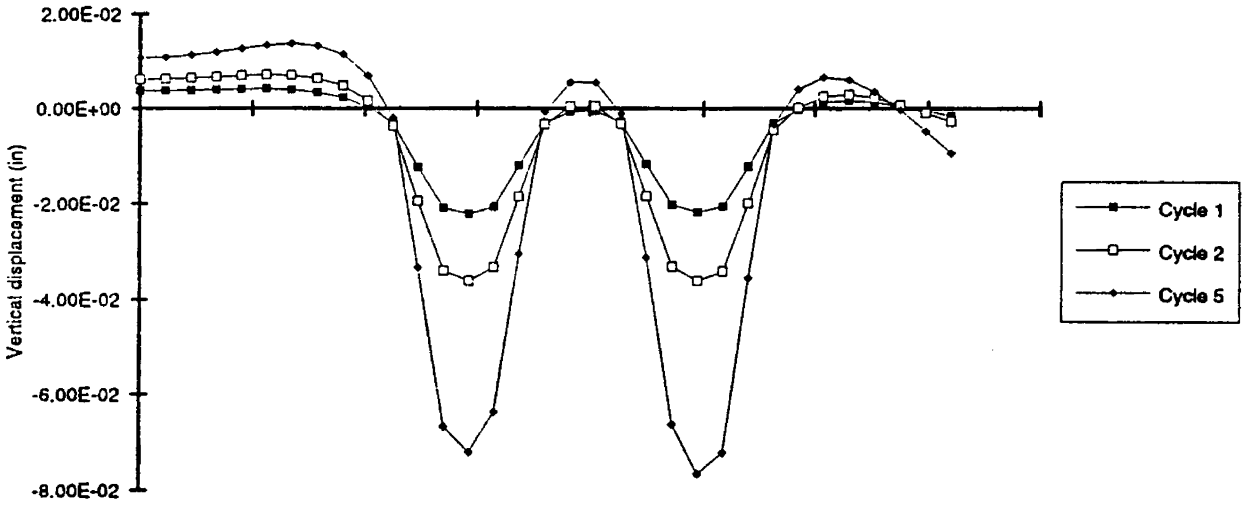

Figure 2-30. Predicted surface profiles under different loading durations with 3,450-kPa stress [11].

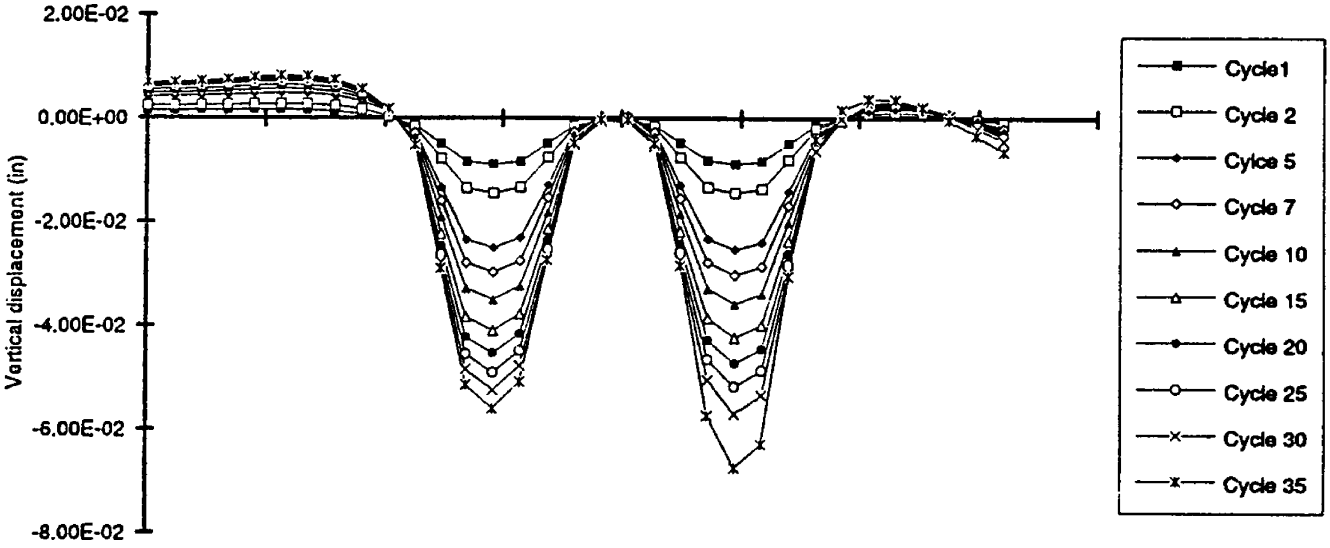

Figure 2-31. Predicted surface profiles under different loading durations with 1,380-kPa stress [11].

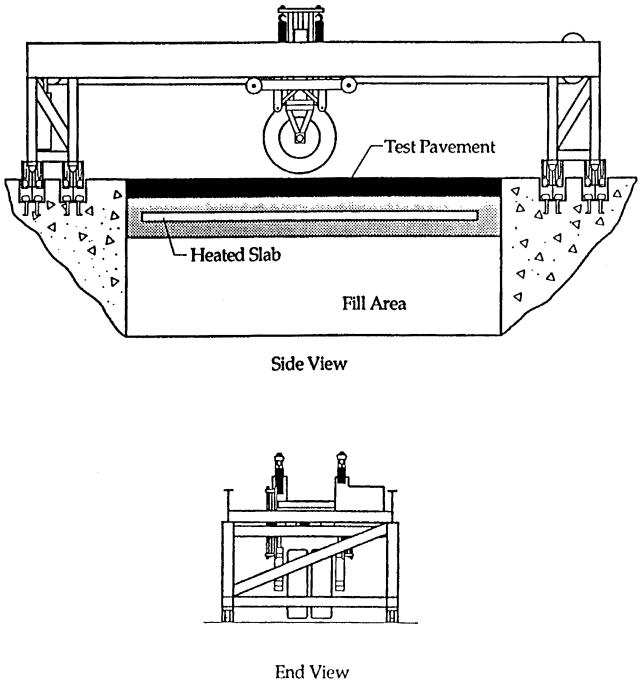

Figure 2-32. Schematic of the INDOT/Purdue University APT [49].

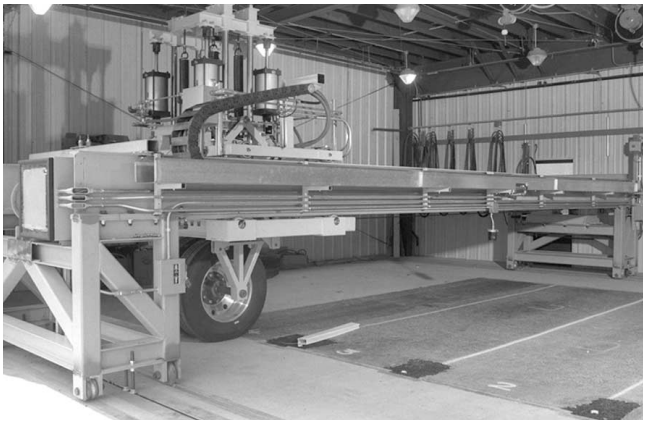

Figure 2-33. INDOT/Purdue University APT.

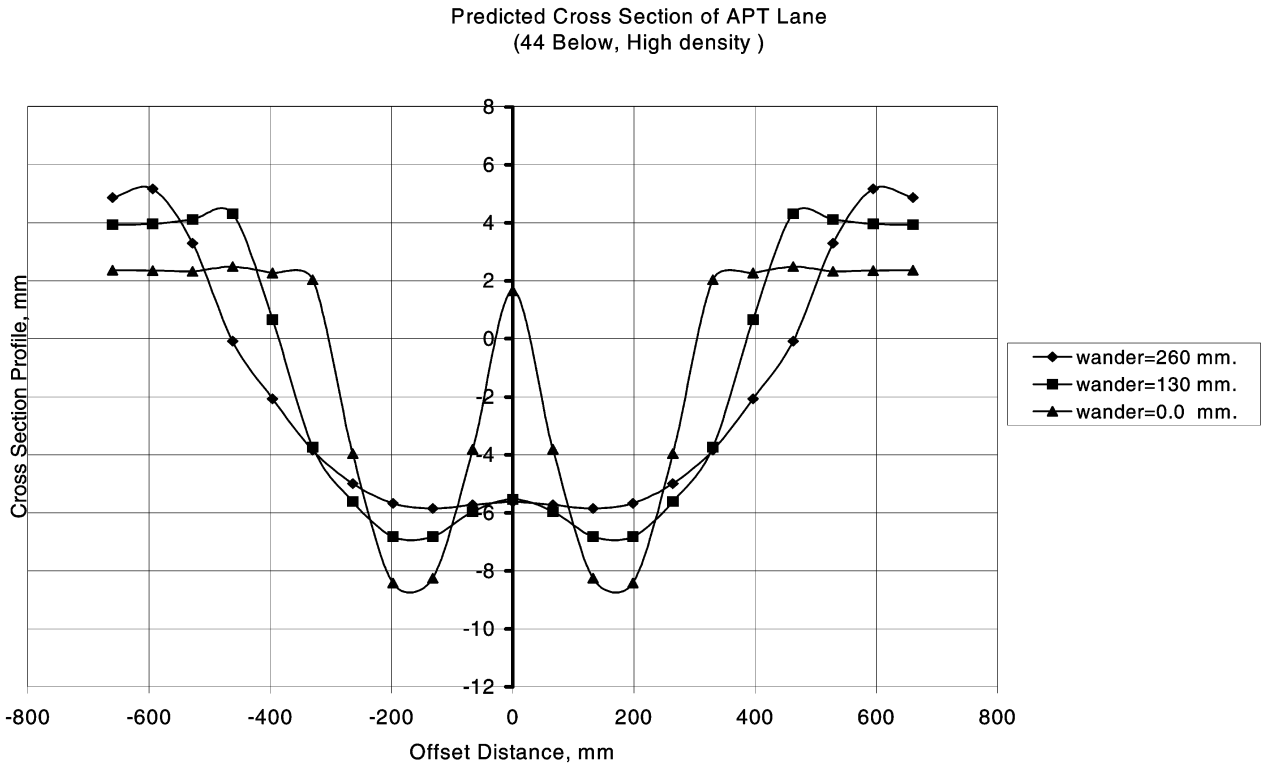

Figure 2-34. Effect of wander on transverse surface profile [47].

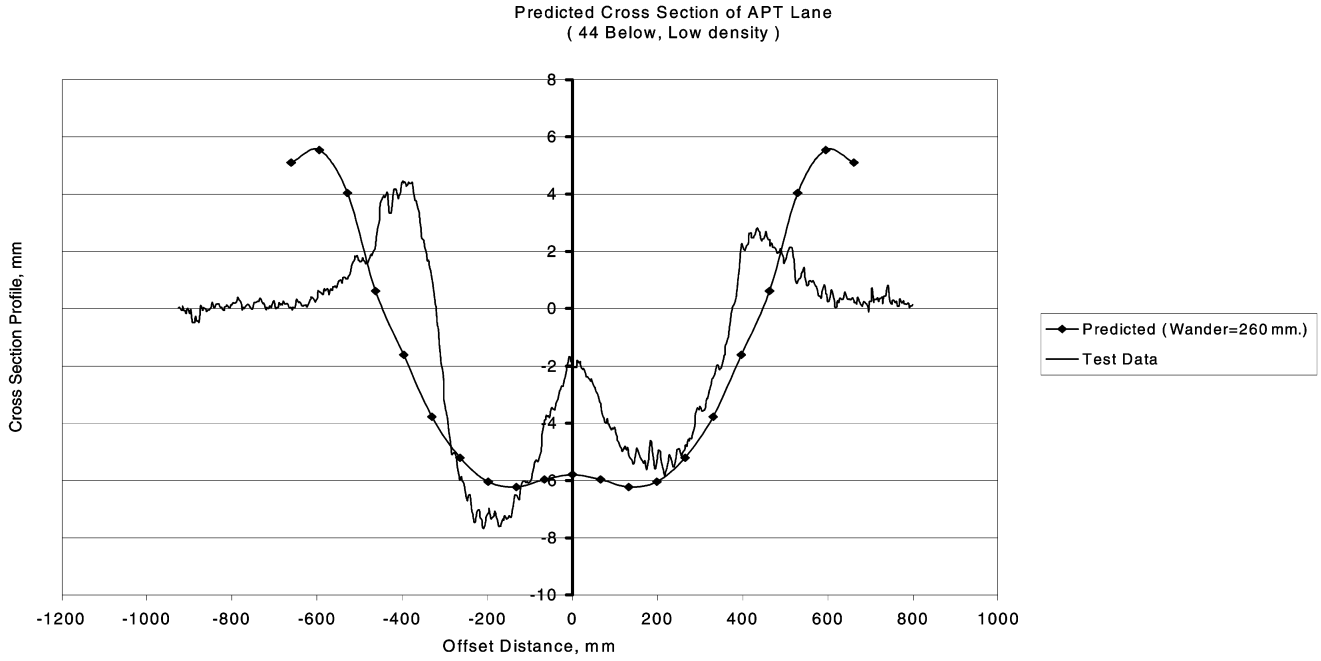

Figure 2-35. Comparison of predicted and measured surface profiles [47].

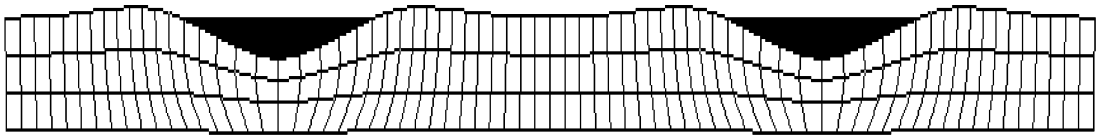

Figure 2-36. Example predicted HMA surface deformation due to HMA failure.

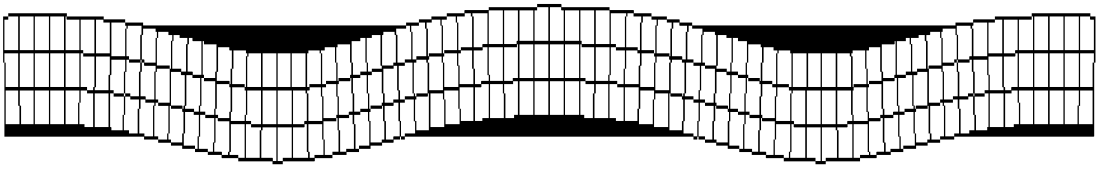

Figure 2-37. Example predicted HMA surface deformation due to base failure.

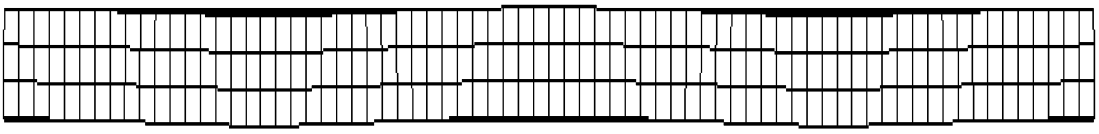

Figure 2-38. Example predicted HMA surface deformation due to subbase failure.

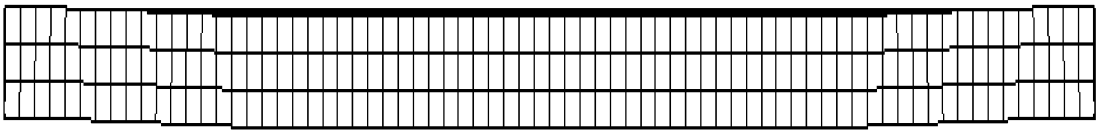

Figure 2-39. Example predicted HMA surface deformation due to subgrade failure.

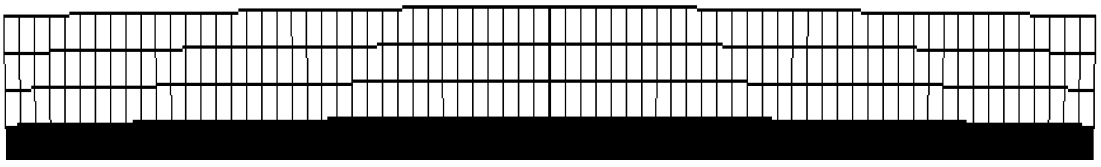

Figure 2-40. Example predicted HMA surface deformation due to subgrade heave.

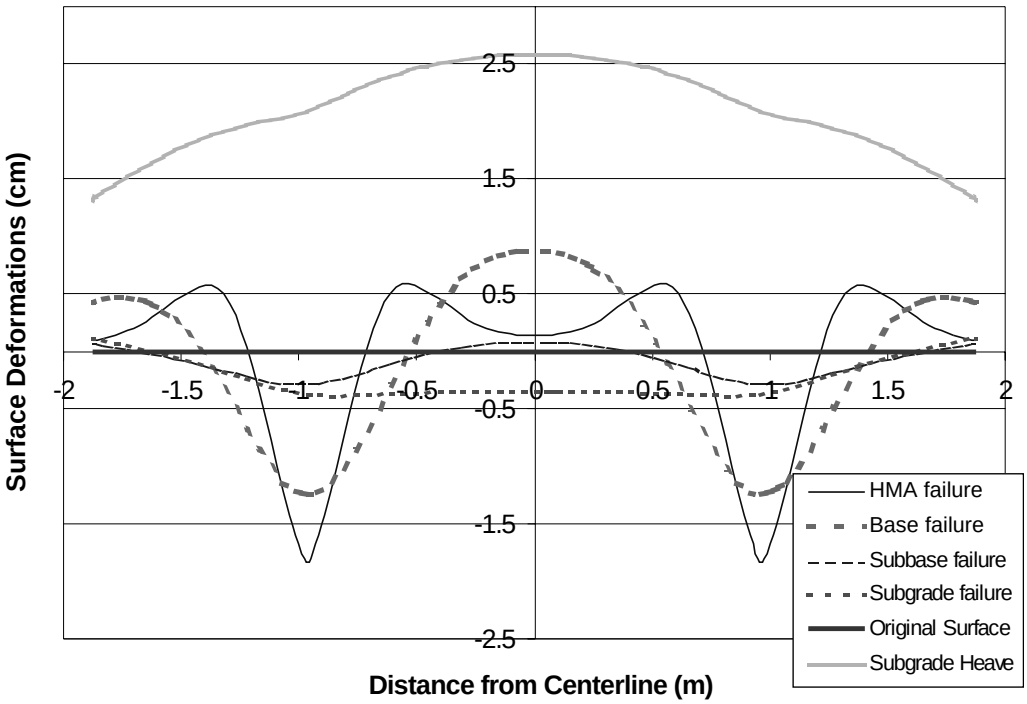

Figure 2-41. Comparison of selected predicted surface profiles (for mesh presented in Figures 2-36 through 2-40).

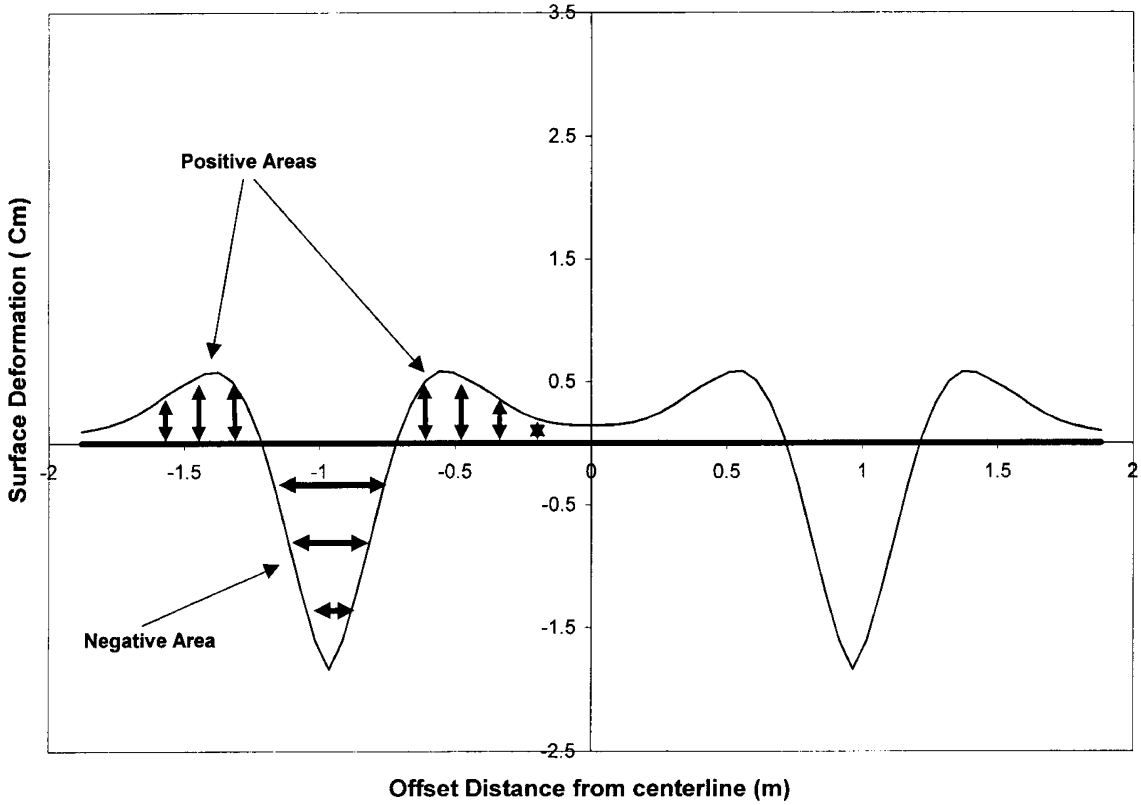

Figure 2-42. Definition of positive and negative distortion area.

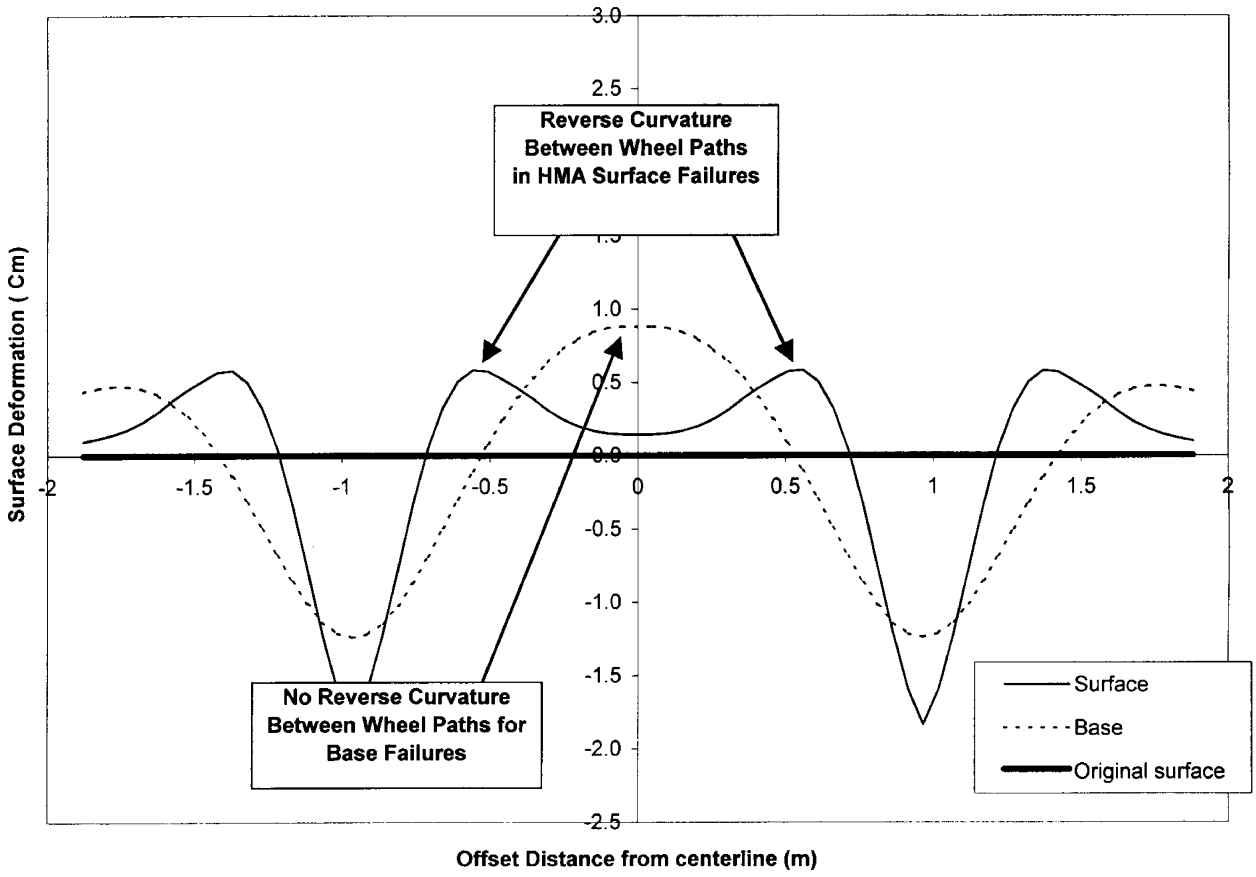

Figure 2-43. Reverse curvature between wheel paths.

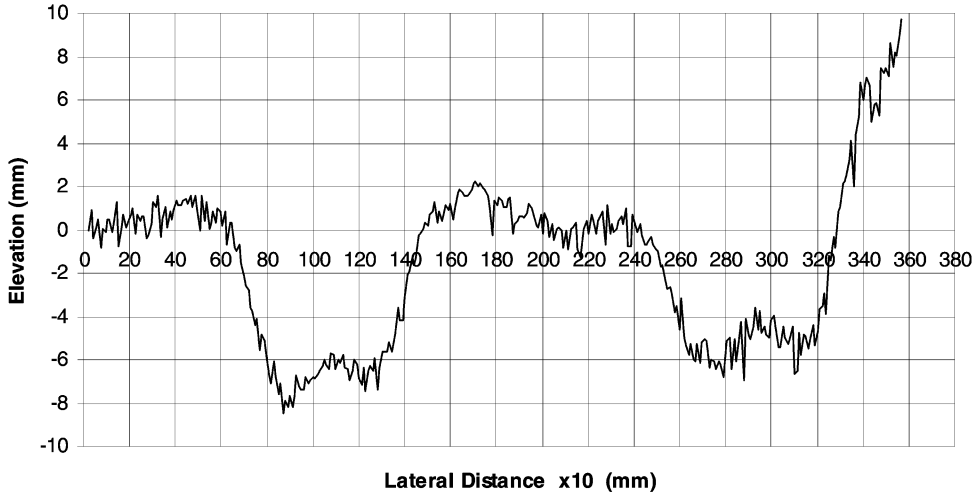

Figure 2-44. WesTrack Section 1 profile after removing cross slope.

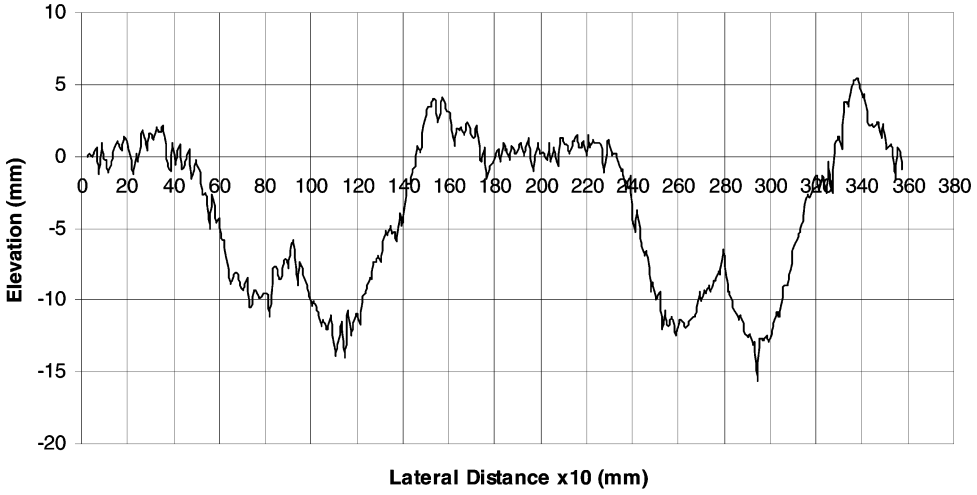

Figure 2-45. WesTrack Section 35 profile after removing cross slope.

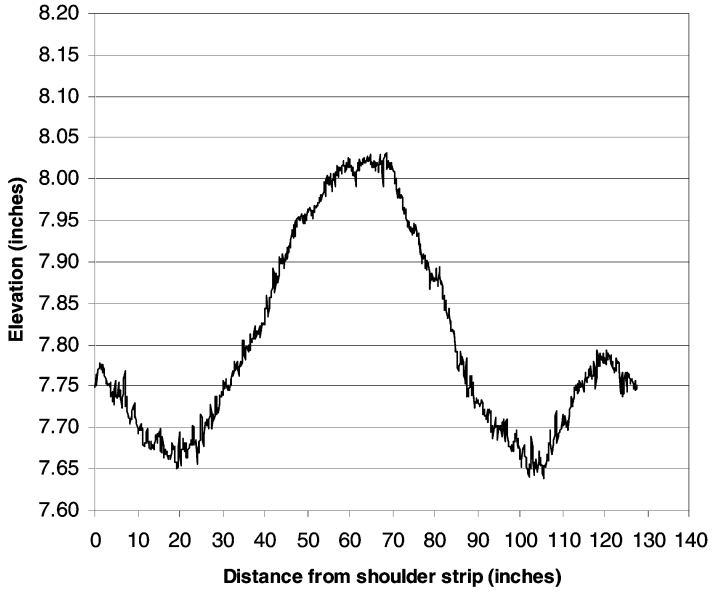

Figure 2-46. MnROAD Cell 15 profile.

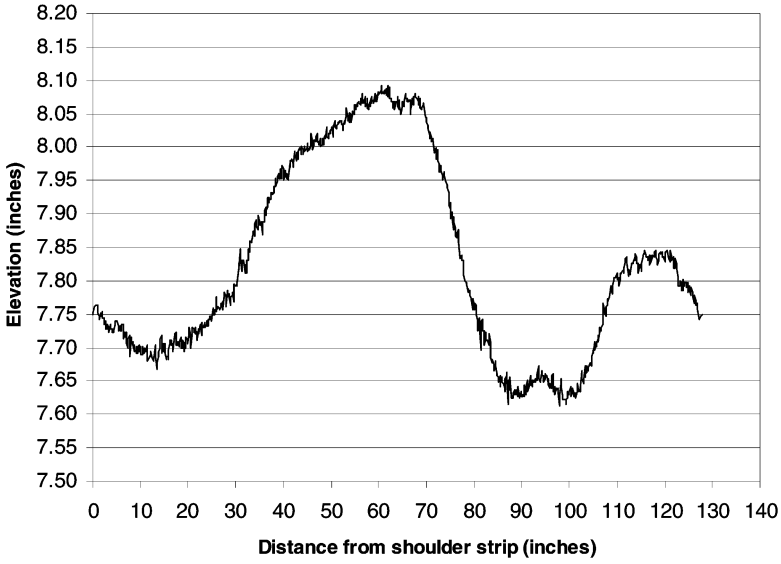

Figure 2-47. MnROAD Cell 21 profile.

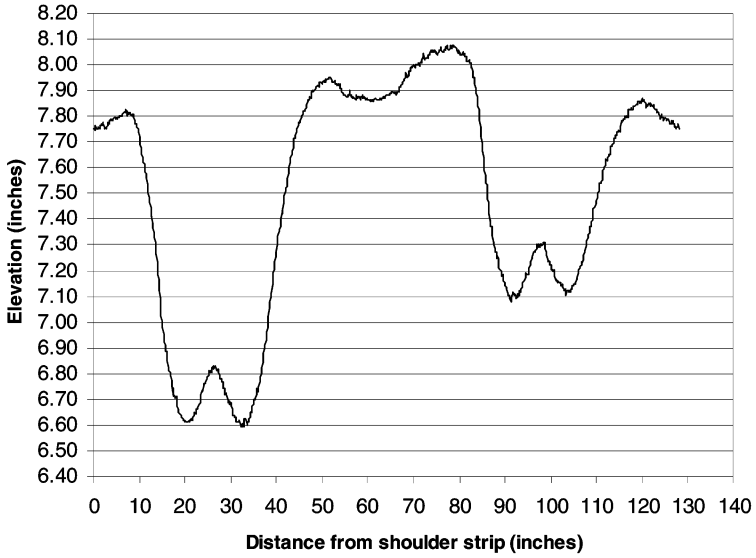

Figure 2-48. MnROAD Cell 28 profile.

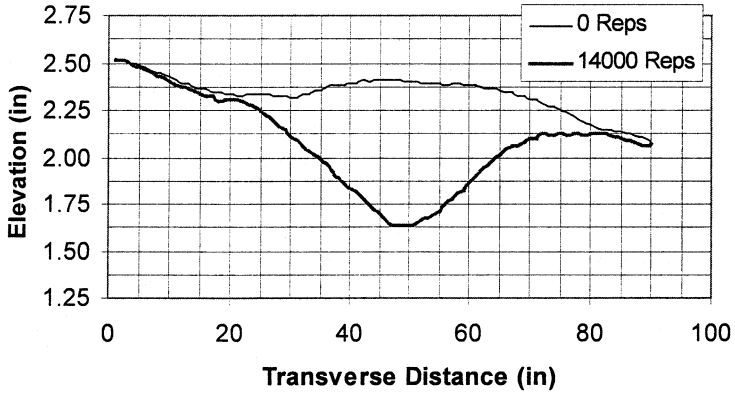

Figure 2-49. FHWA ALF Lane 2 Site 4 surface profiles.

CHAPTER 3

THEORETICAL ANALYSIS

3.1 INTRODUCTION

This chapter gives theoretical analysis details using finite element modeling (FEM). The chapter first considers the relatively simple models identified from the literature review. It then discusses the general issues associated with finite element analysis, such as element selection, determination of mesh size, boundary condition, material properties, and load conditions.

To reasonably simulate pavement structures, this chapter refines the previously noted simple models. A 2-percent pavement cross slope, which is a typical feature of pavements, is introduced into the refined models. Loading conditions include a dual-tire axle instead of single-tire axle and nonuniform contact stress instead of uniform contact stress. Wheel wander (see Chapter 4 for details) has also been carefully incorporated into the loading conditions.

A range of pavement layer thickness is used in the theoretical analysis. Pavement failure in terms of rut depth is set at two deformation levels: a low level, with a maximum rut depth of 5–8 mm (0.2–0.3 in.), and a high level, with a maximum rut depth of 22–25 mm (0.9–1 in.). Results of analysis using the refined models, as well as resolution of some practical issues for FEM analysis, are discussed in Chapter 4. These issues are important in developing and refining the pavement failure criteria.

3.2 INITIAL FINITE ELEMENT ANALYSIS OF RUTTING BEHAVIOR

As an initial approach to analyzing pavement rutting behavior (i.e., surface deformation characteristics caused by rutting) using the finite element method, two simple models were first developed. Analysis results using these models were used in the theoretical analysis included in the literature review. The FEM software used is ABAQUS, which has proven to be a suitable FEM program for the analysis of flexible pavements.

3.2.1 Model Geometry

Two different conventional flexible pavement sections were used to represent high- and low-volume pavements. Conventional flexible pavements are layered systems with high-quality material near the surface, where stress intensity is the greatest, and lower-quality material at the bottom, where the stresses are less intensive. Figure 3-1 shows the pavement cross section geometry of the high-volume model. Starting from the top, the pavement section consists of a surface course, base course, subbase course, and subgrade. Figure 3-2 shows the low-volume pavement cross section geometry used in the study. Also starting from the top, the pavement consists of a surface course, base course, and subgrade. In these two models, only one-half of the pavement cross sections are modeled because of symmetry around the pavement centerlines.

3.2.2 Element Types and Mesh Size

Hua [53] has shown that flexible pavement rutting can be modeled as a plane strain or two-dimensional problem rather than a three-dimensional problem. In doing so, the total computation time is reduced without significant loss in accuracy. As a result, the four-node, quadrilateral plane strain element from the ABAQUS two-dimensional, solid-element library was selected for use in the analysis. The meshing schemes used for the models are given in Figures 3-3 and 3-4, respectively.

A series of finite element analyses were performed with decreasing element size to determine the suitable mesh size. Figure 3-5 shows the trend of surface displacement with change in element size. When the element size is less than 100 mm (4 in.), the difference between the displacements is negligible. The smallest element size used for the high- and low-volume traffic pavement models is 50 mm (2 in.) and 25 mm (1 in.), respectively. Finer meshes were generated in regions of high-stress gradients. The shaded portions of the mesh in Figures 3-3 and 3-4 represent the asphalt pavement surface layer. The deformations on the top surface of this layer reflect the pavement surface transverse profile.

3.2.3 Boundary Conditions

Based on the assumption that there is no deformation beyond a certain depth in the subgrade, the depth of the subgrade was fixed at 1.2 m (4 ft) and 1.6 m (6 ft) for the high- and low-volume pavement models, respectively. Furthermore, the bottom surface of the subgrade is assumed to be fixed, which

means that nodes on the bottom of the subgrade cannot move horizontally or vertically. Also, along the line of symmetry, all nodes are constrained horizontally, but are free to move in the vertical direction. The boundary nodes along the pavement edge are constrained in both horizontal and vertical directions.

3.2.4 Loading Model

In this initial approach, an equivalent 80-kN (18,000-lb) single-axle load with single tires was used. The spacing between two single tires was selected to be 1.8 m (6 ft). Tire contact area depends on contact pressure. In this study, the contact pressure was assumed to equal the tire pressure (no effect of the tire wall). The gross contact area was calculated as 645 cm^2 (100 $in.^2$) for the single tire based on a tire pressure of 620 kPa (90 psi). The contact area is converted into an equivalent rectangular area with a length of 31.75 cm (12.5 in.) and a width of 20.3 cm (8 in.) (contact area = $0.5277*L^2$, length = $0.8712L$, width = $0.6L$). The actual layout and configuration of the contact area is shown in Figure 3-6.

Another factor related to traffic is the vehicle speed. The speed directly relates to the duration of loading on the finite element model. Low speed will give a longer loading duration than high speed and, hence, introduce more rutting in the pavement surface. In this study, 8 km/h (5 mph) was modeled. The loading cycle consisted of using one single-step load function to approximate the wheel loading. The total cumulative loading time of this single step was calculated using the speed and number of load repetitions. This approximation reduced the computation time dramatically while still providing reasonable results.

Unlike the finite element analysis conducted for the project proposal, the number of load repetitions is not fixed for the purpose of developing the failure criteria. Using a trial-and-error method, different numbers of load repetitions were applied for each failure mode to generate both small (5–8 mm [0.2–0.3 in.]) and large (20–25 mm [0.9–1 in.]) deformations.

3.2.5 Wheel Wander

Rutting of in-service pavements includes traffic with wander rather than the single-wheel-path traffic commonly used in FEM analyses. The effect of traffic wander is to distribute the loads over a wider area of pavement. As a result, the loading time on any given wheel path is reduced. For a given number of wheel passes, the total rutting would be reduced by the effect of wander. Also, the heave alongside the wheel paths is greater for single-wheel-path traffic. When wander is incorporated, the heave areas are compacted somewhat by the wandering wheel loads. Consequently, incorporating wander in load models is important in rutting predictions. The load model used had a wander width of 45.7 cm (18 in.). Wheel wander is applied by redistributing the total cumulative traffic loading time in a normally distributed fashion. A more detailed discussion on how the wheel wander distance is selected is given in Chapter 4.

3.2.6 Material Properties

Flexible pavement deformation, which occurs as a result of repeated loading, depends on the total cumulative traffic loading time. In order to simulate flexible pavement permanent deformation, a creep model is used to characterize layer materials. Permanent deformation of pavement asphalt and unbound aggregate and foundation materials is a time- and stress-dependent response. In the case of asphalt layers, there is also temperature dependence. The finite element software ABAQUS was used for analysis of rutting. Stress and time dependency is accounted for using a creep rate model from the ABAQUS material model library. In equation form, the creep rate is represented as

$$\dot{\varepsilon} = A\sigma^n t^m \tag{3-1}$$

where

$\dot{\varepsilon}$ = creep strain rate,
σ = uniaxial equivalent deviatoric stress,
t = total loading time, and
A, m, n = parameters related to material properties.

In this analysis, the effect of temperature is taken as fixed. As subsequently described, nonlinear stress distribution combined with wheel wander are accounted for in the load model. Loading time relates to vehicle speed and the length of loaded area. In actuality, the loaded area is oval and shows distinct treads. As a result, variable-length rectangular segments are used to represent the loaded contact area. Resulting variable loading time is accounted for in the loading model.

In analysis, parameters n and m were fixed, while parameter A was varied. In application, plotting log of rut depth versus log of time is a straight line. Parameter A is the value of the y-axis intercept. Rutting increases linearly with the value of A. By varying the value of A for the creep model of a given layer, the amount of deformation in that layer is controlled. Details of model application are given by Huang [49] and Hua [53].

In this study, layers allowed to rut were assigned the following layer properties:

$$E = 3.1 \times 10^6 \text{ kPa } (45{,}000 \text{ psi}), \tag{3-2}$$

$$\mu = 0.3, \tag{3-3}$$

$$A = 0.8 \times 10^{-4}, \tag{3-4}$$

$$n = 1.2, \text{ and} \tag{3-5}$$

$$m = -0.5. \tag{3-6}$$

Parameters E and μ are elastic modulus and Poisson's ratio, respectively. The parameter A was decreased by a factor of 160 for layers where rutting was not allowed.

3.2.7 Results of Initial Analysis

A detailed analysis of the initial modeling results was presented in Chapter 2. In summary, an examination of the predicted deformations by the finite element model indicates that the deformations represent typical deformations observed from in-service pavements. The predicted surface profiles are consistent with profiles observed for actual rutted pavements due to failures in the specific layers identified. These findings suggested the appropriateness of using finite element analysis in developing the failure criteria. Distortion parameters, which are total area and ratio of area, were calculated from results of finite element analysis and used in developing the initial failure criteria. By comparing the initial criteria with Simpson's criteria found in the literature, it was observed that there existed some deficiencies in Simpson's criteria.

In order to make the initial criteria more applicable to in-service pavements, the finite element models had to be refined so that the conditions in a real pavement structure were more closely simulated and finite element models covered a wider range of pavement structures. A detailed description on the refined finite element models is presented in the next section.

3.3 REFINEMENTS IN FEM ANALYSIS

This section examines the effect of material properties on the failure criteria. It also establishes new pavement models with a 2-percent cross slope. When pavement cross slope was introduced into the analysis, the previously employed half-lane finite element models had to be abandoned because a line of symmetry no longer existed at the center of a lane. All subsequent finite element models were developed with a full-lane width of 3.7 m (12 ft) accompanied by a 1.8-m (6-ft) wide shoulder.

Other modifications were made to both low- and high-volume structures. Different shoulder types were considered for low-volume structures (i.e., both HMA and aggregate shoulders were analyzed). As a result of the preliminary analysis, base and subbase layers were combined for most high-volume structures. This combination was done because the difference in deformations at the pavement surface was small between the base and subbase failure modes, which in turn resulted in very small differences in the proposed distortions parameters. Pavement failures for the subgrade heave mode are not considered in the simple model.

For the new finite element models, the prototype loading condition was changed from a one-half axle, single-wheel assembly to a full axle with dual wheels. A standard 80-kN (18,000-lb) axle load was used with a tire inflation pressure of 620 kPa (90 psi). Nonuniform contact stresses and transverse wheel wander were also incorporated into the loading conditions. Pavement structures subsequently analyzed were still classified into two categories: low and high volume. Within each category, a wide range of typical pavement structural sections was selected for analysis, as recommended by the project panel. All of these new features are addressed separately in the following sections.

3.3.1 Effect of Elastic Modulus on Distortion Parameters

In the analysis of initial models, typical values of elastic modulus were used for the pavement structure layers. Concerns developed about how predicted distortion parameters would be affected by the use of constant modulus values, namely the total area and ratio of area. The definition of total area (positive and negative) is shown in Figure 3-7. The wire method used to determine the rut depth is given in Figure 3-8.

A sensitivity study was therefore conducted by varying the modulus values of the pavement layers. Because rutting in the HMA layer has been found to be the most sensitive case, only HMA failure was considered. Results in terms of total area and ratio of area are shown in Figures 3-9 and 3-10, respectively. It can be seen from these figures that the effects of elastic modulus on distortion parameters are negligible. Consequently, the use of typical modulus values was continued.

3.3.2 Structural Geometry

Geometry of new high- and low-volume traffic pavement structures used in FEM are shown in Figures 3-11 and 3-12, respectively. A 2-percent cross slope was incorporated in the geometry for all layers in the model. The high-volume structure shown in Figure 3-11 includes a separate base and subbase and is compared with a structure having a combined base/subbase layer. The thickness of this combined layer is equal to the sum of the thickness of the base and subbase layers shown in Figure 3-11. There is essentially no difference in the results (see Section 3.3.6). Consequently, in subsequent analysis, the low- and high-volume model structures are both represented by the structure shown in Figure 3-12, except that the combined thickness of the base/subbase layer, denoted simply as the base layer, varies.

It should be noted that Figures 3-11 and 3-12 are used to demonstrate the compositions of the modified structures, the applied cross slope, and the use of full-width pavements. The geometry shown in these figures should not be used to distinguish between high- and low-volume structures. The analysis was performed on a variety of high- and low-volume structures, each with various layer thickness combinations. The exact geometry of the structures is discussed in Section 3.3.8.

A sample finite element mesh in ABAQUS for the refined models is shown in Figure 3-13. The cross slope is apparent on the top surface of each layer.

3.3.3 Consideration of Shoulder Type

An analysis was made of the effect of shoulder type on distortion parameters. The analysis included both HMA and aggregate surfaced shoulders for both low- and high-volume traffic structures. The low-traffic-volume shoulder structure consisted of 75 mm (3 in.) of HMA over 600 mm (12 in.) of base. The high-traffic-volume shoulder structure consisted of 300 mm (6 in.) of HMA, 600 mm (12 in.) of base, and 600 mm (12 in.) of subbase. Both structures were supported by the same subgrade. High- and low-traffic-volume structures were modeled with both HMA and aggregate shoulders using HMA, base, and subbase failure modes. The analysis considered both low- and high-rutting magnitudes (i.e., 5 mm [0.2 in.] versus 25 mm [1 in.] rut depths). The resulting distortion parameter data are presented in Tables 3-1 and 3-2. A comparison of results for the two shoulder surfaces types indicates that aggregate surfaced shoulders produced only nominal differences in the distortion parameters for HMA and base failure modes. It is important to note that regardless of shoulder type, the observed distortion parameters fell within the criteria that were initially proposed for each of these failure modes. Because most high-volume facilities are constructed with paved shoulders and the observed distortion parameters fell within the original criteria under both conditions, it was decided that further analysis of high-volume structures would be conducted with HMA shoulders only. Additional analysis of low-volume structures included both HMA and aggregate shoulders.

3.3.4 Determination of Wheel Path Distribution

Wheel path distribution (i.e., transverse wander) is a very important factor in determining the shape of pavement transverse profiles and, thus, distortion parameter values. As indicated previously, a standard normal distribution is appropriate for wheel wander, and Buiter et al. suggested an average standard deviation of 0.29 m (11.4 in.) [55]. To determine an appropriate wander distance for use in the finite element analysis, analysis was conducted on a high-volume structure consisting of 150 mm (6 in.) of HMA, 300 mm (12 in.) of base, and 300 mm (12 in.) of subbase. The analysis was completed for wander distances of 0.3 m (12 in.), 0.36 m (14 in.), 0.41 m (16 in.), 0.46 m (18 in.), 0.51 m (20 in.), and 0.56 m (22 in.), respectively. Surface profiles associated with the HMA failure mode are most sensitive to wheel wander. Therefore, the analysis was conducted only for this failure mode.

A detailed analysis of the wander effect is presented in Chapter 4. Based upon an examination of these profiles relative to profiles found in the literature and to those observed by the research team members in the field, 0.41 m (16 in.) of wheel wander was considered to be appropriate for the finite element analysis. The application of such a constant distribution in the finite element analysis is equivalent in effect to the total load distribution from the initiation of rutting to the point in time when a maximum rut depth would be exhibited.

3.3.5 Nonuniform Contact Stress

Nonuniform contact stress between the tire and pavement surface was adopted in the finite element models. The distribution of contact stresses employed is based on contact stress measurements found in the literature [56, 57]. The measured contact stresses for a standard dual-tire, 80-kN (18,000-lb) single axle with a tire inflation pressure of 620 kPa (90 psi) were employed. In order to incorporate the measured contact stresses, the tire contact area, which determines the duration of loading, is changed from a single rectangle with constant contact stress to a group of small rectangles with different lengths and contact stresses. Figure 3-14 shows the simplified contact area for a single axle with dual tires. Contact stresses are assumed to be constant within a given rectangular area. The stress distribution on each of the rectangular areas of a single tire is determined from the test data (see Figure 3-15). The distribution of contact stress and the contact area for the two tires

TABLE 3-1 Comparison of HMA and aggregate shoulders with large rut depths

Structure	Failure Mode	Shoulder Type	Distortion Parameters		
			Rut Depth (mm)	Total Area (mm^2)	Ratio (Pos/Neg)
High Volume	HMA	HMA	24.6	-18534.2	0.21
		Aggregate	24.9	-14425.5	0.34
	Base	HMA	24.4	-35495.1	0.02
		Aggregate	24.6	-43939.2	0.00
	Subbase	HMA	23.5	-37467.1	0.00
		Aggregate	23.6	-37545.4	0.00
Low Volume	HMA	HMA	25.3	-20812.2	0.16
		Aggregate	25.4	-18798.0	0.21
	Base	HMA	24.7	-29480.1	0.04
		Aggregate	24.5	-32750.0	0.01

TABLE 3-2 Comparison of HMA and aggregate shoulders with small rut depths

Structure	Failure Mode	Shoulder Type	Distortion Parameters		
			Rut Depth (mm)	Total Area (mm^2)	Ratio (Pos/Neg)
High Volume	HMA	HMA	5.4	-3516.2	0.24
		Aggregate	5.5	-2823.9	0.35
	Base	HMA	5.7	-8481.2	0.02
		Aggregate	6.2	-11057.3	0.00
	Subbase	HMA	5.5	-8650.4	0.00
		Aggregate	5.5	-8641.6	0.00
Low Volume	HMA	HMA	7.1	-3787.2	0.28
		Aggregate	7.1	-3517.7	0.31
	Base	HMA	6.7	-7770.8	0.04
		Aggregate	6.4	-8390.3	0.01

within each dual-tire set can be the same or different. For simplicity, the contact areas and stresses are set equal for the two tires in the finite element models. The contact stresses used are shown in Figure 3-16. Figure 3-17 shows the distribution of loading time corresponding to each level of contact stress using the 0.41-m (16-in.) wheel wander.

It was determined that when a two-dimensional model is employed with transverse wheel wander, nonuniform contact stresses do not play a significant role in determining pavement profiles and distortion parameters. Nevertheless, nonuniform contact stresses were still incorporated in the finite element models so as to simulate real loading conditions as closely as possible.

3.3.6 Consideration of Base and Subbase Layer Combinations

Initial finite element analysis showed that the differences between a base and subbase failure in terms of surface profiles and distortion parameters were small. This finding suggested the possibility of combining the two layers. If the effect of this combination can be determined to be minor, not only will the whole volume of finite element analysis be reduced, but the refined criteria will be simplified, as well.

The use of a subbase layer is more typical in high-traffic-volume structures; low-traffic-volume pavements usually do not have both a base and a subbase layer. To determine the effect of combining base and subbase layers, finite element analysis was conducted for a high-volume structure, addressing HMA, base, and subbase failure mechanisms. The original structure consisted of 150 mm (6 in.) of HMA, 300 mm (12 in.) of aggregate base, and 300 mm (12 in.) of subbase. These sections were compared with similar analysis of structures consisting of 150 mm (6 in.) of HMA and 600 mm (24 in.) of base. The same subgrade was used for all sections. Both low- and high-rutting magnitudes were considered (5 mm [0.2 in.] versus 25 mm [1 in.] rut depths). The comparisons revealed small differences in distortion parameters between the two types of structures for base and subbase failure mechanisms. No differences were observed for the HMA failure mode. The distortion parameters are presented in Tables 3-3 and 3-4, and the surface profiles are shown in Figure 3-18. On the basis of this analysis, it was decided to combine base and subbase layers for subsequent analysis of high-traffic-volume pavement structures. This approach should not be interpreted to suggest that the individual layers are not important, but rather that failures in either layer lead to similar surface deformations that, in turn, lead to similar distortion parameters.

3.3.7 Subgrade Heave

Simpson et al. [20] proposed that a failure of the pavement structure caused by subgrade heave would result in a surface profile with the deformed surface, all above the original pave-

TABLE 3-3 Comparison of high-volume structures with and without subbase (large rutting)

Failure Mode	Structure	Distortion Parameters		
		Rut Depth (mm)	Total Area (mm^2)	Ratio (Pos/Neg)
HMA	150mm HMA + 300mm Base + 300mm Subbase	24.6	-18534.2	0.21
	150mm HMA + 600mm Base	24.6	-18557.3	0.21
Base	150mm HMA + 300mm Base + 300mm Subbase	24.4	-35495.1	0.02
	150mm HMA + 600mm Base	24.7	-37471.5	0.025
Subbase	150mm HMA + 300mm Base + 300mm Subbase	23.5	-37467.1	0.00

TABLE 3-4 Comparison of high-volume structures with and without subbase (small rutting)

Failure Mode	Structure	Distortion Parameters		
		Rut Depth (mm)	Total Area (mm^2)	Ratio (Pos/Neg)
HMA	150mm HMA + 300mm Base + 300mm Subbase	5.4	-3516.2	0.24
	150mm HMA + 600mm Base	5.4	-3504.6	0.24
Base	150mm HMA + 300mm Base + 300mm Subbase	5.7	-8481.2	0.02
	150mm HMA + 600mm Base	5.5	-8843.2	0.016
Subbase	150mm HMA + 300mm Base + 300mm Subbase	5.5	-8650.4	0.00

ment surface. The initial finite element analysis conducted by the research team also indicated similar results, as shown in Figure 3-19. After close examination of the subgrade heave mechanism, the previous models are believed to be inappropriate in that the material properties of the subgrade are held unchanged after heave occurs in these models.

In reality, when heave occurs, the subgrade goes through a positive volume change (i.e., expands) and upheaval occurs in the pavement structure. However, when these changes occur, the subgrade is in an expanded, high-moisture state. Application of wheel loads can cause subgrade densification and shear deformation. Densification will cause rutting, as well as subgrade strengthening; the strengthened subgrade will, in turn, reduce the rate of further rutting. Although this whole process cannot be simulated exactly by one finite element procedure, average material properties can be selected for analysis. The results of this analysis show that the subgrade failure mode due to heave is essentially the same as that of subgrade rutting (see Figure 3-20). Although heave may still be present in the pavement structure, it cannot be measured from a 3.7-m (12-ft)-wide transverse surface profile; the net result is that the entire pavement surface simply moves up. As a result, the subgrade heave failure mode has been pooled with the standard subgrade failure mode.

3.3.8 Structural Sections Considered in Finite Element Analysis

An attempt has been made to analyze a range of typical pavement sections representative of those in existence in both high- and low-traffic-volume facilities throughout the United States. Typical pavement sections considered in the modeling analysis are presented in Table 3-5. In selecting these structures, comments and suggestions provided by the project panel members were incorporated. The panel members recommended that analysis be conducted for a pavement structure with 50 mm (2 in.) of HMA and 300 mm (6 in.) of base, as well as thick and thin, full-depth HMA sections. Table 3-5 also indicates the AASHTO structural numbers ($SN = a_1d_1 +$

TABLE 3-5 Modal contributions to rutting

Structural Layers	Volume															
	Low					High										
HMA (mm)	50	75	100	130	130	150			230			300			380	
Base (mm)	150	300	150	0	300	300	300	600	0	300	600	0	300	600	0	600
Subbase (mm)						300										
Subgrade (m)	1.8	1.8	1.8	1.8	1.8	1.8	1.8	1.8	1.8	1.8	1.8	1.8	1.8	1.8	1.8	1.8
AASHTO SN	1.3	2.25	2.0	1.75	2.95	4.5	3.3	4.5	3.15	4.35	5.55	4.2	5.4	6.6	5.25	7.65
Analysis Series No.	01	02	03	04	05	01	02	03	04	05	06	07	08	09	10	11
Shoulder Conditions	2	2	2	2	2	2	1	1	1	1	1	1	1	1	1	1
Rut Depths	2	2	2	2	2	2	2	2	2	2	2	2	2	2	2	2
Failure Modes	3	3	3	2	3	4	3	3	2	3	3	2	3	3	2	3
FE Analyses Required	12	12	12	8	12	16	6	6	4	6	6	4	6	6	4	6
FE Analyses/Volume	56					70										
Total FE Analyses	126															

Notes:
1. The 2 Rut Depths are small (approximately 5mm) and large (approximately 25mm).
2. The 3 Failure Modes are HMA, Base, and Subgrade (assuming Base and Subbase are lumped together).
3. The shoulder conditions are: 2 = HMA and Aggregate, 1 = HMA only.
4. FE = finite element.
5. SN = structural number.

$a_2d_2m_2 + a_3d_3m_3$) assuming the following layer and drainage coefficients:

$$a_1 = -0.35; \quad (3\text{-}7)$$

$$a_2 \text{ and } a_3 = -0.10; \text{ and} \quad (3\text{-}8)$$

$$m_2 \text{ and } m_3 = 1.0 \quad (3\text{-}9)$$

Other information in the table simply indicates the total number or levels associated with each analysis parameter for a given structural section. For example, the value of 2 in the second column for the "Rut Depths" parameter in the first column of Table 3-5 indicates that analysis was conducted considering two rut-depth magnitudes: low and high (5 mm [0.2 in.] and 25 mm [1 in.]). The value of 2 in the same column for "Shoulder Conditions" indicates that two shoulder-surface conditions were considered in the analysis of a given structural section: HMA and aggregate. Similarly, a value of 3 for "Failure Modes" indicates that three rutting-failure modes were considered in the analysis of a given structural section. The value of 12 in the second column of the table for "FE Analysis Required" indicates that 12 finite element analyses were conducted. In this case, the factors incorporated in the analyses were HMA and aggregate shoulders; low and high rut depths; and HMA, base, and subgrade rutting failure modes.

Table 3-5 also indicates that 126 finite element runs would be required to obtain distortion parameters for each of the structures analyzed: 56 for the low-traffic-volume structures and 70 for the high-traffic-volume structures. As many as 378 runs were completed because the finite element analyses were performed using a fixed rut depth. If the first attempt with the finite element program did not produce the desired amount of rutting, the analysis would have to be done again with the appropriate parameters changed. Up to three finite element program runs were required to obtain the desired rut depth for each combination of structural, geometric, and loading conditions. The program developed during the last quarter of 1999 to assist with the finite element analysis has proven to be extremely useful in that it saves a significant amount of time in preparing initial data and analyzing results. This program also calculates distortion parameters and is named "Profile Analysis Assistant Program (PAAP)." It was used in the analysis of both FEM results and field transverse surface profiles.

3.3.9 Results From Finite Element Analysis

Distortion parameters for high-traffic-volume structures are presented in Tables 3-6 to 3-16. Tables 3-17 to 3-21 summarize the distortion parameters for low-traffic-volume structures. All the profiles presented in these figures have been magnified by a factor of ten to enhance visual interpretation.

TABLE 3-6 Results from high-volume structure HVS01

Structure: 150mm HMA, 300mm Base, and 300mm Subbase				
Failure	Shoulder	Rut Depth (mm)	Total Area (mm^2)	Ratio (+/-)
HMA	HMA	24.6	-18534.2	0.21
"	"	5.4	-3516.2	0.24
Base	"	24.4	-35495.1	0.018
"	"	5.7	-8481.2	0.016
Subbase	"	23.5	-37467.1	0.0
"	"	5.5	-8650.4	0.0
Subgrade	"	25.3	-55975.5	0.0
"	"	6.6	-15898.8	0.0
HMA	Aggregate	24.9	-14425.5	0.337
"	"	5.5	-2823.9	0.352
Base	"	24.6	-43939.2	0.0
"	"	6.2	-11057.3	0.0
Subbase	"	23.6	-37545.4	0.0
"	"	5.5	-9641.6	0.0
Subgrade	"	25.5	-56634.9	0.0
"	"	6.8	-16535.4	0.0

TABLE 3-7 Results from high-volume structure HVS02

Structure: 150mm HMA and 300mm Base				
Failure	Shoulder	Rut Depth (mm)	Total Area (mm^2)	Ratio (+/-)
HMA	HMA	24.6	-18527.0	0.210
"	"	5.3	-3503.4	0.240
Base	"	24.5	-35662.7	0.018
"	"	5.7	-8529.0	0.016
Subgrade	"	23.4	-56004.8	0.0
"	"	6.9	-14623.9	0.0

TABLE 3-8 Results from high-volume structure HVS03

Structure: 150mmHMA and 600mm Base				
Failure	Shoulder	Rut Depth (mm)	Total Area (mm^2)	Ratio (+/-)
HMA	HMA	24.6	-18557.3	0.21
"	"	5.4	-3504.6	0.24
Base	"	24.7	-37471.5	0.025
"	"	5.5	-8843.2	0.016
Subgrade	"	24.2	-53866.0	0.0
"	"	5.0	-12164.5	0.0

TABLE 3-9 Results from high-volume structure HVS04

Structure: 230mm Full-Depth HMA				
Failure	Shoulder	Rut Depth (mm)	Total Area (mm^2)	Ratio (+/-)
HMA	HMA	24.4	-21925.8	0.158
"	"	5.1	-4207.4	0.178
Subgrade	"	25.8	-58039.8	0.0
"	"	6.3	-13495.4	0.0

TABLE 3-10 Results from high-volume structure HVS05

Structure: 230mm HMA and 300mm Base				
Failure	Shoulder	Rut Depth (mm)	Total Area (mm^2)	Ratio (+/-)
HMA	HMA	24.2	-21849.7	0.158
"	"	5.5	-4511.5	0.174
Base	"	24.8	-39688.8	0.015
"	"	5.6	-9211.1	0.012
Subgrade	"	24.1	-51665.3	0.0
"	"	6.7	-17367.8	0.0

TABLE 3-11 Results from high-volume structure HVS06

Structure: 230mm HMA and 600mm Base				
Failure	Shoulder	Rut Depth (mm)	Total Area (mm^2)	Ratio (+/-)
HMA	HMA	24.2	-21841.2	0.157
"	"	5.5	-4496.1	0.175
Base	"	25.2	-38812.5	0.0024
"	"	5.7	-9064.3	0.0004
Subgrade	"	23.9	-46511.4	0.0
"	"	6.1	-12827.8	0.0

TABLE 3-12 Results from high-volume structure HVS07

Structure: 300mm Full-Depth HMA				
Failure	Shoulder	Rut Depth (mm)	Total Area (mm^2)	Ratio (+/-)
HMA	HMA	24.2	-21841.2	0.157
"	"	5.5	-4496.1	0.175
Subgrade	"	25.2	-38812.5	0.0024
"	"	5.7	-9064.3	0.0004

TABLE 3-13 Results from high-volume structure HVS08

Structure: 300mm HMA and 300mm Base				
Failure	Shoulder	Rut Depth (mm)	Total Area (mm^2)	Ratio (+/-)
HMA	HMA	25.3	-25624.8	0.117
"	"	6.4	-6138.4	0.119
Base	"	25.0	-40011.2	0.009
"	"	6.2	-10118.9	0.005
Subgrade	"	24.7	-50055.2	0.0
"	"	7.6	-17411.9	0.0

TABLE 3-14 Results from high-volume structure HVS09

Structure: 300mm HMA and 600mm Base				
Failure	Shoulder	Rut Depth (mm)	Total Area (mm^2)	Ratio (+/-)
HMA	HMA	25.2	-25605.3	0.117
"	"	6.4	-6118.9	0.120
Base	"	24.1	-40122.9	0.0
"	"	5.8	-9747.5	0.0
Subgrade	"	21.6	-41732.6	0.0
"	"	6.1	-12601.2	0.0

TABLE 3-15 Results from high-volume structure HVS10

Structure: 380mm Full-Depth HMA				
Failure	Shoulder	Rut Depth (mm)	Total Area (mm^2)	Ratio (+/-)
HMA	HMA	24.6	-27059.3	0.082
"	"	7.1	-7609.2	0.080
Subgrade	"	21.5	-50982.9	0.0
"	"	5.8	-15128.2	0.0

TABLE 3-16 Results from high-volume structure HVS11

Structure: 380mm HMA and 600mm Base				
Failure	Shoulder	Rut Depth (mm)	Total Area (mm^2)	Ratio (+/-)
HMA	HMA	24.3	-26804.8	0.083
"	"	7.0	-7451.3	0.083
Base	"	24.4	-43706.0	0.0
"	"	5.9	-10518.6	0.0
Subgrade	"	22.8	-43693.3	0.0
"	"	6.1	-12386.0	0.0

TABLE 3-17 Results from low-volume structure LVS01

Structure: 50mm HMA and 150mm Base				
Failure	Shoulder	Rut Depth (mm)	Total Area (mm^2)	Ratio (+/-)
HMA	HMA	24.0	-28828.4	0.03
"	"	5.7	-5166.6	0.065
Base	"	21.5	-9010.4	0.44
"	"	5.7	-2253.3	0.46
Subgrade	"	25.3	-46650.0	0.0
"	"	6.4	-11791.3	0.0
HMA	Aggregate	20.0	-26971.4	0.01
"	"	5.3	-5133.8	0.046
Base	"	24.8	-7693.6	0.564
"	"	6.8	-2113.0	0.556
Subgrade	"	24.3	-44014.6	0.0
"	"	6.9	-12589.7	0.0

TABLE 3-18 Results from low-volume structure LVS02

Structure: 75mm HMA and 300mm Base				
Failure	Shoulder	Rut Depth (mm)	Total Area (mm^2)	Ratio (+/-)
HMA	HMA	25.3	-20812.2	0.162
"	"	7.1	-3787.2	0.275
Base	"	24.7	-29480.1	0.04
"	"	6.7	-7770.8	0.036
Subgrade	"	26.5	-60916.0	0.0
"	"	7.5	-15529.2	0.0
HMA	Aggregate	25.4	-18798.0	0.212
"	"	7.1	-3517.7	0.311
Base	"	24.5	-32750.0	0.011
"	"	6.4	-8390.3	0.014
Subgrade	"	25.2	-54829.5	0.0
"	"	6.5	-12874.9	0.0

TABLE 3-19 Results from low-volume structure LVS03

Structure: 100mm HMA and 150mm Base				
Failure	Shoulder	Rut Depth (mm)	Total Area (mm^2)	Ratio (+/-)
HMA	HMA	23.3	-18366.5	0.170
"	"	5.7	-3631.3	0.216
Base	"	21.9	-25954.9	0.03
"	"	7.0	-10514.0	0.004
Subgrade	"	24.5	-47538.7	0.0
"	"	7.5	-14132.3	0.0
HMA	Aggregate	23.3	-16296.7	0.232
"	"	5.7	-3271.7	0.270
Base	"	22.2	-28625.5	0.006
"	"	7.1	-11677.0	0.0
Subgrade	"	25.9	-50008.7	0.0
"	"	7.7	-14597.6	0.0

TABLE 3-20 Results from low-volume structure LVS04

Structure: 130mm Full-Depth HMA				
Failure	Shoulder	Rut Depth (mm)	Total Area (mm^2)	Ratio (+/-)
HMA	HMA	23.5	-17206.6	0.213
"	"	5.3	-3260.9	0.248
Subgrade	"	24.8	-45001.6	0.0
"	"	6.6	-12138.9	0.0
HMA	Aggregate	23.7	-14152.3	0.313
"	"	5.4	-2720.5	0.345
Subgrade	"	25.9	-46881.2	0.0
"	"	6.9	-12730.1	0.0

TABLE 3-21 Results from low-volume structure LVS05

Structure: 130mm HMA and 300mm Base				
Failure	Shoulder	Rut Depth (mm)	Total Area (mm^2)	Ratio (+/-)
HMA	HMA	23.6	-17586.0	0.203
"	"	5.3	-3366.0	0.238
Base	"	23.5	-33005.9	0.017
"	"	5.9	-8438.8	0.015
Subgrade	"	20.8	-50369.3	0.0
"	"	7.7	-16293.1	0.0
HMA	Aggregate	23.7	-14559.3	0.300
"	"	5.4	-2844.4	0.323
Base	"	24.4	-42391.3	0.0
"	"	6.1	-10560.7	0.0
Subgrade	"	23.5	-56265.1	0.0
"	"	8.2	-17369.9	0.0

In reviewing the results (surface profiles and distortion parameters), the low-volume structure, consisting of 50 mm (2 in.) of HMA, was found to exhibit a different rutting behavior than all other low- and high-volume structures. A discussion will be presented later in this section.

For structures other than the low-volume structures, visual inspection indicates that the surface profiles delineate the failure modes. This indication supports the premise that distortion parameters determined from the transverse profiles can be used to predict layer failure. The distortion parameters do, in fact, vary in terms of total area and ratio of area as failure transitions from HMA to subgrade. Despite the difference in structures and layer thickness, in this transition the total area increases in absolute value and the ratio of area decreases. As noted previously, the low-volume pavement structure with the 50-mm (2-in.) HMA layer behaves differently than all other structures do. In the analysis, it was difficult to force this structure to exhibit a 25-mm (1-in.) rut depth and maintain a profile similar to that of the other structures because the thin HMA layer does not have the capacity to deform internally. As a result, the base layer contributes significantly to the rutting, resulting in a decreased ratio of area for HMA failure. As a further consequence, a base failure for this thin, low-volume structure appears to be an HMA failure. In this case, the HMA layer is not thick enough to distribute load to the base layer in the same way as a thick HMA layer would.

After review, this case was not used in developing the aggregate failure criteria, but treated as a special case. The validity of finite element analysis for this structure was confirmed by trenching data obtained from SH 28 East in Mississippi. The analysis of these data will be presented in Chapter 6.

3.4 SUMMARY

A comprehensive matrix of pavement structures was analyzed using finite element analysis. Results from this analysis clearly show differences in transverse surface profiles and distortion parameters for different pavement failure modes. These results can be used to develop criteria for identifying pavement layer failure from measured transverse surface profiles. The special case of the thin, low-volume traffic section has been carefully checked and will not be used in developing the general-purpose failure criteria.

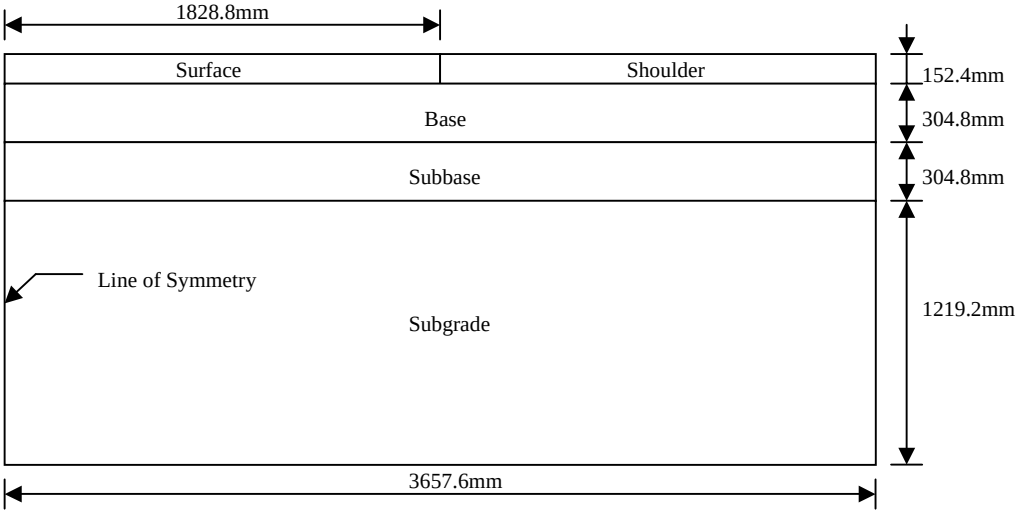

Figure 3-1. Cross section of modeled high-volume structure.

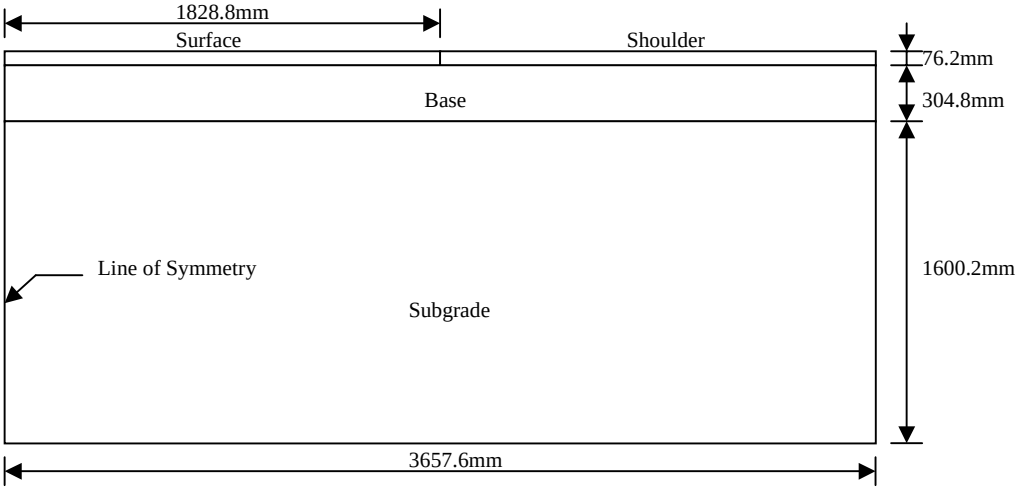

Figure 3-2. Cross section of modeled low-volume structure.

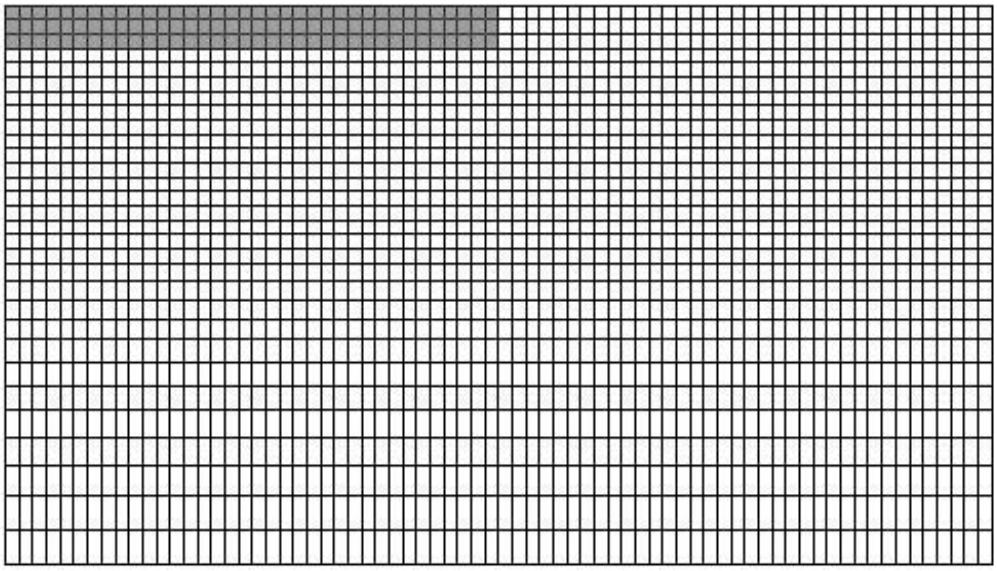

Figure 3-3. Finite element mesh used for high-volume structures.

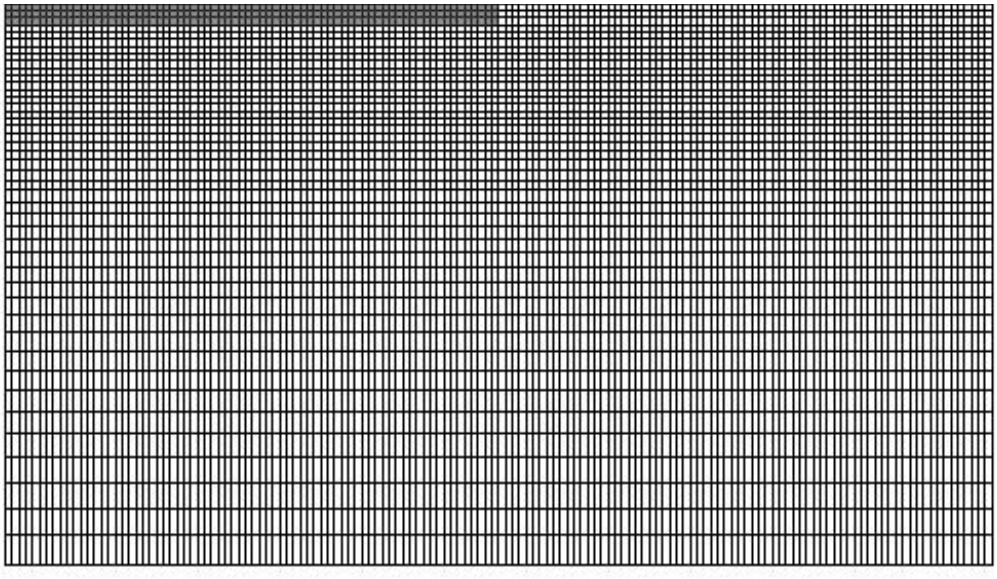

Figure 3-4. Finite element mesh used for low-volume structures.

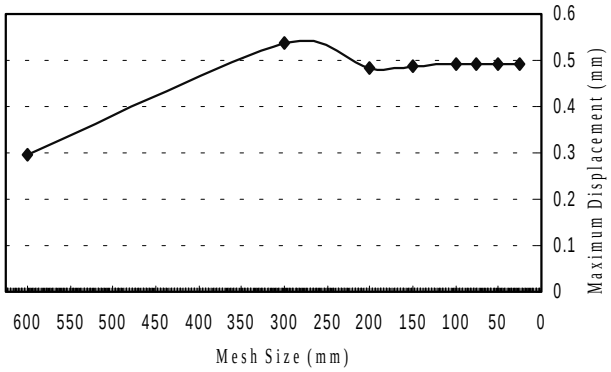

Figure 3-5. Relationship between maximum displacement and mesh size.

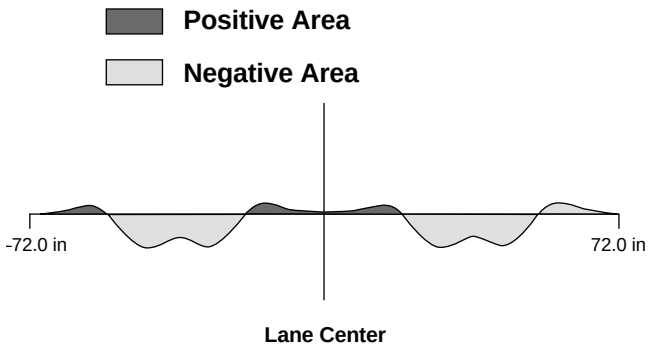

Figure 3-7. Definition of positive area and negative area.

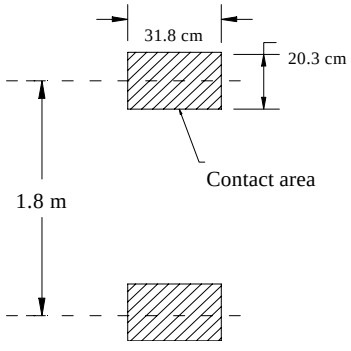

Figure 3-6. Tire contact areas of single-tire axel.

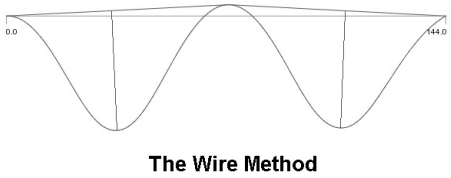

Figure 3-8. The wire method of rut determination.

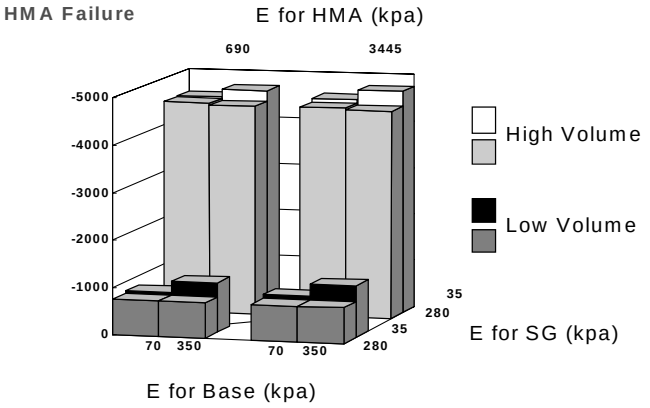

Figure 3-9. Effect of "E" on total area.

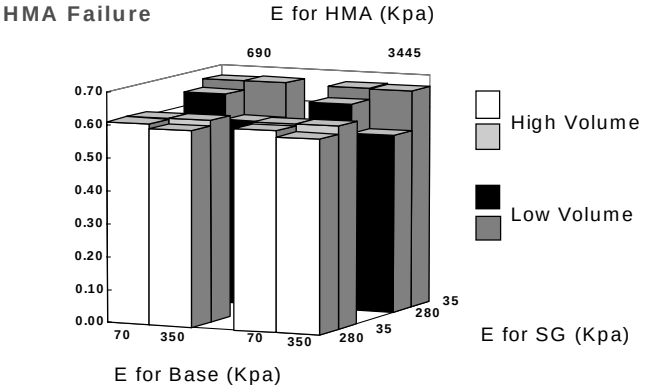

Figure 3-10. Effect of "E" on ratio of positive to negative area.

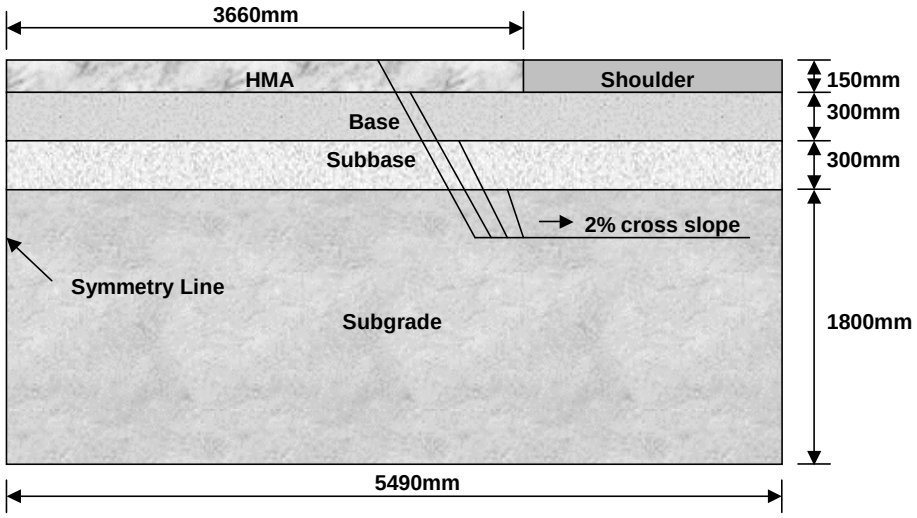

Figure 3-11. Geometry of structure, Refined Model 1.

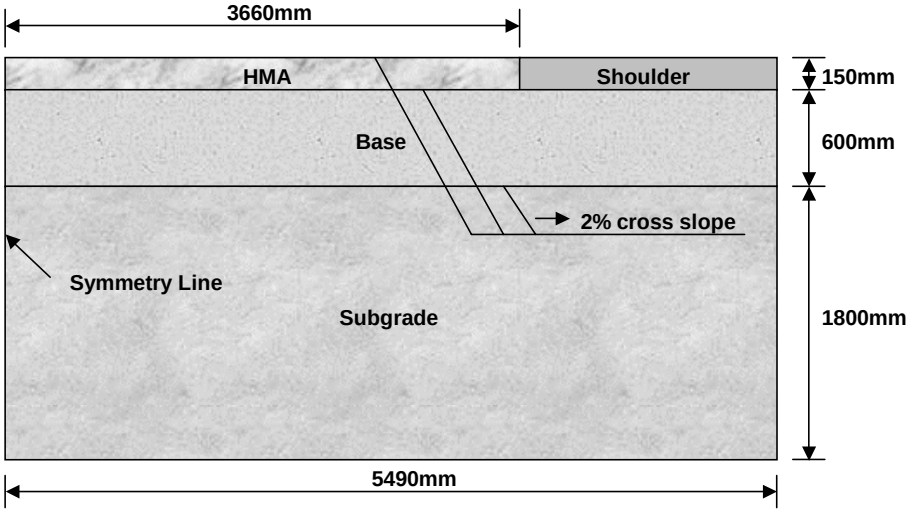

Figure 3-12. Geometry of structure, Refined Model 2.

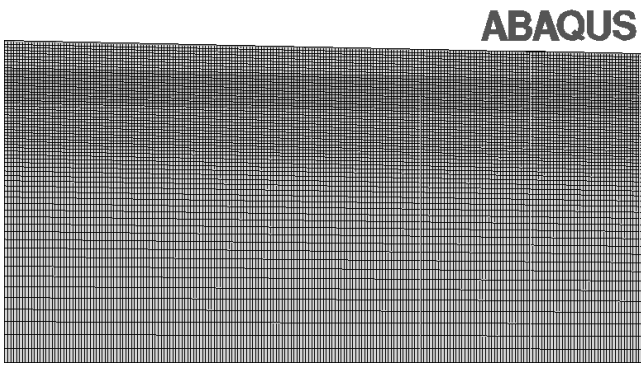

Figure 3-13. A finite element model in ABAQUS for the refined model.

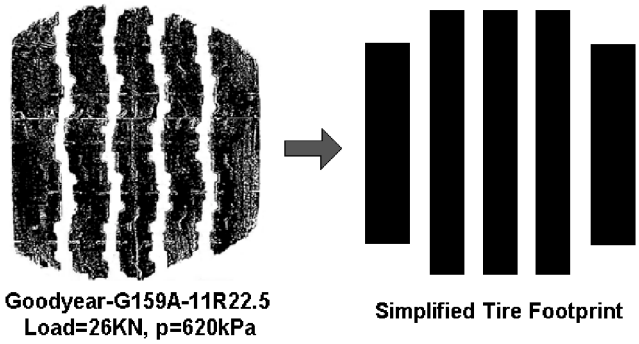

Figure 3-14. Simplification of tire footprint.

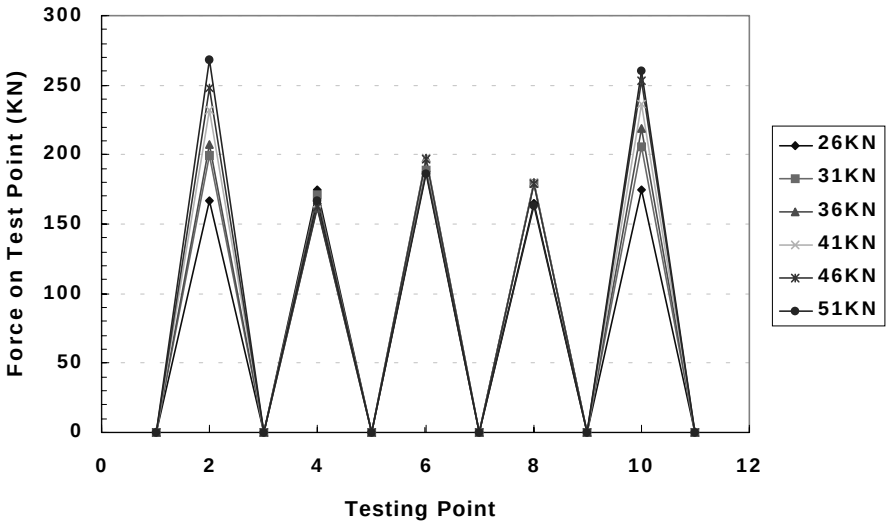

Figure 3-15. Distribution of nonuniform contact stresses.

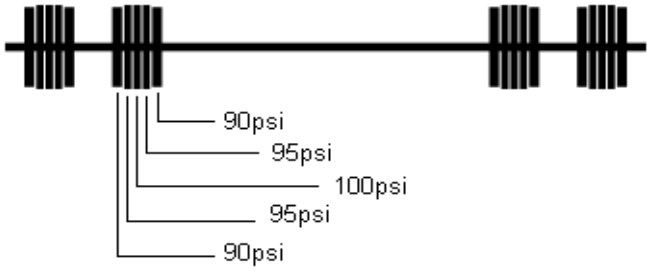

Figure 3-16. Contact area and contact stresses.

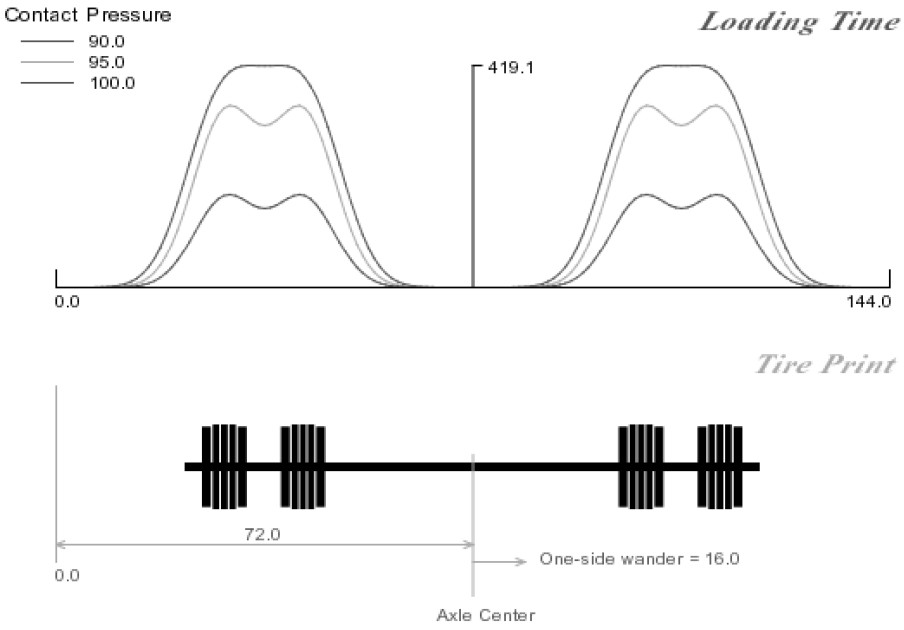

Figure 3-17. Load distribution of different stress levels.

Profile for HMA failure mode, 150mm HMA + 300mm base + 300mm subbase

Profile for HMA failure mode, 150mm HMA + 600mm base

Profile for base failure mode, 150mm HMA + 300mm base + 300mm subbase

Profile for subbase failure mode, 150mm HMA + 300mm base + 300mm subbase

Profile for base failure mode, 150mm HMA + 600mm base

Note: These profiles are magnified by a factor of 10, and all have rut depths of approximately 24 mm.

Figure 3-18. Effects of combined base and subbase on surface profiles.

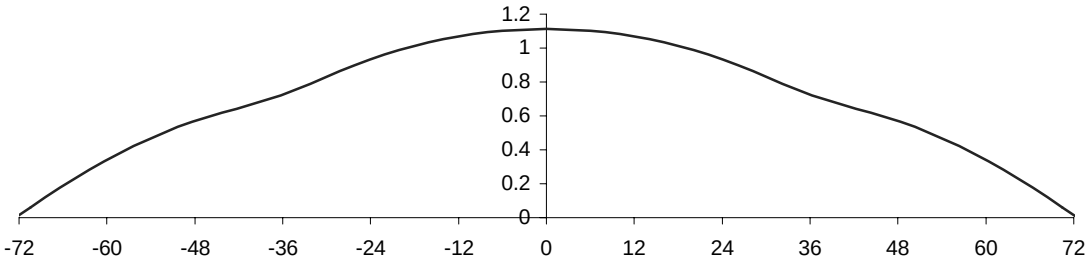

Figure 3-19. Subgrade heave from old finite element model (mm).

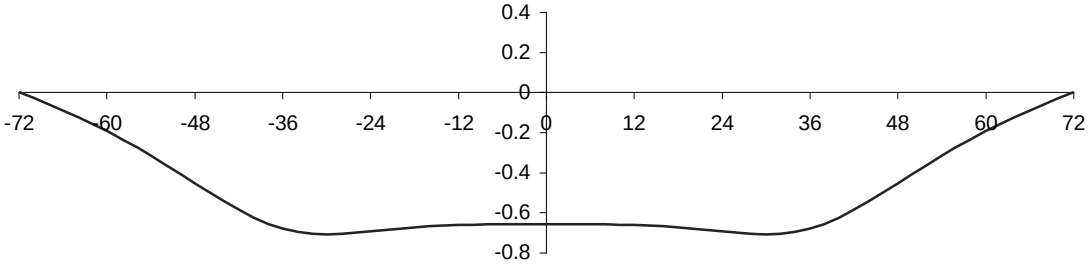

Figure 3-20. Subgrade heave from new finite element model (mm).